Integrating desalination with concentrating solar power: Large scale cogeneration of water and electricity

by
Ernest Peter Dall

Thesis presented in partial fulfilment of the requirements for the degree of Master of Engineering (Mechanical) in the Faculty of Engineering at Stellenbosch University

Supervisor: Dr J.E. Hoffmann

March 2017

Stellenbosch University https://scholar.sun.ac.za

Declaration

By submitting this thesis electronically, I declare that the entirety of the work contained therein is my own, original work, that I am the owner of the copyright thereof (unless to the extent explicitly otherwise stated) and that I have not previously in its entirety or in part submitted it for obtaining any qualification.

March 2017

Copyright © 2017 Stellenbosch University

All rights reserved

Stellenbosch University https://scholar.sun.ac.za

Abstract

The demand for fresh water is a growing concern that is shared globally. Finite fresh water resources, accompanied by an exponential population growth will demand the need for additional installed desalination plants worldwide. However, desalination is extremely energy intensive with the costs thereof depending on the availability of local energy resources (coal, oil, gas, etc.). Fortunately, most arid regions generally also have high solar energy resources that could be utilized instead of conventional fossil fuel resources. Concentrating solar power (CSP) is steadily gaining more market acceptance as the cost of electricity from CSP power plants progressively declines. Cogeneration is an attractive prospect for future CSP developments as the simultaneous production of power and potable water can have positive economic implications towards increasing the feasibility of CSP plant developments. This is a theoretical case study, within the context of Namibia, in Southern Africa, investigating the possible benefits and concerns of integrating a multiple-effect desalination (MED) plant with a $100MW_e$ concentrating solar power (CSP) tower plant for the large scale cogeneration of electricity and potable water (CSP+D). The focus of this study is set on the analytical modelling of a MED plant which captures the sensitivities of the parameters required for cogeneration analysis. A simplified CSP and Rankine cycle is modelled in terms of the optical-to-thermal conversion of energy. The high capital costs of thermal desalination heat exchangers as well as the pumping of seawater far inland is the most significant barrier in making this approach competitive against more conventional desalination methods such as reverse osmosis. The compromise between the lowest levelized cost of electricity and potable water depends on the sizing and the top brine temperature of the desalination plant. Additionally, the feasibility and final sizing of a CSP+MED plant would ultimately depend on the Namibian CSP tariffs and structures as well as the tariff for desalination.

Keywords: concentrating solar power (CSP), Multiple-effect distillation (MED), cogeneration, desalination, central receiver

Stellenbosch University https://scholar.sun.ac.za

Opsomming

Die aanvraag vir vars water is ŉ groeiende kwessie wat wêreldwyd ervaar word. Beperkte vars water bronne gekombineer met ŉ eksponensiële groei in bevolking sal aandring op die addisionele konstruksie van ontsoutings aanlegte wêreldwyd. Die probleem is dat ontsoutingsprosesse ongelooflik energie intensief is en dat die koste daarvan afhanklik is van die lokale beskikbaarheid van energiebronne, byvoorbeeld steenkool, gas en olie. Gelukkig het die meerderheid van woestyn areas ook die meeste sonkrag potensiaal wat gebruik kan word in plaas van fossiel brandstowwe. Die mark vir gekonsentreerde sonkrag (CSP) is stadig maar seker besig om te groei soos wat die elektrisiteitskostes daarvan jaarliks daal. Die mede-generasie van elektrisiteit en ontsoute seewater is ŉ aantreklike vooruitsig vir die toekomstige ontwikkeling van CSP kragstasies. Die gelyke produksie van elektrisiteit en water kan positiewe ekonomiese implikasies hê en dus die haalbaarheid van CSP projekte verder motiveer. Hierdie is ŉ teoretiese gevallestudie, binne die konteks van Namibië, wat die moontlike voordele en kwessies aangaande die integrasie van ŉ meervoudige-effek distillasie (MED) prosesse binne-in ŉ CSP toring aanleg bespreek. Die netto-elektriese kapasiteit van die CSP aanleg is ŉ 100 MW_e. Die fokus van hierdie studie is gemik op die analitiese modellering van ŉ MED aanleg wat die sensitiwiteitseienskappe van parameters vasvang wat benodig is vir die analise van ŉ mede-generasie aanleg. ŉ Vereenvoudigde CSP en Rankine siklus word gemodelleer in terme van die optiese tot termiese omskakeling van energie. Die hoe kapitale kostes van korrosiebestande hitteruilers as ook die pompkostes om seewater na die binneland te vervoer is die hoof struikelblok wat hierdie benadering minder kompeterend maak in vergelyking met “tru-osmose”. Die kompromie tussen die koste van elektrisiteit en water hang af van die grootte en boonste pekel temperatuur van die MED aanleg. Verder sal die haalbaarheid en gekose grootte van die CSP+MED aanleg afhanklik wees van die tariewe wat toegeken sal word vir CSP en ontsoute water in Namibië.

Stellenbosch University https://scholar.sun.ac.za

Acknowledgments

I would like to express my sincere gratitude to the following individuals and organizations who have contributed to making this work possible:

- NamPower for providing the financial support for my studies at Stellenbosch University
- My supervisor, Dr J.E. Hoffmann, for your guidance and providing the resources and additional funding which facilitated the realization of this study
- Prof. F. Dinter for your guidance and support
- STERG for providing the resources, space and exposure that encourages doing research in concentrating solar power
- GeoSun for providing the required climate data for Arandis
- My friends, Frank Duvenhage, Arvind Pidaparthi for your assistance, support and interest in my research
- My family for your continuous support and encouragement to further my studies in engineering
- The Cyprus Institute for inviting me to the 2016 Networking of Excellence in Solar Thermal Energy Research (NESTER) autumn school. It gave me the opportunity to engage with the top CSP research institutions and helped to streamline my research and expand my knowledge in the field of CSP and desalination
- Dr Diego Alarcón-Padilla and Dr Patricia Palenzuela from CEIMAT-PSA (Spain) for sharing your knowledge regarding CSP and desalination processes

Stellenbosch University https://scholar.sun.ac.za

Table of contents

Stellenbosch University https://scholar.sun.ac.za

Stellenbosch University https://scholar.sun.ac.za

Stellenbosch University https://scholar.sun.ac.za

Stellenbosch University https://scholar.sun.ac.za

Stellenbosch University https://scholar.sun.ac.za

List of figures

Stellenbosch University https://scholar.sun.ac.za

Stellenbosch University https://scholar.sun.ac.za

Stellenbosch University https://scholar.sun.ac.za

List of tables

Stellenbosch University https://scholar.sun.ac.za

Nomenclature

Constants

g	Gravitational constant	[m/s^2]
σ	Stefan-Boltzmann constant	[W/m^2/K^4]

Dimensionless numbers

f	Coefficient of resistance	[-]
Re	Reynolds number	[-]

Variables

$A_{e,[i]}$	Heat transfer area of ith effect	[m^2]
$A_{ph,[i]}$	Area of ith preheater	[m^2]
$A_{Rec,ref}$	Receiver reference outside surface area	[m^2]
A_{rec}	Receiver exposed outside surface area	[m^2]
$C_{HX,Ti/SS}$	Ti-SS shell-in-tube heat exchanger capital cost	[USD]
C_{Rec}	Receiver total cost	[USD]
$C_{T,tot}$	Tower total cost	[USD]
D	Diameter of bulk water pipeline	[m]
DR_n	Nominal discount rate	[%]
$E_{mes,in}$	Total thermal energy flow into the MES plant	[kW]
$E_{mes,out}$	Total thermal energy out of the MES plant	[kW]
$h_{b,[i]}$	Enthalpy of brine in ith effect	[kJ/kg]

Stellenbosch University https://scholar.sun.ac.za

$h_{dv,f,[i]}$	Enthalpy of saturated distillate fluid in i^{th} flash-box	[kJ/kg]
$h_{dv,fg,out[i]}$	Enthalpy of distillate vapour exiting i^{th} PH	[kJ/kg]
$h_{dv,g,[i]}$	Enthalpy of saturated distillate vapour in i^{th} flash-box	[kJ/kg]
$h_{dv,out,[i]}$	Enthalpy of condensed distillate vapour in i^{th} effect	[kJ/kg]
$h_{f,[i]}$	Enthalpy of feed-water in i^{th} effect	[kJ/kg]
H_{helio}	Heliostat height	[m]
H_{Rec}	Receiver height	[m]
$h_{s,in}$	Enthalpy of heating steam entering first effect of MES plant	[kJ/kg]
$h_{s,out}$	Enthalpy of heating steam exiting first effect of MES plant	[kJ/kg]
$h_{shv,[i]}$	Enthalpy of superheated distillate vapour in i^{th} effect	[kJ/kg]
$h_{sw,in}$	Enthalpy of seawater entering condenser	[kJ/kg]
$h_{sw,out}$	Enthalpy of seawater exiting condenser	[kJ/kg]
H_T	Tower height	[m]
h_c	Receiver convective heat transfer coefficient	[W/m K]
L	Length of bulk water pipeline	[m]
$LMTD_{ph,[i]}$	Log-mean temperature difference of i^{th} preheater	[°C]
$M_{b",[i]}$	Brine formed after flashing in i^{th} effect	[kg/s]
$M_{b,[i]}$	Brine formed in the i^{th} effect	[kg/s]
$M_{d,tot}$	Total distillate formed in MES plant	[kg/s]
$M_{dgc,[i]}$	Distillate formed via condensation in i^{th} flash-box of the $M_{d,[i-1]}$ stream	[kg/s]
$M_{dgf,[i]}$	Distillate vapour formed via flashing of the $M_{d,[i-1]}$ stream in i^{th} flash-box	[kg/s]
$M_{dv,[i]}$	Distillate vapour formed in i^{th} effect	[kg/s]
$M_{dv,gc,[i]}$	Distillate formed via condensation in i^{th} flash-box of the $M_{dv[i-1]}$ stream	[kg/s]

Stellenbosch University https://scholar.sun.ac.za

$M_{dv,gf,[i]}$	Distillate vapour formed via flashing of the $M_{dv[i-1]}$ stream in i^{th} flash-box	[kg/s]
M_f	Feed-water entering first effect of MES plant	[kg/s]
$M_{gb,[i]}$	Distillate produce via boiling in the i^{th} effect	[kg/s]
$M_{gf,[i]}$	Distillate vapour formed in i^{th} effect via flashing of brine	[kg/s]
$M_{mes,in}$	Total mass flow into the MES plant	[kg/s]
$M_{mes,out}$	Total mass flow out of the MES plant	[kg/s]
M_S	Saturated steam entering first effect of MES plant	[kg/s]
$M_{sw,rej}$	Rejected seawater (excess cooling water)	[kg/s]
M_{sw}	Seawater flow rate	[kg/s]
n	Life time cycle	[years]
N	Number of effects	[-]
P_{annual}	Annual electricity produced	[kWh]
Q	Volume flow rate in bulk water pipeline	[m^3/s]
Q_{PB}	Required heat input to the power block	[W]
$Q_{r,in}$	Thermal energy from heliostat field incident on receiver	[kW]
$Q_{r,loss}$	Receiver thermal energy losses	[kW]
$T_{b,[i]}$	Brine temperature in i^{th} effect	[°C]
T_{db}	Ambient dry-bulb temperature	[°C]
$T_{dv,[i]}$	Temperature of distillate vapour in i^{th} effect	[°C]
$T_{f,[i]}$	Temperature of feed-water in i^{th} effect	[°C]
T_L	Condensing temperature of Rankine cycle	[°C]
T_s	Heating steam temperature of 1^{st} MES effect	[°C]
T_{wall}	Receiver average surface temperature	[°C]
$U_{e,[i]}$	Heat transfer coefficient of i^{th} effect	[W/m^2 K]
$U_{ph,[i]}$	Heat transfer coefficient of i^{th} preheater	[W/m^2 K]

Stellenbosch University https://scholar.sun.ac.za

v_m	Mean velocity in bulk water pipeline	[m/s]
v_w	Wind velocity	[m/s]
$X_{b,[i]}$	Salinity of brine in the i^{th} effect	[g/kg]
X_f	Salinity of feed-water	[g/kg]
z_1	Sea level reference elevation	[m]
z_2	Arandis elevation	[m]

α	Receiver solar absorbtance	[%]
ε	Receiver thermal emittance	[%]
ε_{ps}	Roughness of the bulk water pipe surface	[m]
η_{hf}	Overall heliostat optical efficiency	[%]
η_{nc}	Nominal heliostat cleanliness	[%]
η_{pump}	Efficiency of bulk water pump	[%]
η_{rec}	Receiver efficiency	[%]
$\eta_{\rho,nom}$	Nominal heliostat reflectivity	[%]
η_{ρ}	Actual heliostat field reflectivity	[%]
θ_z	Zenith angle	[°]
ρ_{sw}	Seawater density	[kg/m^3]

Stellenbosch University https://scholar.sun.ac.za

Abbreviations

BPE	Boiling point elevation
CAPEX	Capital expenditure
CEIMAT	Centro de Investigaciones Energéticas Medioambientales y Technológicas
CF	Capacity factor
CSES	Centre for Solar Energy Studies
CSP	Concentrating solar power
DLR	Deutschen Zentrums für Luft- und Raumfahrt
DNI	Direct normal irradiance
DP	Design point
EES	Engineering equation solver
EPC	Engineering procurement and construction
FTC	Fixed tower cost
FWH	Feed-water heater
FWP	Feed-water pump
GHG	Greenhouse gas
GIS	Geographic information systems
HPT	High pressure turbine
HTF	Heat transfer fluid
IEA	International Energy Agency
ITD	Initial temperature difference

Stellenbosch University https://scholar.sun.ac.za

LCA	Life cycle assessment
LCOE	Levelized cost of energy
LCOW	Levelized cost of water
LMTD	Logarithmic mean temperature difference
LPT	Low pressure turbine
MED	Multiple effect distillation
MENA	Middle East North Africa
MES	Multiple-effect stacked
MSF	Multiple-flash distillation
NEA	Non-equilibrium allowance
NPV	Net present value
NREL	National Renewable Energy Laboratory
O&M	Operation and maintenance
PB	Power block
PR	Performance ratio
PSA	Plataforma Solar de Almería
PT	Parabolic trough
PV	Photovoltaic
RE	Renewable energy
REFIT	Renewable energy feed-in tariff
REIPPPP	Renewable energy independent power producer procurement program
RO	Reverse osmosis
RRC	Receiver reference cost

Stellenbosch University https://scholar.sun.ac.za

RSE	Receiver scaling exponent
SA	Specific area
SAM	System Advisor Model
SAPP	Southern African Power Pool
SBP	Schlaich Bergerman und Partner
SM	Solar multiple
TBT	Top brine temperature
TCSE	Tower cost scaling exponent
TDS	Total dissolved solids
TES	Thermal energy storage
TESS	Thermal energy storage systems
TMY	Typical meteorological year
TTD	Terminal temperature difference
TVC	Thermal vapour compression
UCRF	Uniform capital recovery factor
UNWWD	United Nations World Water Development
UR	Usability ratio

Stellenbosch University https://scholar.sun.ac.za

1. Introduction

1.1 Background

Electricity security is the ultimate factor responsible for any country's economic growth and prosperity. It is directly related to the main challenges that countries face globally such as: poverty mitigation, global environmental change and food and water security (Purohit, Purohit & Shekhar, 2013).

During the 2015 COP21 conference in Paris, more than 150 countries representing 90 % of global economic activity and nearly 90 % of energy-related greenhouse gas (GHG) emissions, have submitted commitments stating their goals and plans to reduce emissions by the year 2030 (International Energy Agency, 2015).This will have pronounced implications for the progressive acceptance and market security for alternative energy technologies world-wide as relevant proceeding renewable energy (RE) policies are set into place.

Energy is closely interlinked with water as almost all forms of energy require some amount of water as part of their production, generation or processing. Conversely, energy is necessary for the production, collection, treatment and delivery of water. According to the United Nations World Water Development (UNWWD) Report of 2015, an estimated 5 % to 30 % of the overall operating costs of water and wastewater utilities are attributed to electricity (UN-Water, 2015).

1.1.1 Namibia's electricity situation

The electricity demand for Namibia is relatively low. According to NamPower's annual report (Viranyi, 2015), in 2015 the country had a peak demand of approximately 656 MW. The country also imported more than 60 % of the annual electricity usage from the Southern African Power Pool (SAPP). Namibia's local electricity generation fleet consists of the following plants:

- Ruacana, 337 MW hydro plant
- Van Eck, 120 MW coal fired plant (dry-cooled)
- Anixas, 23 MW diesel fired plant
- Paratus, 12 MW diesel fired plant

The Ruacana hydropower scheme is Namibia's flagship power station providing more than 90 % of the local electricity generation (Viranyi, 2015: 62). However, being ultimately dependent on the seasonal rainfall the reliability of the hydropower

Stellenbosch University https://scholar.sun.ac.za

station is compromised. There are future prospects for the construction of the Baynes Hydropower Project 200 km downstream of the Ruacana project. The scheme aims to build one of the highest concrete faced rock dams in Africa and will have an installed generation capacity of 600 MW (NamPower, 2016a). The project is anticipated to commence in 2017 and will take six years to complete.

Initial commissioning of the Van Eck coal fired station was in 1972 and was the first power station in Africa to implement dry-cooling (NamPower, 2016b). The power station has recently (2014) undergone refurbishment in order to extend the life time of the plant and has not been running at full load since. NamPower has considered running the plant using a mixture of imported coal and "green coal". Green coal is produced by a torrefaction process of harvested invader bush (MBH Energy, 2016). Torrefaction is a thermal process that is used to convert biomass into a coal-like material that has improved fuel characteristics compared with the original biomass product (Biomass Technology Group, 2016).

The Paratus and ANIXAS diesel power stations are only used for emergency operation. Paratus was commissioned in 1976 and ANIXAS recently came into operation in late 2011 (NamPower, 2011a,b). The 800 MW Kudu Gas Project to be built close to Oranjemund has been delayed since 2009. This involves the extraction of offshore gas to be transported via 170 km underwater pipeline to the gas fired power plant. The Kudu field has proven gas reserves of 40 billion m^3 of gas and was discovered by Chevron in 1974 (Roelf, 2015). An independent power producer (IPP) bid has been awarded to Xaris Energy to build a 250 MW gas fired plant in Walvis Bay. It is a short-term contingency project to alleviate the effects of the delayed Kudu Gas Project. Ironically, the Xaris project is experiencing delays itself due to political issues (Hartman, 2016).

Despite the delays of the planned gas fired power plants, the REIPP programs in Namibia are steadily gaining momentum. A 4.5 MW photovoltaic (PV) plant built by InnoSun and a 5 MW PV plant built by HopSol Africa along with another 30 MW of IPP tenders that will be released in the near future will strengthen Namibia's solar energy generation capacity. InnoWind's 5 MW wind farm will start construction in July 2017 with future plans to construct a 500 MW farm along the southern coast of Namibia.

At the end of 2015, Namibia's power utility (NamPower) set out a tender for an impact assessment to construct Namibia's first CSP plant. The plant capacity will be between 50 MW_e and 200 MW_e and will be located close to Arandis on a site previously allocated for a coal-fired power plant (CSP Today, 2015).

Stellenbosch University https://scholar.sun.ac.za

Namibia's energy mix roadmap aims to have 70 % of its electricity generated by renewable energy sources (Sawin, Seyboth, Sverrisson & Martinot, 2016). Being a country with limited fossil fuel resources, but having an abundance of insolation resources (see Figure 1) creates a preference for the use of RE technologies over conventional electricity generation methods.

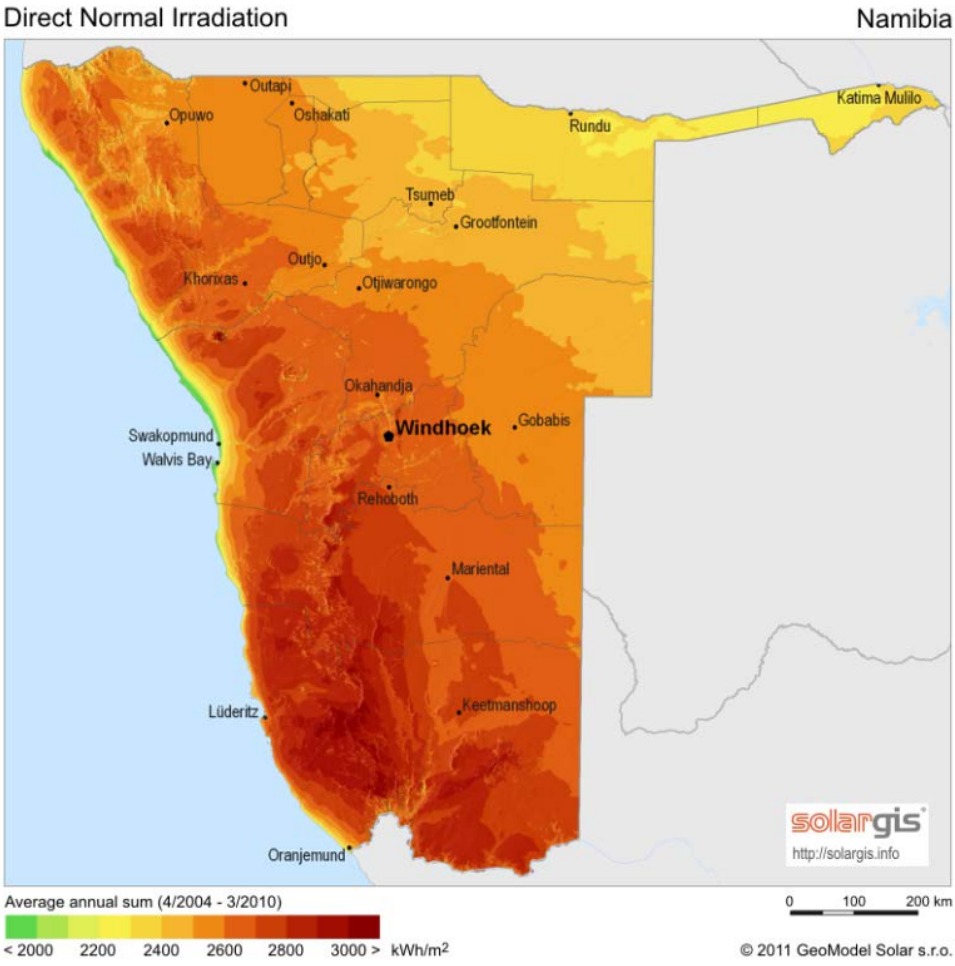

Figure 1: DNI map of Namibia, (solarGIS Geomodel Solar, 2016)

Stellenbosch University https://scholar.sun.ac.za

1.1.2 Commercial desalination technologies

Water can be defined to be fresh when it contains less than 1 g/L of salts or total dissolved solids (TDS) (Sandia, 2003). The standard for drinking water varies from country to country, however the World Health Organisation has defined a threshold for drinking water taste at 250 mg/L (WHO, 1970). The process of removing salt from water to produce potable water is known as desalination. Desalination was initially introduced as a commercial technology for use on ocean-bound ships. Thermal distillation was used to provide potable water to eliminate the risk of diminishing fresh water supplies during extended voyages (Seigal & Zelonis, 1995). Later on in the 1950's, the Middle Eastern countries were the first to utilize desalination on a large scale for the use of municipal drinking water (Greenlee *et al.*, 2009). The cumulative capacity of desalination has increased exponentially (Figure 2) and is expected to continue on the same trend as the global population expands.

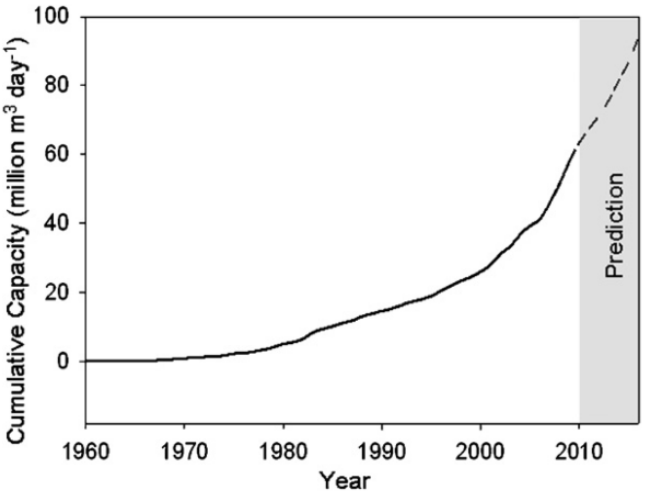

Figure 2: Global collective desalination capacity from 1960 to 2016, (Lee, Arnot & Mattia, 2011)

Reverse osmosis

Reverse osmosis (RO) is a process in which water molecules are forced through a semi-permeable membrane, leaving behind the dissolved elements in a more saline solution otherwise known as brine. RO has experienced significant advancements in the past 40 years, surpassing conventional thermal technology i.e. multi-stage flash (MSF) and becoming the current leading desalination technology. Advancements include significant membrane cost reductions (Figure 3a) as well energy recovery

Stellenbosch University https://scholar.sun.ac.za

systems (Figure 3b). Note that the low value of 2 kWh/m^3 would be the energy requirement for brackish water, 3 to 10 g/L, and that this would typically increase for the treatment of seawater, 35 to 45 g/L (Gebel, 2014: 12).

The performance of RO plants are easily affected by the feed-water quality which comprises of factors that includes turbidity, salinity and temperature (Isaka, 2012), thus making the pre-treatment of feed-water compulsory. This would increase the capital cost of the system compared to more robust thermal desalination technologies.

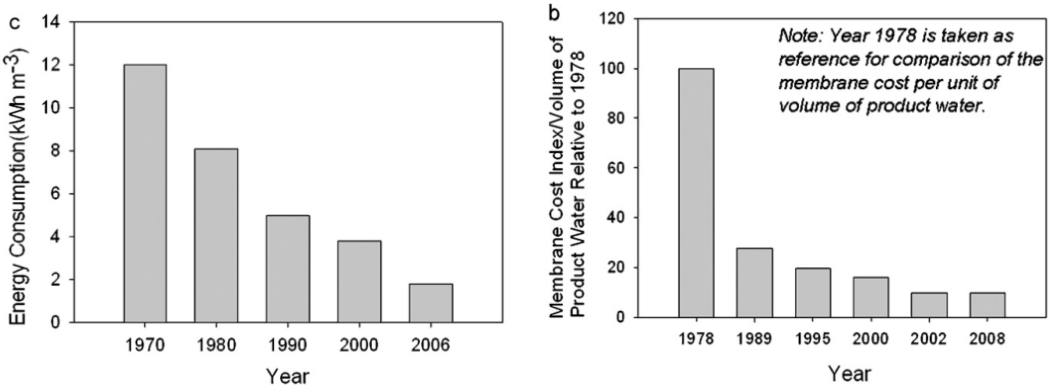

(a) (b)

Figure 3: RO (a) Reduction in energy consumption; (b) Reduction in membrane cost, (Lee *et al.*, 2011)

Multiple-effect flash (MSF) distillation

This thermal distillation process (Figure 4a) involves the evaporation and condensation of water. Incoming feed water is preheated through a series of pre-heaters, each recovering the latent heat of evaporation and coupling the evaporation and condensation stages in the plant. The feed water enters the first stage where the flash process begins and progresses with each succeeding stage operating at a slightly lower pressure.

MSF is the most established thermal desalination technology and constituted more than 54 % of the global desalination capacity in the year 2000 (El-Dessouky & Ettouney, 2002: 15). Commercial installations are designed with 10 – 30 stages with an approximate 2 °C temperature drop per stage. (Kalogirou, 1997) The number of stages in an MSF system only increases the desalination capacity and does not affect

Stellenbosch University https://scholar.sun.ac.za

the plant efficiency. Temperature requirements range from 90 °C to 110 °C and approximately requires 4 kWh/m^3 for pumping of feed-water and brine (Al-Karaghouli & Kazmerski, 2013).

Multiple-effect distillation

Multi-effect desalination (MED) is also a thermal process in which the majority of the distillate produced is by boiling accompanied by a small quantity of flashing. The distillate created in the first effect is condensed in the succeeding effect and also used for heating the incoming feed water. The temperature requirement for MED systems ranges between 100 °C and 50 °C; however, to reduce scaling ideal temperatures below 70 °C are considered ideal (Darwish, Al-Juwayhel & Abdulraheim, 2006).

The plant efficiency (specific heat requirement per m^3 distillate) is a function of the number of effects and increases as effects are added in the system. The temperature drop between effects ranges between 1.5 °C and 2.5 °C (Ophir & Lokiec, 2005; Gebel, 2014). The implementation of MED systems for cogeneration (electricity and desalinated water production) has the advantage over traditional MSF systems because of the lower temperature requirement of MED plants.

MED plant effects are typically arranged horizontally next to one another; however vertical stacked configurations can also be used to reduce the pumping requirements of the system. Figure 4b is an illustration of a multiple-effect stacked (MES) configuration. The stacked MED configuration is considered the most suitable to be used for solar energy applications due to the plant being stable in operation between nearly zero and 100 % output, even while sudden alterations in the operational load are made (Kalogirou, 1997).

Stellenbosch University https://scholar.sun.ac.za

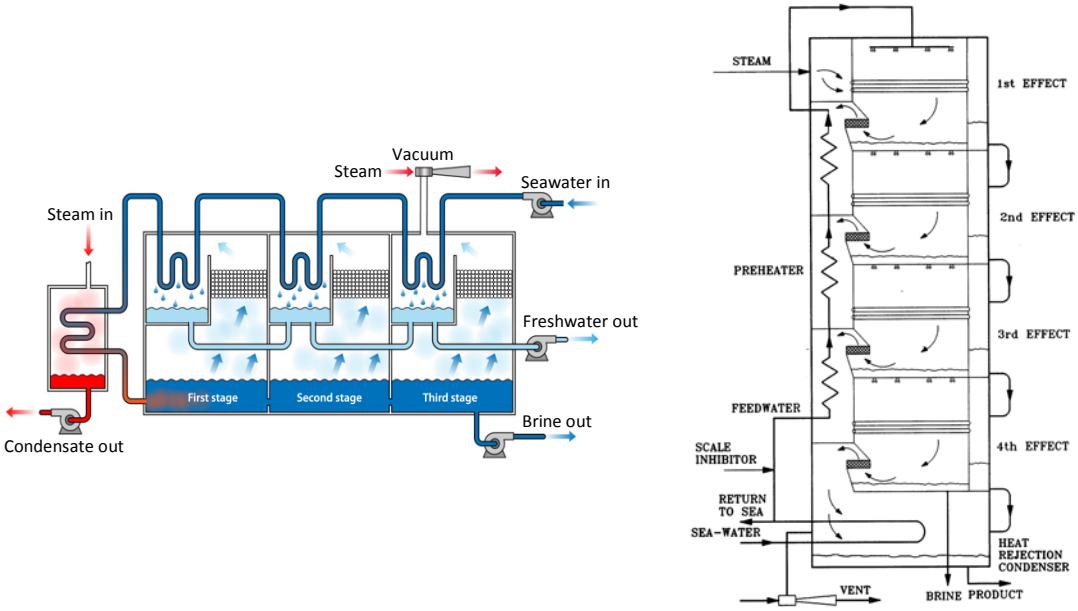

(a) (b)

Figure 4: Schematic diagram of (a) MSF system, (Al-Karaghouli & Kazmerski, 2013); (b) MES evaporator, (Kalogirou, 2005)

1.1.3 Concentrating solar power

The rapid declining prices of PV are confronting the CSP industry which has placed the focus on increasing its value through thermal energy storage systems (TESS) (Sawin *et al.*, 2016). Considering Figure 5a there has been a slowdown in the Spanish market and the United States, however the rest of the world has seen a greater expansion of CSP capacity. The world could see an exponential growth of CSP plants with the following developments due for construction:

- Egypt (2.8 GW by 2020)
- Algeria (2 GW by 2030)
- Kuwait (1.1 GW by 2030)
- Saudi Arabia (25 GW by 2025)
- China (5-10 GW by 2020)

Stellenbosch University https://scholar.sun.ac.za

Although the global installed capacity for CSP is nowhere close to that of PV (Figure 5b), the cost of CSP is expected to continue to decline as demonstrated with the competitive bidding process used in South Africa. Cogeneration of water and electricity might possibly create an additional niche market for CSP as it distinguishes itself from other RE technologies with its ability to run as base load electricity plants with the addition of TESS.

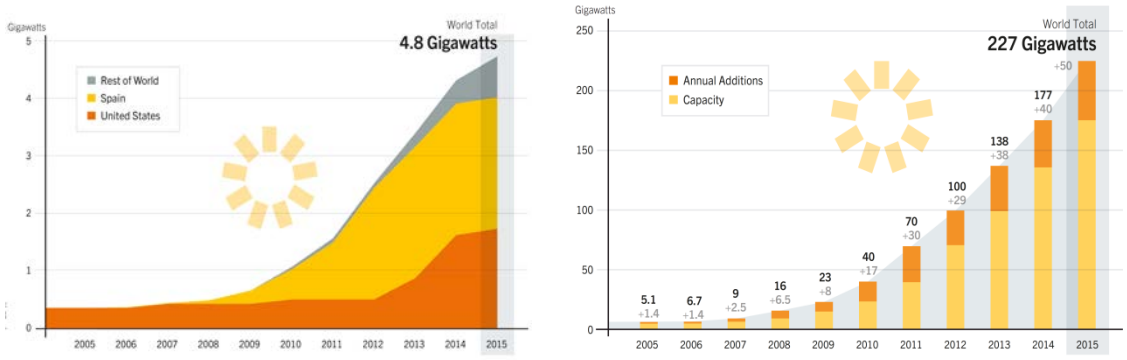

(a) (b)

Figure 5: Global capacity and annual additions of (a) CSP and (b) PV, (Sawin *et al.*, 2016)

1.2 Motivation

1.2.1 The need for desalination

The oceans make up 96.5 % of the earth's water resources and another 1 % is made up of brackish and slightly salty water situated as surface and groundwater sources. That leaves 1.7 % to be found at the polar ice caps and the remainder 0.8 % is considered available fresh water (Gleick, 1996). The demand for fresh water is a growing concern that is shared globally. Finite fresh water resources, accompanied by an exponential population growth have resulted in an increased demand for additional installed desalination plants worldwide Shannon *et al.* (2008). Current predictions state that by the 2030 the global water requirements will increase by more than 50 % (from 4500 billion m^3 to 6900 billion m^3) and if so, the current surface water resources will not be sufficient (WRC, 2009).

Desalination is extremely energy intensive with the costs thereof depending on the availability of local energy resources such as coal, oil and gas. If desalination is to be

Stellenbosch University https://scholar.sun.ac.za

a globally rapid growing technology, the exploration of alternative energy resources to desalinate water is of significant concern. Fortunately, most arid regions generally also have abundant solar energy resources that could be utilized instead of conventional fossil fuel resources.

The map in Figure 6 is a study done by Ulster University in the United Kingdom and is an attempt to identify where solar desalination is most applicable. A ranking score approach is used and includes factors such as water scarcity and stress, saline water resources and insolation levels. On the global DNI resource map in Figure 7 one can see that the regions with the highest annual DNI solar resources are situated relatively close to the western coastal areas and the Middle East and North African (MENA) region as well.

From these maps it is evident that there is a relatively big scope for CSP and desalination worldwide. The ability of CSP plants to store excess thermal energy and operate at base load level, distinguishes itself from other RE technologies such as PV and wind. The capability of running a RE driven desalination technology at base load would further decrease the levelized cost of water for a given plant life cycle. The relevance of this study is supported by the given water and electricity circumstances of Namibia and the country's target of having a 70 % share in renewable electricity generation by 2030 (Sawin *et al.*, 2016: 166).

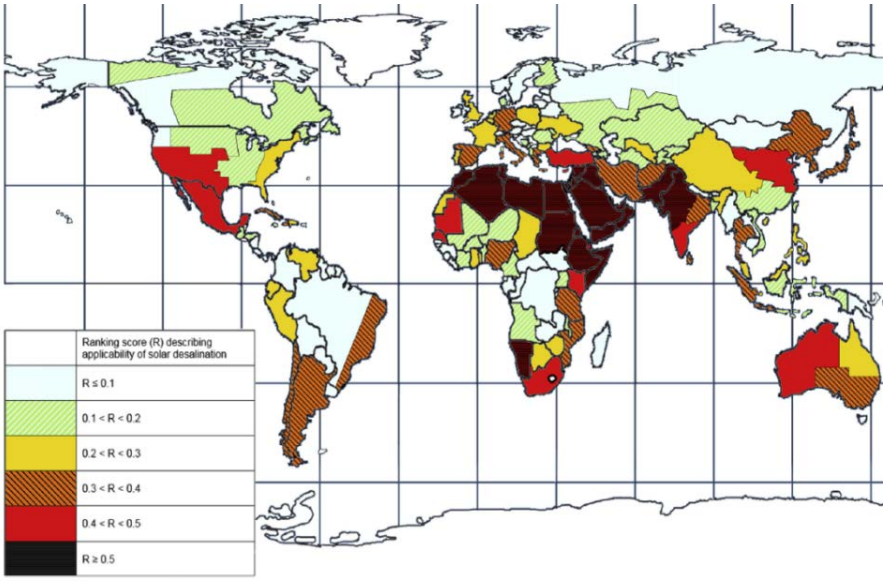

Figure 6: The global applicability of solar desalination (Pugsley, Zacharopoulos, Mondol & Smyth, 2016)

Stellenbosch University https://scholar.sun.ac.za

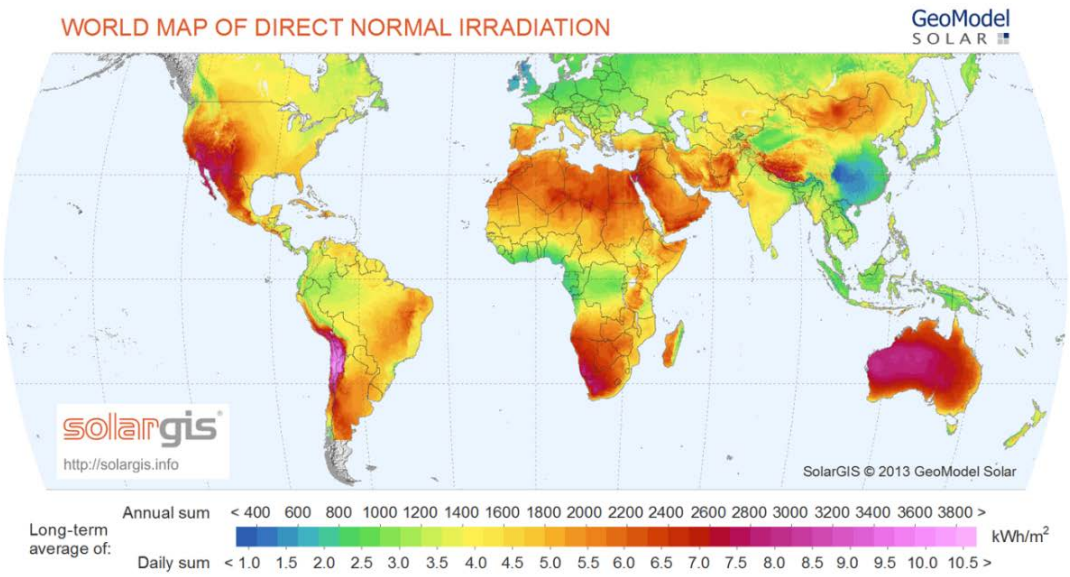

Figure 7: World map of direct normal irradiation, (SolarGIS Geomodel Solar, 2013)

1.2.2 Selection of case study

This study is done in the context of Namibia with Arandis chosen as the site location. A comprehensive pre-feasibility study for the construction of a pre-commercial CSP plant in Namibia was led by the Renewable Energy and Energy Efficiency Institute at the Polytechnic of Namibia. The study evaluated numerous sites across Namibia based on elements that include DNI, slope, water availability, grid accessibility, etc. Arandis ranked as one of the top 20 sites for CSP projects in Namibia and having the closest proximity to the coast, makes Arandis an ideal site for a CSP and desalination study. Figure 8 illustrates the locations for the top 20 CSP sites, including Arandis, in Namibia and also includes components of the current grid network. Table 1 is a summary of the geographical position of Arandis and will be used as the location for the case study.

Stellenbosch University https://scholar.sun.ac.za

Table 1: Geographical information of Arandis

Parameter	Value
Latitude	-22.4167 °
Longitude	14.9667 °
Elevation	572 m

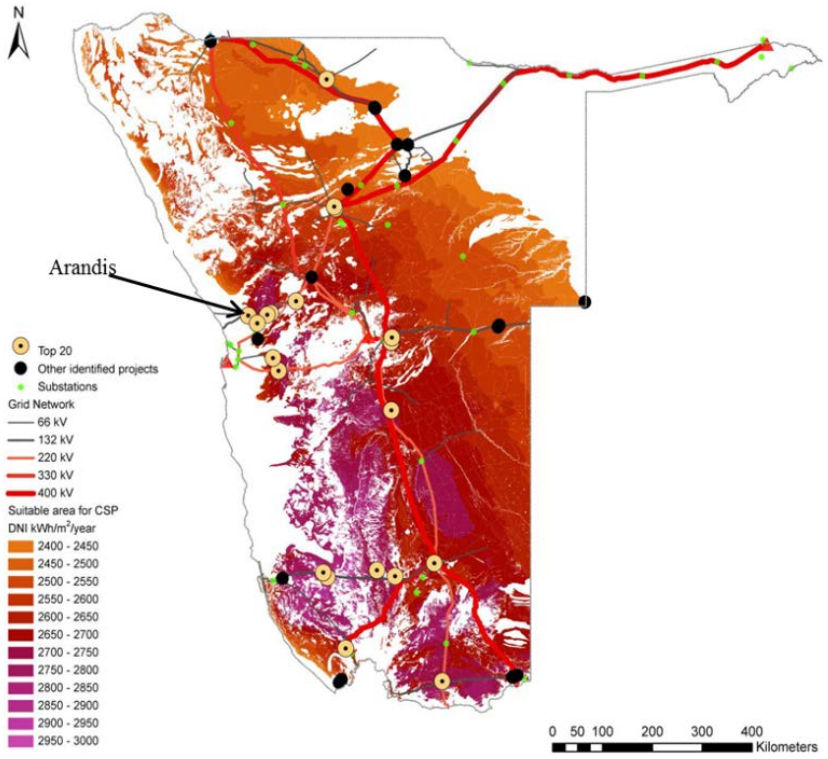

Figure 8: Top 20 ranked CSP sites in Namibia, (REEEI, 2012: 198)

Coastal communities of Walvis Bay, Swakopmund, Henties Bay, Arandis and the three Uranium mines currently use approximately 15 million cubic metres of water a year; most of which is extracted from the Omdel and Kuiseb aquifers. The UN Comprehensive Freshwater Assessment of 1997 (Pryor & Blanco, 2010) classified Namibia's water resources as stressed and moving towards vulnerable by the year 2025. The exhaustion of groundwater aquifers will almost certainly give rise to dire environmental consequences such as an increase in groundwater salinity due to

Stellenbosch University https://scholar.sun.ac.za

ingress of seawater into fresh water aquifers and lowering the water table which increases well and bore depths, leading to increased energy required for pumping. (Pugsley *et al.*, 2016)

The concern that the increased water extraction from the local aquifers could potentially result in it being permanently damaged was a key driver for desalination; hence the Trekkoppje RO plant was built. The plant was built by Areva and has the capacity to deliver 20 million m^3 of water annually. From a consumer's perspective, desalination can have negative economic implications on the mining industry as opposed to receiving water from an aquifer. The cost escalation experienced by Rössing Uranium when switching over to desalinated water in 2013 can be seen in Figure 9. In 2012 water from the Omdel aquifer cost approximately 13 N$/$m^3$ rising more than 400 % to approximately 54 N$/$m^3$ for desalinated water from Trekkoppje. What is also noted is that the water demand for the Rössing mine decreased in this period by about 20 %. Demand side management (DSM) of water resources should always be implemented to ensure the most efficient consumption of water before considering desalination as an expensive alternative.

The addition of a cogeneration plant (CSP-desalination) could increase the future security of the country's electricity and water supply. It is therefore necessary to investigate the economic feasibility of such a plant in the context of Namibia.

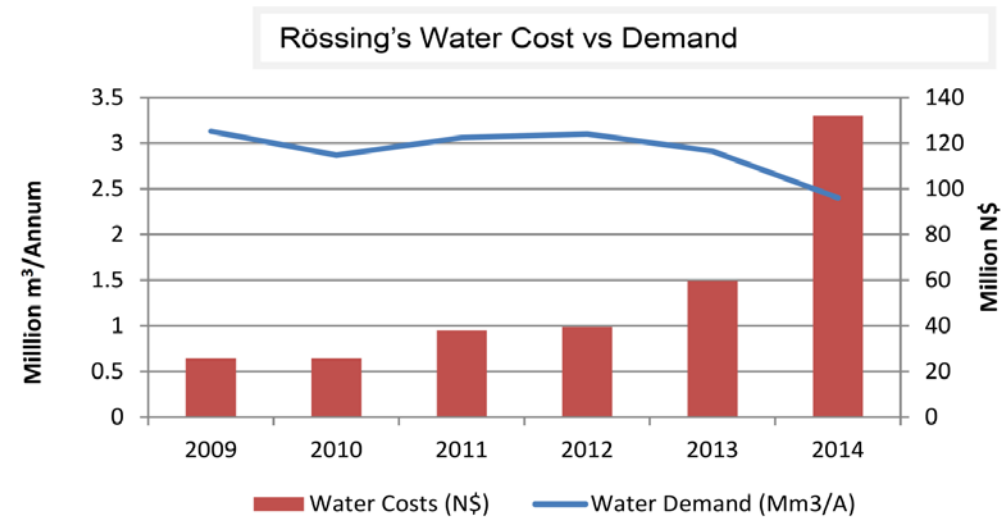

Figure 9: Rössing Uranium's water cost vs. demand (Duvenhage, 2014)

Stellenbosch University https://scholar.sun.ac.za

1.3 Research objectives

The purpose of a cogeneration plant is that the overall energy efficiency is increased by producing both useful electricity as well as useful heat for thermal desalination. Consequently, a cogeneration plant enables the same level of end-use energy demand to be met with less energy inputs (International Energy Agency, 2011). The economic implication of a cogeneration system is that the total product costs are reduced as opposed to having two separate systems, i.e. a power plant and desalination plant.

In this study a vertically stacked MED plant is integrated into the power block of a 100 MW_e central receiver plant as the primary cooling cycle. All the steam exiting the steam turbine is condensed in the first effect of the MED plant. The MED plant essentially replaces the need for a dry-cooled condenser.

The aim of this study is to:

- Investigate the economic feasibility of a large scale CSP+MED plant for the cogeneration of potable water and clean electricity
- Identify the optimal MED plant size for various condensing temperatures, also referred to as the top brine temperatures, ranging between 55 and 70 °C

1.4 Limitations of research

The main hurdle of this study is obtaining access to reliable financial inputs/data for the economic model. Regarding the cost of large scale MED desalination plants, the majority of data available in the literature is generally high-level costing data, i.e. presenting the cost of MED as \$/m^3/day installed capacity. Not having access to the detailed cost breakdown presents difficulties with the physical sizing of the MED plant. This issue is dealt with using Hall's equation and is discussed in the Economics chapter.

The CSP+MED cogeneration model involves numerous sub model components. To avoid from straying into too many different aspects of the cogeneration system, the focus of this work has been set on the modelling of a vertically stacked MED plant with sufficient detail in order to capture the sensitivities of parameters that are significant in cogeneration system analysis. Handling and disposal of the reject brine and excess cooling water is not taken into account. The construction of reservoirs or salt pans would increase the project capital cost; however the salt could also be an added by-product and would then add value to the system.

Stellenbosch University https://scholar.sun.ac.za

2. Literature review

2.1 Introduction

In this chapter an overview is given of some planned cogeneration systems involving CSP and MED desalination. As of yet, no large scale cogeneration CSP+MED plant that produces electricity and desalinates water has been built. Therefore most of the available data regarding this topic is in the form of theoretical case studies which are also discussed. A simplified approach for the modelling of a central receiver plant is investigated and compared with a benchmark software package (SAM) in order to identify the impact that certain simplifications might have on the model accuracy. Finally a brief review is done on various MED modelling approaches in which the most suitable approach for the purpose of this study is selected.

2.2 CSP desalination projects

2.2.1 Libya

In the near future, a large demand for water desalination is anticipated in Libya. Confident that solar powered systems could be a solution for this scenario, the Libyan government has signed a cooperation agreement with Solar Power Group in collaboration with MAN for the construction of 3000 MW_e of solar thermal power plants within the next decade. A preliminary pilot plant will be built at the Centre for Solar Energy Studies (CSES) near Tripoli and will consist of a 15 MW_e Fresnel CSP plant and a MED plant with an installed capacity of 700 m^3/h (German Aerospace Center (DLR), 2007).

2.2.2 Republic of Yemen

The City of Sana'a is the capital of Yemen and is one of the oldest continuously inhabited cities in the world. Other than harnessing rainwater, the city's main water supply comes from a ground water basin with a current reserve of 2 to 3 billion m^3. The annual extraction of 260 million m^3 per year with a recharge rate of 52 million m^3 per year leads to the likelihood that the basin would be depleted between the years 2015 and 2020.

Stellenbosch University https://scholar.sun.ac.za

The country's fossil fuel reserves are not considered to be sufficient in a long term scenario, therefore solar desalination via CSP is perceived to be the solution providing long-term security. The project proposal is that seawater from the Red Sea is desalinated near the coastal city of Hudaidah. The desalinated water would then be transported over a distance of 250 km at an elevation of 2700 m inland to the City of Sana'a. The Sana's Solar Water Project consists of the following components (German Aerospace Center (DLR), 2007):

- CSP plant capacity of 1250 MW_e
- Multiple-effect desalination capacity of 700 million m^3/year
- Reverse osmosis desalination capacity of 300 million m^3/year
- Steel pipeline of 250 km length and 3000 mm diameter

2.3 Co-generation studies

2.3.1 CSP+MED vs. CSP+RO (CEIMAT-PSA)

Palenzuela *et al.* (2015) did a techno-economic analysis on the integration of desalination with a 50 MW_e parabolic trough CSP plant in the Mediterranean and MENA region. The aim of the study was to find the most suitable CSP+D configuration for the respective regions by evaluating the thermodynamic and economic plant performance. The study concluded that the integration of a MED into a CSP plant is the most efficient choice for both locations. Four different integrations were evaluated with more detail of this study summarised in the CSP+MED vs. CSP+RO (CEIMAT-PSA) appendix.

2.3.2 CSP+MED vs. CSP+RO (DLR)

A study done by (Moser, Trieb & Fichter, 2013), from the German Aerospace Agency (DLR), investigated long-term scenarios for the demand of water and electricity which are based on the potential integration of desalination with CSP. The two main desalination technologies considered is reverse osmosis (RO) and multiple-effect distillation (MED). A parabolic trough with synthetic oil is the reference CSP technology choice as the study found it to be the most mature technology and represented about 88 % of the global installed CSP capacity at the time. The study found MED to be the cheaper option in the Arabian Gulf due to its robust behaviour against higher seawater salinity and temperature. Additional details regarding the methodology and results of this study can be found in A.1 Cogeneration studies appendix.

Stellenbosch University https://scholar.sun.ac.za

2.3.3 Solar desalination in Chile

A theoretical case study in Northern Chile was done on the synergies of solar power and desalination by (Servert, Cerrajero & Fuentealba, 2016). The study investigated the feasibility of two solar desalination alternatives (PV+RO and CSP+MED) compared to the conventional grid connected RO plant solution. The case study scenario involved desalinating seawater to be used for the mining industry located 100 km from the coast and 2200 m above sea level (Figure 10). The levelized cost of water (LCOW) was used as an indicator to compare the feasibility of the investigated configurations and was calculated for plant lifetime scenarios of 10, 15, 20 and 25 years using a real discount rate of 12%. The study determined that solar desalination in the Atacama Desert in Chile could technically be feasible with MED + CSP being the most favourable option. The details of this study can be found in the A.1 Cogeneration studies appendix.

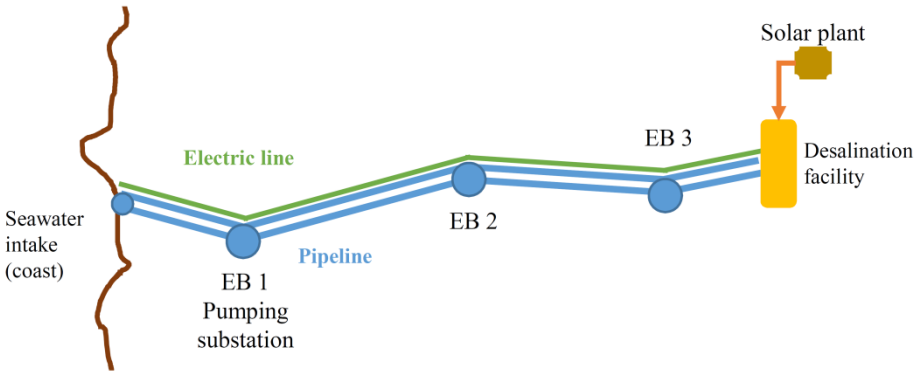

Figure 10: Schematic depiction of the seawater pumping process, (Servert *et al.*, 2016)

2.3.4 Central receiver and MED

A thermal analysis study was done by (Frantz & Seifert, 2015) that investigated the theoretical performance of an MED desalination plant integrated into a 3 MW_e solar tower CSP plant. Al-Kosseir in Egypt was the location of choice for the case study with the aim of illustrating the trade-off between electricity and water production in such a cogeneration plant. This study demonstrates the trade-off dynamics between the production of electricity and desalinated water in a cogeneration CSP+D plant. Detailed results of this study can be found in the A.1 Cogeneration studies appendix. CSP+MED cogeneration pilot plant (Cyprus)

Stellenbosch University https://scholar.sun.ac.za

At the Cyprus Institute's Pentakomo Field Facility, the first phase of a small scale CSP+MED pilot plant has recently came into operation (Papanicolas *et al.* 2015). The current setup drives a 15 kW steam turbine integrated with a 4 effect MED plant with a rated capacity of 2 m^3 per day. The system also incorporates a single molten salt storage tank with a thermal capacity of 0.6 MWh. The second phase of the project would increase the plant capacity from 2 MW to 8 MW to increase the maturity and confidence of such a cogeneration setup.

2.3.5 CSP+MED+RO cogeneration (Cyprus Institute)

A Cyprus case study done by (Ghobeity *et al*, 2011) in which time-invariant conditions of a summers day are presented. Existing RO and MED models from the literature are amended and incorporated in the study. A validated steam cycle is used which permits the optimization over a wide range of steam extraction scenarios. The study concluded that for the 4 MW_e capacity of the CSP plant, RO is the preferred desalination technology over MED from an energy efficiency perspective. Nonetheless, when current (at the time of the study) rates for electricity and water in Cyprus are used then extracting steam at low pressures for MED generates the maximum income. Additionally the study suggests that for given circumstances such as Cyprus in which the electricity to water price ratio ranges from 6 to 10; that cogeneration with MED is favourable over only electricity production.

2.4 Central receiver system modelling

Predicting the performance of a CSP system is an intricate process. It involves numerous subsystems whose performance are time dependent on the instantaneous conditions of the entire system, as well as the recent history of its operation (AUSTELA, 2016). Modelling a central receiver plant can be done in extensive detail considering all of the system's key comprising components i.e. the heliostat field, receiver, storage, power block etc. System Advisor Model (SAM) is a freeware program that is used to simulate, design and evaluate the performance and economics of CSP systems. SAM has become an international "benchmark" for high level analyses of CSP system performance studies (AUSTELA, 2013). The software was developed by the National Renewable Energy Agency (NREL) in collaboration with SANDIA National Laboratories and is intended to facilitate decision making for individuals in the renewable energy industry. In this section alternative methods for modelling the subcomponents of central receiver systems are investigated and compared to that used in SAM.

Stellenbosch University https://scholar.sun.ac.za

2.4.1 Heliostat field efficiency

The heliostat field geometry used in SAM is of the radial staggered type (Figure 11b), but can be altered using the SolarPILOT^{TM} software also developed by NREL. Various algorithms can be used within SAM to optimize the heliostat field with respect to the tower height, receiver height and the receiver height to diameter ratio. A simplified method that provides near instantaneous results is suggested by (Gauché, Backström & Brent, 2011) in which the heliostat field efficiency is approximated to be a function of the zenith angle. The method is based on a cornfield layout illustrated in Figure 11b and considers only the cosine, shading and blocking losses of the field. The results of this study is compared to the results of eSolar's pilot plant (Schell, 2011) and demonstrates a good agreement with the simulated and measured plant data.

The method proposed by Gauché *et al*. demonstrates acceptable accuracy for smaller plants like eSolar's Sierra SunTower plant, however further validation is required for other heliostat field variants and sizes. Therefore a simple comparison with SAM was done using the solar data from Daggett, California. Heliostat field sizes were arbitrarily chosen (SM's of 1, 2, 3 and 4) and compared with Gauché *et al.*'s correlation as illustrated in Figure 12. Considering the annual field efficiency, the approximation seems to correlate the best at a SM of 3 and the worst at a SM of 4. In Appendix A.2 Central receiver plant modelling, the hourly field efficiency of each SM case is compared to Gauché *et al.*'s approximation on each solstice and equinox. In Figure 64 to Figure 67, the significant adverse effects due to cosine losses can easily be seen and is not captured by the simplified approximation of Gauché *et al*.

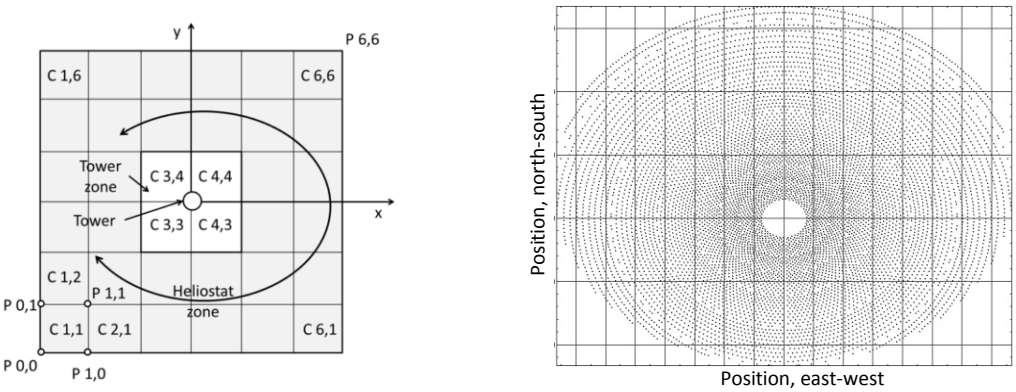

(a) (b)

Figure 11: Heliostat field layouts (a) cornfield and (b) radial staggered layout, (Gauché *et al.*, 2011; NREL, 2015)

Stellenbosch University https://scholar.sun.ac.za

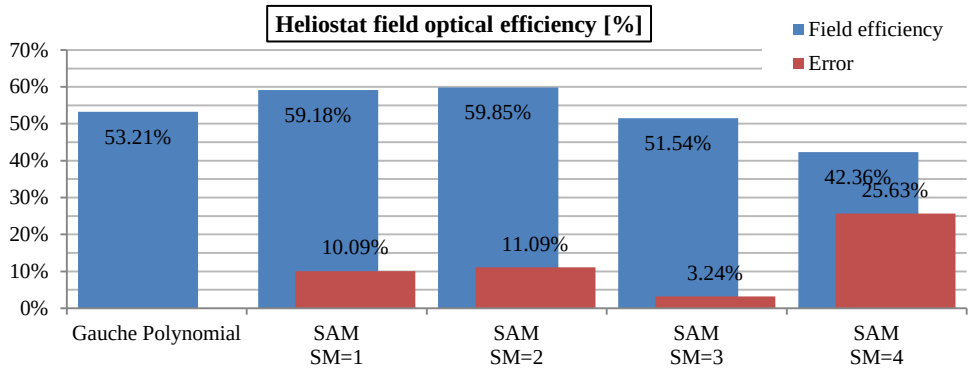

Figure 12: Annual field optical efficiency comparison

2.4.2 Receiver

There has been a great deal of development in various receiver designs involving various heat transfer fluids for external and cavity receivers to falling film receivers using fluidized sand particles. Figure 13a shows the external receiver of the Gemma Solar plant by Torresol in Spain and the unique cavity receiver design in Figure 13b of the Khi Solar One plant by Abengoa in South Africa. Cavity receivers generally have lower radiation heat loss, but more convective losses than external receivers (Ho & Iverson, 2014). An experimental study by (Bergan, 1986) suggests that external receivers have higher overall efficiencies, but external receivers have the advantage of quicker start-ups.

The main issue of modelling cavity receivers is calculating the natural convection heat losses by performing intricate CFD analyses (Samanes, García-Barberena & Zaversky, 2015). Due to the complex geometry of a cavity receiver, it is challenging to derive a simplified model to approximate the receiver efficiency. Conversely, the losses of an external receiver can be approximated with relative accuracy by the simple energy equation (6), which is discussed in the Central receiver plant model chapter in more detail.

Stellenbosch University https://scholar.sun.ac.za

(a) (b)

Figure 13: (a) Gemma Solar external receiver and (b) Khi Solar One cavity receiver, (Torresol Energy, 2010; ABENGOA SOLAR, 2016)

2.4.3 Rankine cycle

The aim of the power cycle in SAM is to characterise the off-design performance of the power block as accurate as possible while providing sufficient flexibility to handle typical Rankine cycle designs. The power block model in SAM is based on a detailed process model of a characteristic 10 MW_e steam Rankine cycle that is developed in Engineering Equation Solver (EES). The output of this model is converted into an off-design response surface and uses a statistical method to characterise relationships between variables. This regression model approach captures the effect of the heat transfer fluid (HTF) inlet temperature, condenser pressure and the HTF mass flow rate on the power output and heat input (Michael J. & Gilman, 2011).

The integration of a thermal desalination plant into the power block is an important aspect of this study and therefore a regression model would not suffice when accurate steam conditions at the outlet of the low pressure turbine (LPT) is required. Modelling a semi-detailed Rankine cycle in EES and incorporating the efficiency and steam mass flow rate outputs into the CSP+MED model would be the most accurate alternative to SAM and is discussed in more detail in the Central receiver plant model chapter.

Stellenbosch University https://scholar.sun.ac.za

2.5 MED modelling

Various approaches have been made in the modelling of multiple-effect distillation systems, some simpler than others based on different assumptions. What is clear from the models discussed in this section is that the intended use of each model is different. Some are intended for high level optimization like Mistry *et al.*, while the detailed model from El-Dessouky is beneficial for the analyses of a specific MED plant configuration.

2.5.1 El-Sayed and Silver

A simple model for a forward-feed MED system with flash evaporation was developed by (El-Sayed & Silver, 1980). The following assumptions are made:

- Fluid properties are constant i.e. latent heat, specific heat and boiling point elevation
- Fluids are considered an ideal solution
- Friction pressure drop modelled based on a mean saturation temperature drop increased by the effect of the BPE

Using the listed assumptions, Equation (1) is derived to explicitly solve for the performance ratio (PR) of the system, where $h_{fg,S}$ is the enthalpy of vaporization of steam, n the number of effects, m_f and m_D are the mass flow rates of the feed-water and the distillate, TTD_{fh} is the terminal temperature difference of the feed heater, ϵ is the sum of the BPE and temperature change due to loss of pressure and ΔT_e the temperature difference between two effects.

This approach is very simple and is suitable for swift performance ratio approximations and heat transfer areas for a forward feed (FF) MED system at known operating conditions. The limitation to this approach is that detailed information about the mass and energy streams cannot be assessed in order to analyse the system and perform sensitivity analyses. The PR is given by:

$$PR = \frac{h_{fg,S}}{\frac{h_{fg}}{n} + \frac{m_f}{m_D} c(TTD_{fh} + \epsilon) + \frac{n-1}{2n} c\Delta T_e} \quad (1)$$

Stellenbosch University https://scholar.sun.ac.za

2.5.2 Darwish *et al*.

Darwish *et al*. (2006) also developed a simplified correlation, Equation (2), that is used to approximate the performance ratio of a FF MED system by assuming the following:

- Equal amounts of vapour is generated by boiling in all effects except the first
- BPE is equal for all effects
- Equal temperature rise of feed-water in feed heaters
- The BPE equals the temperature rise in each feed heater
- Constant specific heat
- Constant latent heat

where m_D, m_S and $m_F$are the mass flow rates of the distillate, steam and feed-water, n is the number of effects, TTD_{fh} the terminal temperature difference between the first effect and the feed at the exit of the last feed heater and h_{fg} the latent heat.

$$PR=\frac{m_D}{m_S}=\frac{n}{1+n\frac{m_F c(TTD_{fh})}{m_D h_{fg}}} \quad (2)$$

2.5.3 El-Dessouky and Ettouney Basic Model

A simplified mathematical model is presented by (El-Dessouky & Ettouney, 2002). It involves only the brine and distillate flow rates, brine salinity, temperatures and heat transfer area. Mass and energy balances for the flash boxes and preheaters are excluded in the model. The following assumptions are made:

- Feed-water enters the first effect at the saturation temperature of the effect
- Constant specific heat
- Thermodynamic losses are constant across all effects
- No flashing of vapour occurs in effects
- Produced vapour has no salinity concentration
- Equal thermal loads in all effects
- Driving temperature difference in effects are equal to difference in condensation and evaporation temperatures
- Energy losses to environment is negligible

This simplified model shares more detail than that of El-Sayed and Silver as well as Darwish *et al*.; however it still does not fully capture the dynamics of practical plants

Stellenbosch University https://scholar.sun.ac.za

due the assumptions listed above. It does provide a rudimentary understanding of the MED process.

2.5.4 El-Dessouky and Ettouney detailed model

A more detailed model is presented by (El-Dessouky, Alatiqi, Bingulac & Ettouney, 1998) which builds up on the basic model and includes the preheaters and flash boxes. The following assumptions are made in their methodology:

- Constant heat transfer areas for evaporators in all effects
- Constant heat transfer areas for preheaters in all effects
- Accounts for vapour leak in the venting system
- Considers variation in thermodynamic losses from one effect to another
- Physical properties are a function of salinity and temperature
- Account for the influence of non-condensable gasses on the heat transfer coefficients and pressure losses

This model suggests that the top brine temperature has a significant effect on the required heat transfer area. The main advantage of this model compared to the abovementioned methods is the calculation of the overall heat transfer coefficients in each process from fundamental principles. However, being composed of a set of highly non-linear equations the use of a numerical procedure is required to solve the system which becomes computationally expensive when optimising MED systems. Using regression, correlations are derived for the overall heat transfer coefficients, specific area, cooling water and performance ratio which become useful for optimization studies of MED systems.

2.5.5 Mistry *et al*.

An improved model is presented by Mistry *et al*. (2012) and suggests to provide a more accurate depiction of the MED process by relying on fewer assumptions and simplifications. The following approximations are made:

- Steady-state operation
- Distillate contains no salt
- Exchanger area in effects are just large enough to condense vapour to saturated fluid condition
- Seawater properties are functions of salinity and temperature only
- Energy losses to environment are negligible
- Non-equilibrium allowance (NEA) is negligible

Stellenbosch University https://scholar.sun.ac.za

- Liquid brine leaves each effect at the temperature of that effect
- Distillate vapour is slightly superheated by the BPE
- Overall heat transfer coefficient is averaged of the length of an exchanger
- Overall heat transfer coefficient in each effect and preheater is a function of temperature only

This model distinguishes itself from other modelling approaches that require computationally expensive iterative solution algorithms and uses simultaneous equation software packages i.e. Engineering Equation Solver (EES) or JACOBIAN. Parametric analyses of various outputs such as the performance ratio, specific area and recovery ratio shows good agreement with the other models reviewed in the literature. A comparison of the MED system performance is illustrated in Figure 68 and Figure 69 in the A.3 MED model comparisons appendix.

2.6 Heat transfer

There are numerous correlations available for the overall heat transfer coefficient of condensers and evaporators. A review of these correlations have been presented by (El-Dessouky & Ettouney, 2002: 596) with a comparison illustrated in Figure 14. Most of these correlations are given in Appendix A.4 Heat transfer coefficient correlations. The fouling correlations from (El-Dessouky *et al.*, 1998) are used in the MED modelling methodology of Mistry *et al*. and considering Figure 14 they appear to be the most conservative.

Stellenbosch University https://scholar.sun.ac.za

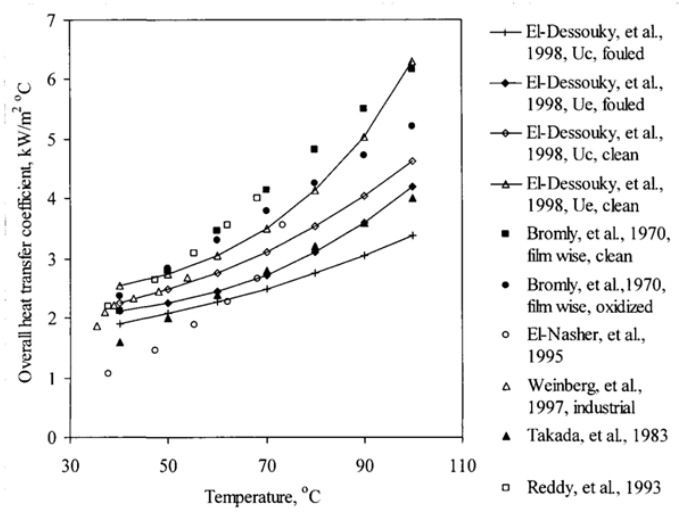

Figure 14: Variations in overall heat transfer coefficient predicted by various correlations as a function of temperature, (El-Dessouky & Ettouney, 2002)

2.7 Summary

In the study done by CEIMAT-PSA, the site locations are relatively low above sea level (150 m), but the 60 km distance from the coastline would still contribute to additional pumping requirements, making the CSP+MED plant configurations less competitive. However, the study still suggests that CSP+MED is more attractive than RO, but not by far and could have had a different outcome if the elevation were higher.

The site selection criteria of the study done by the DLR involve much lower elevations (< 20 m) and closer proximities to the coast. In terms of LCOE, the CSP+RO only outperformed the CSP+MED plant when once-through cooling was used, but not in the case of dry-cooling. In the MENA region, using a hybrid mode to run the plant at base load makes sense, because of the availability of cheap fossil fuels.

The study done in Chile highlights that currently, the cheapest option for desalination is still probably RO and the grid. However, it also illustrates the advantage that CSP has over other RE technologies in terms of storage. The RO+PV configuration was significantly more expensive (LCOW) than the CSP+MED option, because the latter had greater plant availability. The configurations in these studies do not focus on the production of a large amount of excess electricity.

Stellenbosch University https://scholar.sun.ac.za

The thermal analysis study done with the central receiver and MED plant outlines the importance that the TBT has on the sizing of a CSP+MED plant. The study suggests that increasing the TBT leads to much higher yields in water production while the electricity production is reduced by only a small amount. Still, it is difficult to compare units of water with units of electricity. Only when adding economic value to these products within the context of Namibia, a sensible comparison can be made in terms of revenue gained and whether such a project would make economic sense.

SAM's method of using a regression method to predict the PB performance is sufficient when CSP-only analyses are done. However, integrating a desalination plant into the PB as a condenser is a crucial component of this study and therefore it is suggested that a semi-detailed Rankine cycle be modelled for this study. Using the approach of Gauché *et al.* significantly reduces the computational time when calculating the hourly heliostat field efficiency. Large differences occur between this method and SAM at SM's higher than 3. This is an issue that occurs because of attenuation losses that are not captured by Gauché *et al.*'s polynomial and should therefore only be used for high-level studies such as this one.

The MED modelling approach of Mistry *et al.* provides more detail than the other existing models from the literature i.e. El-Sayed, Darwish, El-Dessouky basic and detailed. An added advantage is the use of a simultaneous equation solver (EES) that avoids the requirement for additional algorithms for solving the system and consequently reduces computational time. This model meets the requirement for high-level cogeneration system design; however the transient operation is not captured by this model. It also assumes heat transfer coefficients derived from empirical methods and when considering a more specific configuration, it is suggested that more modelling detail would be required regarding each effects heat transfer and pressure losses.

Stellenbosch University https://scholar.sun.ac.za

3. Methodology

The purpose of this study is to gain a better understanding of the economic and performance implications of a large scale CSP and MED (CSP+MED) cogeneration system. This chapter sheds light on the approach that is followed in modelling and analysing the CSP+MED cogeneration system. A sensitivity analysis is done on a CSP+MED system with the focus on varying the TBT of the MED plant. The LCOE and LCOW values will be the main performance metrics used to evaluate each system scenario. Additionally, the pumping requirements of each system can be compared to the existing Trekkoppje RO plant.

3.1 Case study setup

Five CSP+MED scenarios are investigated in which the top brine temperature (55 °C to 85 °C) is altered in each case with a step size of 7.5 °C. Therefore in each configuration, a MED desalination plant is integrated into the power block of the 100 MW_e CSP (central receiver) plant. The MED plant acts as the condenser for the power block as opposed to conventional wet or dry-cooling. Seawater is pumped 50 km inland to the CSP site in Arandis where it is desalinated via the MED plant. A schematic of the CSP+MED plant configuration is shown in Figure 15.

In order to compare the impact of a CSP+MED system on the LCOE, a dry-cooled plant (sixth configuration) is also modelled in the same location and serves as the reference plant. The conventional approach would be to have a reverse osmosis plant at the coast that is powered by an independent CSP plant located further inland. The modelling of a RO plant is beyond the scope of this study, but the electricity requirements of the existing Trekkoppje RO plant (4.1 to 4.5 kWh/m^3) is known (Pryor & Blanco, 2010). Therefore the electricity consumption of the MED vs. RO plants could therefore be compared.

Stellenbosch University https://scholar.sun.ac.za

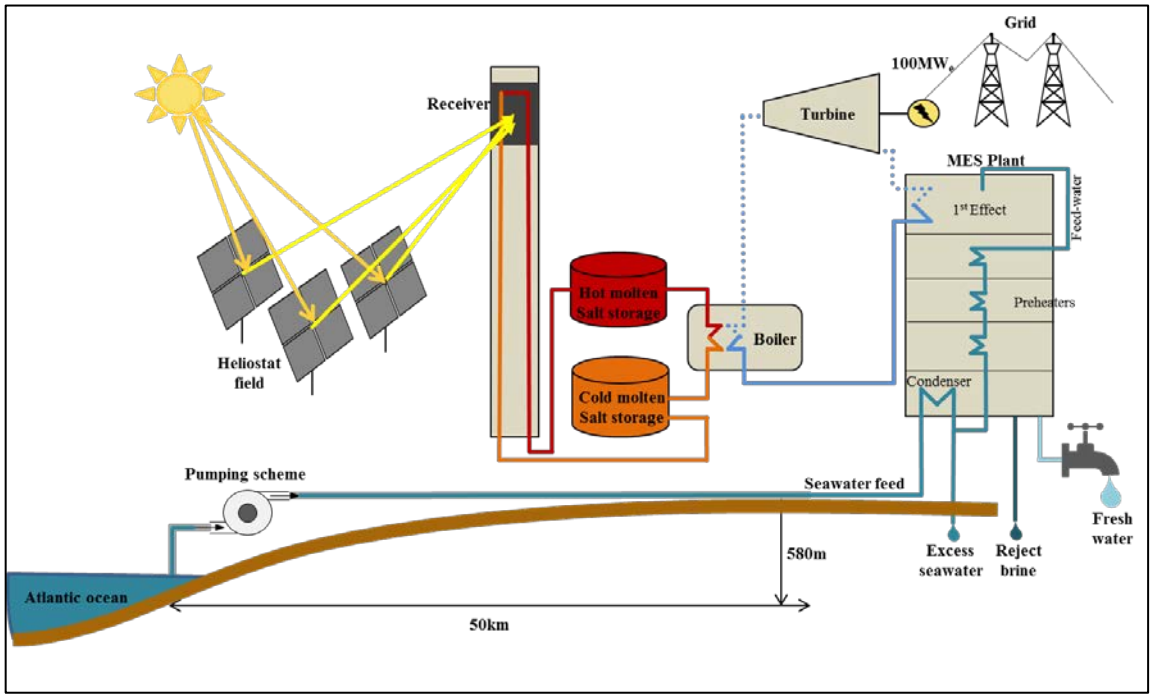

Figure 15: Arandis CSP+MED cogeneration plant schematic

3.2 Design point conditions

The reference design point (DP) conditions used for optimizing the CSP plant models is chosen to be at the autumnal equinox at solar noon conditions. Therefore the weather data used is for the DP conditions are taken at 11:30 am on the 20th March and summarised in Table 2.

Table 2: CSP reference design point conditions

Design point parameter	Value
Zenith angle	22.95°
DNI	827 kWh/m^2
Dry-bulb temperature	34.9 ℃
Wind speed	2.9 m/s

Stellenbosch University https://scholar.sun.ac.za

3.3 Technology selection

As MED desalination requires lower operating temperatures than the MSF (70 °C vs. 120 °C), it can be considered to be more thermodynamically efficient, especially when integrated into a cogeneration plant as it would impose a lower electricity production penalty on the power generation system. The multiple-effect stacked (MES) configuration is an alternative arrangement of the MED process with effects stacked on top of one another. The advantage of MES is that the auxiliary pumping requirements are significantly reduced. Also, the plant can operate under transient conditions with the capability to follow a fluctuating steam supply making it the most suitable desalination technology for solar energy applications (Kalogirou, 2005).

A central receiver configuration is chosen as it is currently the most mature commercial CSP technology that is able to produce electricity using molten salt as the heat transfer fluid (HTF). Using molten salt enables the plant cycle to reach much higher temperatures than most other commercial HTF's (such as thermal oil) and consequently increases the power plant efficiency.

3.4 Cogeneration plant modelling

The CSP+MED cogeneration system is modelled segmentally, using output values of a subsequent model as the input values of a succeeding model. The main subdivisions are as follows:

- The Rankine cycle
- CSP plant components (heliostat field, receiver and storage)
- Stacked MED plant
- Seawater pipeline
- Economics (LCOE and LCOW)

The main difference between each CSP+MED configuration is the specified TBT. Therefore after specifying the TBT of a given configuration, the following procedure is performed:

1. The bleeding pressure locations of the feed water heaters (FWH) and the pressure outlet of the high pressure turbine (HPT) is optimized to yield the maximum Rankine cycle efficiency. The required heat input (Q_{PB}) for the power block and the available saturated steam mass flow rate exiting the low pressure turbine (M_{MES}) are calculated as output parameters

Stellenbosch University https://scholar.sun.ac.za

2. The heat input Q_{PB} is used in the CSP model in order to determine the heliostat field aperture area equating to a solar multiple (SM) value of 1 at the design point conditions
3. A parametric study is performed in order to size the SM and the thermal hours of storage (TES) in order to produce the minimum LCOE value
4. The saturated steam mass flow rate (M_S) from the Rankine cycle and the LCOE value from the CSP plant are used as input parameters in the MES model.
5. A parametric study is done to arrive at the optimal MES plant size by varying the number of effects used to determine the minimum LCOW value. Additionally, the bulk seawater pipeline diameter is determined using the total seawater mass flow rate required for the MES plant based on the design mean velocity in the pipeline

3.5 Cost distribution

The CSP+MED cogeneration plant is one integrated system, but produces two products namely electricity and potable water. In order to size the system optimally, it is necessary to predefine how the costs of the cogeneration plant are distributed between the electricity and water subsystems. In the economics model, the cogeneration system is seen as two separate plants, i.e. a CSP plant producing electricity and a MED plant producing potable water. A simplified method is used to calculate the LCOE and LCOW values involving the installed capital costs (CAPEX), the operational and maintenance costs (O&M) and the plant life cycle.

The economics of the CSP plant model is similar to the method used in the National Renewable Energy Laboratory's (NREL) System Advisor Model (SAM) software. The LCOE is primarily influenced by the cycle efficiency of each configuration which in turn is dependent on the TBT.

The MES capital costs include the costs of building the bulk water pipeline. Revenue is excluded in this study; therefore the electricity consumed by the MES plant auxiliaries along with the pumping of the seawater is purchased by the CSP plant at the LCOE price.

Currently, Namibia does not have approved tariffs for electricity produced by CSP plants and therefore revenue could not be calculated in this study. It is anticipated that the tariffs and tariff structures for electricity and water from such a cogeneration plant would significantly influence the sizing of the plant in terms of SM, TES and the number of effects of the MES plant.

Stellenbosch University https://scholar.sun.ac.za

4. Central receiver plant model

4.1 Introduction

The modelling of the CSP tower plant is simplified in order to reduce the computational time, but provides sufficient detail of the plant performance in an hourly resolution over the span of a year. The simplified model should ideally deliver results that are reasonably accurate and comparable to SAM. The focus of the CSP model is set on the optical to thermal conversion of energy.

The following simplifications/ assumptions have been made in the CSP model:

- Steady-state operation
- Start-up times for the receiver and power block are accounted for by "dumping" the first hour of the day's electricity production
- Cosine, blocking and shading losses are approximated using a function dependent on the zenith angle
- Parasitics are excluded (HTF pumping, heliostat tracking, heat tracing, etc.)
- Attenuation losses are excluded

4.2 Solar resource data

At the time of this study, no hourly ground measured weather data for Arandis in Namibia was available. Hourly satellite derived data was made available by GeoSUN^{TM} Africa for the year period starting from 1 November 2014 to 31 October 2015. The climData SolarGIS hourly time series includes the following parameters:

- Direct normal irradiance
- Sun elevation angle
- Sun azimuth angle
- Dry-bulb temperature
- Wind velocity

Stellenbosch University https://scholar.sun.ac.za

4.3 Heliostat field

The heliostat field is modelled at a macro level. The field is considered to be a single aperture area with its optical efficiency being a function of the solar zenith angle (Gauché *et al.*, 2011). The heliostat field optical efficiency is characterized by the following polynomial and only represents the cosine, blocking and shading losses:

$$\eta_{opt} = 0.4254\theta_z^6 - 1.148\theta_z^5 + 0.3507\theta_z^4 + 0.755\theta_z^3 - 0.5918\theta_z^2 + 0.0816\theta_z + 0.832 \quad (3)$$

In addition the losses caused by the mirror reflectance and soiling are also included. In Collado *et al.*'s (Collado & Guallar, 2013) review of optimized heliostat field layouts, the actual reflectivity of the field is characterised as the nominal reflectivity multiplied by the nominal cleanliness.

$$\eta_\rho = \eta_{\rho,nom} \cdot \eta_{nc} \quad (4)$$

Based on the heliostats from PS10, a nominal reflectivity of 0.88 is used as suggested by (Wei, Lu, Wang, Yu, Zhang & Yao, 2010) and a mirror nominal cleanliness value of 0.95 from (Sargent, 2003). The overall optical efficiency of the heliostat field can therefore be represented as:

$$\eta_{hf} = \eta_{opt} \cdot \eta_\rho \quad (5)$$

4.4 Tower and receiver

For modelling simplicity, an external receiver is considered opposed to a thermally more efficient cavity receiver. The receiver's hourly efficiency is approximated by Equation (6) from Christian *et al.* (2016), where α is the receiver solar absorbtance, ε the receiver thermal emittance and σ the Stefan-Boltzmann constant, A_{rec} the exposed surface area, T_{wall} the average receiver surface temperature, h_c is the convective heat transfer coefficient and T_{db} is the ambient dry-bulb temperature. The temperature data is measured at 2 m above the ground and for this study it will be assumed that the change in temperature at the height of the receiver will not vary significantly.

$$\eta_{rec} = \frac{Q_{r,in} - Q_{r,loss}}{Q_{r,in}} = \frac{\alpha Q_{r,in} - \varepsilon\sigma A_{rec} T_{wall}^4 - h_c A_{rec}(T_{wall} - T_{db})}{Q_{in}} \quad (6)$$

Stellenbosch University https://scholar.sun.ac.za

The convection heat transfer coefficient from the receiver is approximated using the following relation from (Kröger, 2002) and is only function of the wind speed;

$$h_{conv} = 2.8+3v_w \quad (7)$$

Table 3: Receiver technical specifications

Parameter	Value	Reference
Receiver area	1100 m^2	(Sargent, 2003)
Maximum incident flux	1100 kW/m^2	(Christian *et al.*, 2016)
Thermal emittance	0.88	(Pitz-Paal, Dersch & Milow, 2005)
Thermal absorbtance	0.94	(Sargent, 2003)
Wall temperature (avg.)	600 °C	(Christian *et al.*, 2016)

4.5 Thermal energy storage system

A two-tank molten salt storage system is chosen as it currently is the most commercially dominant approach (Lovegrove & Stein, 2012). The storage fills up during periods where surplus heat falls onto the receiver and is drained during times of intermittency and evening periods. Increasing the storage capacity will increase the plant capacity factor (CF); however thermal energy storage (TES) systems are costly and need to be sized accordingly. An ideal insulated thermal storage system has been simplified by assuming no losses to the surrounding environment. Typical losses experienced by the molten salt tanks are 0.5 °C to 1 °C per day (Pennsylvania State University, 2014; SOLARRESERVE, 2016).

4.6 Rankine cycle

A reheat Rankine cycle is modelled in Engineering Equation Solver (EES) with one open- and four contact feed-water heaters as illustrated in Figure 16. The cycle is modelled using mass and energy governing equations solving the system of equations simultaneously. The cycle is solved in terms of specific work and heat, calculating the required steam mass flow to yield a net 100 MW_e output.

Stellenbosch University https://scholar.sun.ac.za

The following assumptions/ simplifications are made for the Rankine cycle model:

- Steady-state operation
- Pressure drops are excluded
- Perfect feed-water heaters are considered
- No losses to the environment

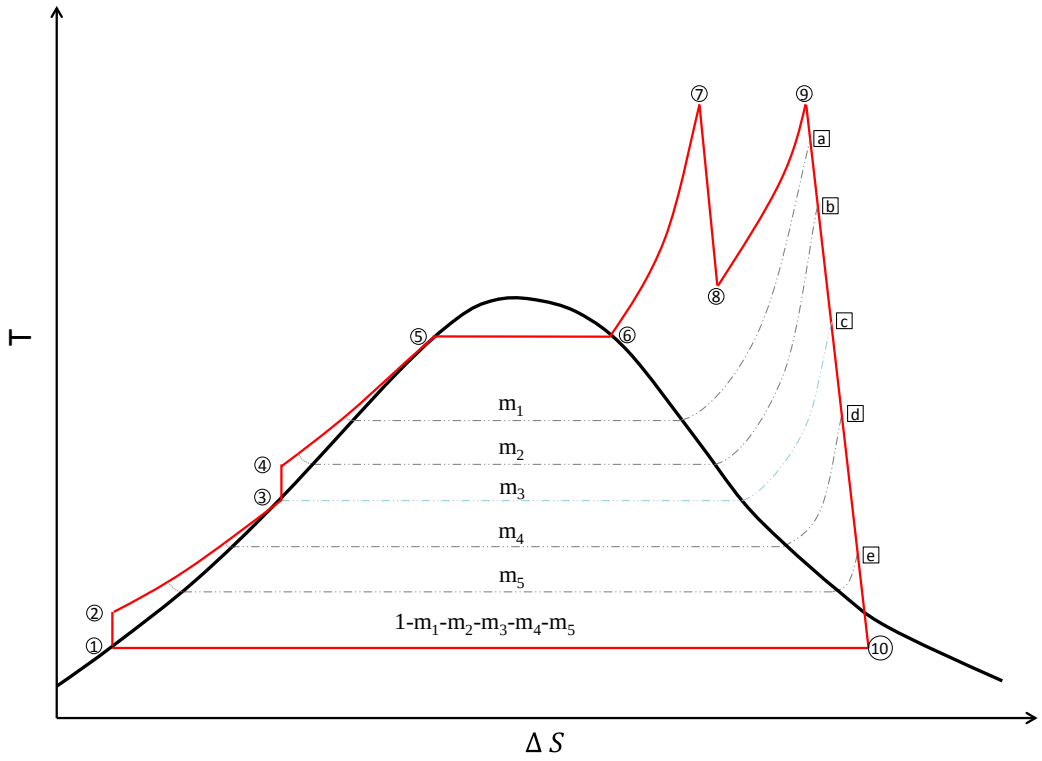

Figure 16: Rankine cycle T-s diagram

Condenser

In the dry-cooled scenario, the condenser pressure is determined by the lower temperature limit of the power cycle. It is the sum of the ambient dry-bulb temperature and initial temperature difference (ITD) as calculated in Equation (8). The ITD is the temperature difference between the inlet condensing steam and the air entering the condenser. ITD's of dry-cooled condensers have experienced a decline as

Stellenbosch University https://scholar.sun.ac.za

the increasing cost of energy is demanding power cycles to be more efficient. A value of 24 °C is chosen for the dry-cooled reference case (GEA, 2012).

$$T_L = T_{db} + ITD \quad (8)$$

In the CSP+D scenario, the MED desalination plant performs the role of the condenser in the Rankine cycle. The temperature at which the steam exiting the turbine condenses is therefore calculated in Equation (10) as the sum of the MED plant's temperature requirement in the first effect, also known as the top brine temperature (TBT), and the terminal temperature difference (TTD) between the condensing steam and the feed-water. An acceptable TTD value for current seawater desalination plants is 2.5 °C (Gebel, 2014).

$$T_L = T_{TBT} + TTD \quad (9)$$

The condensing temperatures for the four configurations investigated are as follows:

1. Dry-cooled CSP plant, T_{db}=34.9 °C
2. CSP+MED, TBT=70 °C
3. CSP+MED, TBT=62.5 °C
4. CSP+MED, TBT=55 °C

Steam turbine

The maximum inlet temperature and pressure conditions of the steam are based on similar values of the Siemens SST-600 steam turbine (Table 4) This turbine is designed for CSP applications and allows for fast start-up times and is compatible for both condenser and back-pressure applications, making it suitable for a CSP-desalination system. The high pressure turbine (HPT) outlet (point 8 in Figure 16) is optimised by performing a parametric study in which the HPT outlet pressure that produces the maximum cycle efficiency is chosen.

Table 4: SST-600 live steam inlet conditions, (Siemens AG, 2012)

Parameter	Value
Pressure	16 MPa
Temperature	565 °C
HPT isentropic efficiency	85 %
LPT isentropic efficiency	85 %

Stellenbosch University https://scholar.sun.ac.za

Generator efficiency	99 %

Feed-water heating

Feed-water heating is implemented in order to improve the cycle efficiency. Steam is bled from the turbine and by transferring the super- and latent heat to the feed water; less of the external heat source is required to generate steam. Four closed and one contact feed heater (FH) are implemented into the Rankine cycle design (Point a-e in Figure 16). Therefore two feed water pumps (FWP) are required (point 1 and 2 in Figure 16) chosen with conservative isentropic efficiencies of 75 %. Boiler feed-water pumps can have isentropic efficiencies of up to 85 % (Nasal, 2003).

Rankine optimization

Each configuration's Rankine cycle, having different cooling conditions at the condenser side, is optimized by means of a parametric study procedure in order to reach its peak potential cycle efficiency. The optimization procedure involves an iterative process in which the pressure values of the HPT turbine (Figure 16, point 8) and the FH bleeding locations (Figure 16, points a-e) are determined. The procedure is repeated until the value of Rankine efficiency reaches convergence; which is considered when the third significant figure stops varying. Each step of the procedure involves varying the pressure of the considered variable in a parametric study with the cycle efficiency as an output. The optimization procedure sequence is as follows (consider Figure 16):

1. Optimize the direct contact FH bleed-off pressure location (Point c)
2. Optimize 4th closed FH bleed-off pressure location (Point e)
3. Optimize 3rd closed FH bleed-off pressure location (Point d)
4. Optimize 2nd FH bleed-off pressure location (Point b)
5. Optimize 1st FH bleed-off pressure location (Point a)
6. Optimize 2nd FH bleed-off pressure location (Point b)
7. Optimize 3rd closed FH bleed-off pressure location (Point d)
8. Optimize 4th closed FH bleed-off pressure location (Point e)
9. Optimize HPT outlet pressure location (Point 8)
10. Optimize the direct contact FH bleed-off pressure location (Point c)
11. Revise all pressure bleed-off values by checking the steam dryness quality is above 100 % for lower bleed-off locations

Stellenbosch University https://scholar.sun.ac.za

After the TBT is changed for the next case, the condensing temperature is changed and the above procedure is repeated in order to optimize the Rankine efficiency for this changed boundary condition.

4.7 SAM comparison

System advisor model (SAM) is a freeware program developed by the National Renewable Energy Laboratory (NREL). It is a performance and financial model that is intended to assist the decision making process of individuals that are involved in the renewable energy industry. SAM is considered an internationally accepted tool amongst industry professionals such as project managers, engineers, policy analysts, technology developers and researchers. SAM is considered as one of the benchmark tools used for CSP simulation software and will therefore be used to verify the performance of the simplified model used in this study.

The SAM simulation setup needs to be set in such a manner that it conforms to the assumptions made in the simplified CSP model created in Excel. The SAM simulation set-up procedure is listed in the B.1 SAM set-up appendix. All values in SAM not mentioned in the following procedure are left at their default values.

After the values were set in the SAM simulation, a parametric study was performed varying the SM between 0 and 4 with increments of 0.2 for 0, 6, 13.5 and 18 hours of TES which are arbitrarily chosen. In Figure 17 the CF's of the Excel CSP model are compared to that of SAM. Given the simplicity of the Excel CSP model and the assumptions made, the results seem to follow that of SAM with relative accuracy. The absolute errors between the two models are illustrated in Figure 18, with the maximum absolute error being below 10 % for all storage cases.

Stellenbosch University https://scholar.sun.ac.za

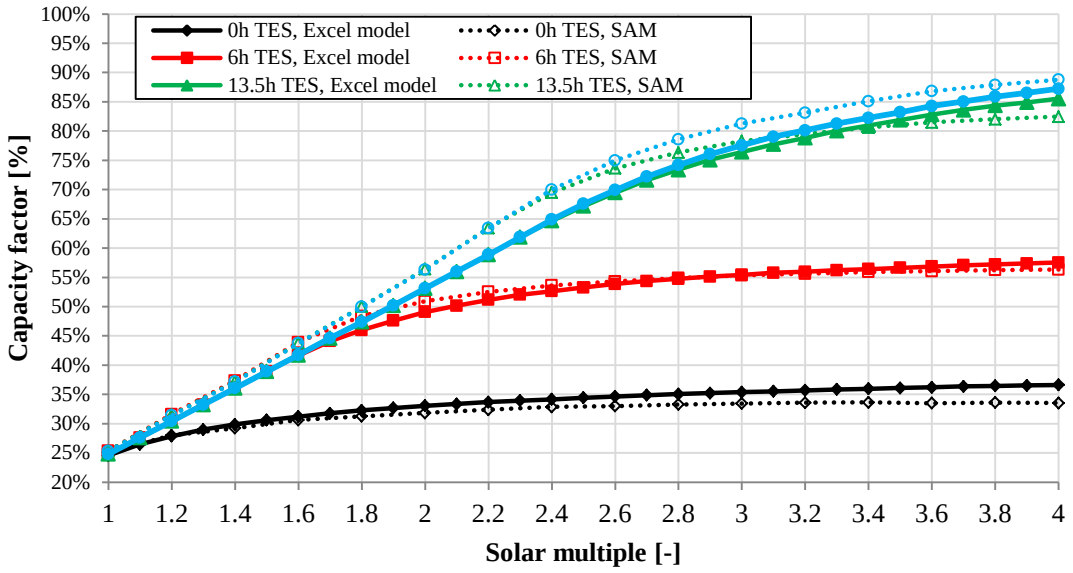

Figure 17: Excel CSP model validation with SAM in terms of CF

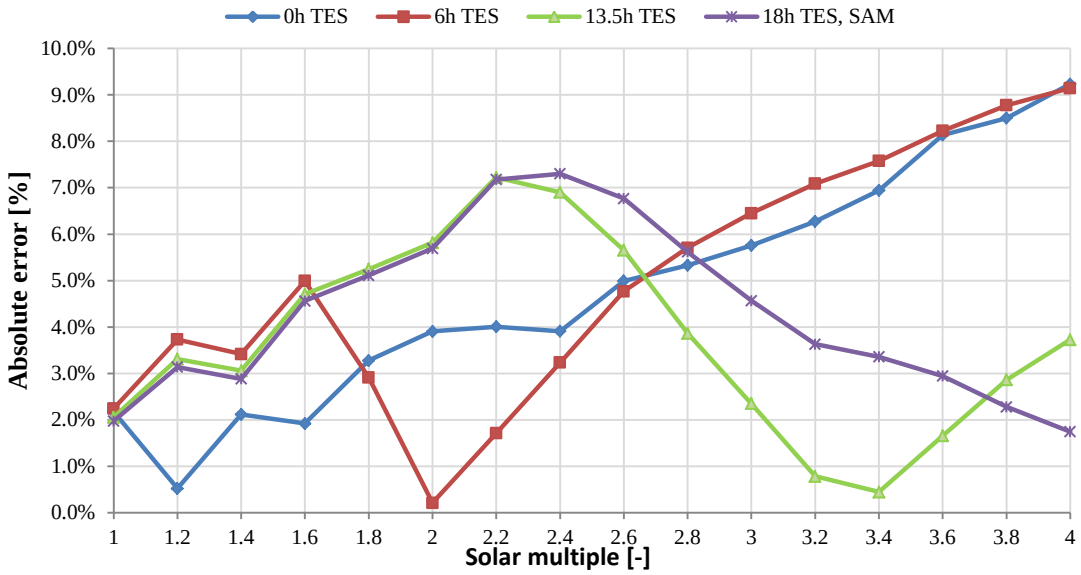

Figure 18: Excel CSP model absolute errors compared to SAM

Stellenbosch University https://scholar.sun.ac.za

4.8 Summary

After the EES Rankine cycle optimisation of each configuration, the resulting cycle efficiency is built into the Excel CSP model. Using the chosen design point conditions the heliostat field solar multiple value of 1 is determined. The CSP model can then be solved for each hour of the year, given a user specified solar multiple as well as the hours of thermal energy storage. A fair correlation between the results of the Excel model and SAM is demonstrated for the dry-cooled reference case and should serve as sufficient validation for the CSP+MED cases as well.

Stellenbosch University https://scholar.sun.ac.za

5. MED desalination plant model

5.1 Introduction

This multiple effect stacked (MES) desalination system is a vertically stacked arrangement of the forward feed multiple-effect distillation (MED) configuration. The modelling approach of Mistry *et al*. (Mistry *et al.*, 2012) has been followed in developing this model in the Engineering Equation Solver (EES) software. Mistry *et al*.'s modelling approach is unique compared to most models presented in literature, because it makes use of a simultaneous equation solver. This approach has the key advantage in avoiding the need to develop algorithms for reaching solution convergence.

This is a modular method in which each subcomponent is modeled individually and coupled to one another by mass flow, salt and energy balance equations. This model relies on fewer assumptions than conventional numerical models. The following assumptions are made:

- Steady-state operation
- Seawater properties are only a function of temperature and salt content (using built-in EES functions)
- Seawater temperature stays constant
- Heat exchange area is sufficient to condense vapour to saturated liquid at the previous effect's pressure
- Pressure losses are negligible
- Non-equilibrium allowance (NEA) is negligible (Mistry *et al.*, 2012)
- Distillate (vapour) and brine (liquid) streams leave each effect at that effect's temperature
- Distillate vapour is slightly superheated
- Energy losses to the environment are negligible
- Distillate produced is pure (zero salinity)
- The distillate vapour generated via boiling and via flashing of the brine is slightly superheated by an amount equal to the effect's boiling point elevation (BPE)
- The overall heat transfer coefficient in each effect, preheater and condenser is a function of temperature only (Mistry *et al.*, 2012)

Stellenbosch University https://scholar.sun.ac.za

5.2 First effect

All effects are identical to one another, although there are some slight differences between the first effect and the succeeding ones. In the first effect (Figure 19) the feed water enters the effect at a sub-cooled condition, while in other effects feed enters slightly above the saturation temperature resulting in some flash evaporation to occur. Furthermore, an external steam source is used for the heating in the first effect, while the succeeding effects receive their heating from the distillate vapour produced in the preceding effects.

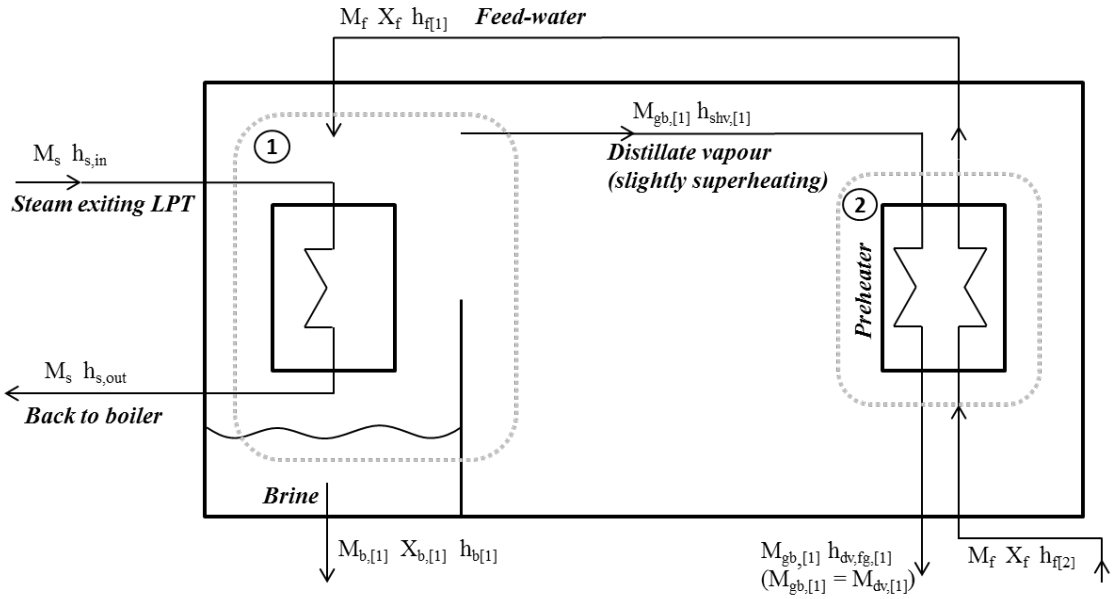

Figure 19: Schematic diagram of 1st effect

5.2.1 Boiling (control volume 1)

The boiling of the feed-water in the first effect takes place using the latent waste heat energy from the steam exiting the low pressure turbine. The boiling feed-water produces the only source of distillate in the first effect. After boiling the remaining feed-water's salinity slightly increases and is called the brine.

Stellenbosch University https://scholar.sun.ac.za

Heating steam

Assumptions for the heating steam are as follows:

- The heating steam entering the first effect is assumed to be saturated vapour
- The heating steam exiting the first effect is assumed to be fully condensed

The steam temperature T_s required for heating in the first effect is the sum of the top brine temperature (TBT) and the limitation of the terminal temperature difference TTD_s.

$$T_s = TBT + TTD_s \tag{10}$$

Mass flow balance

The feed water entering the first effect (M_f) is then separated into the steam generated via boiling ($M_{gb,[1]}$) and the leftover brine ($M_{b,[1]}$):

$$M_f = M_{gb,[1]} + M_{b,[1]} \tag{11}$$

Salt balance

Assuming the distillate produced contains no salt, the remainder of the feed-water with an initial salinity (X_f) forms the leftover brine ($M_{b,[1]}$) with a slight increased salinity of $X_{b,[1]}$.

$$M_f \cdot X_f = M_{b,[1]} \cdot X_{b,[1]} \tag{12}$$

Energy balance

The following energy balance is used for governing the boiling evaporation process in the first effect:

$$M_f \cdot h_{f,[1]} + M_s \cdot h_{s,in} = M_{gb,[1]} \cdot h_{shv,[1]} + M_{b,[1]} \cdot h_{b,[1]} + M_s \cdot h_{s,out} \tag{13}$$

5.2.2 Preheater (control volume 2)

The distillate vapour formed in the first effect ($M_{gb,[1]}$) passes through the counter flow preheater and some steam condenses before moving on to the next effect. In the counter flow direction, the feed-water (M_f) gains a slight temperature rise across the

Stellenbosch University https://scholar.sun.ac.za

preheater and enters the first effect. The following energy balance is done for the first preheater:

$$M_{dv,[1]} \cdot (h_{shv,[1]} - h_{dv,fg,out[1]}) = M_f \cdot (h_{f,[1]} - h_{f,[2]}) \quad (14)$$

5.3 Effects: i to n

Solving the mass and energy flows for the i^{th} to n^{th} effects (Figure 20) are very similar to the first effect. Flash boxes are added where the condensed distillate vapour from each effect is collected. Note that regarding the second effect, there is no condensed distillate steam ($M_{d,[i-1]}$) flowing to the flash-box as the first effect does not have a flash-box in which distillate is accumulated. A vacuum pump system is used to regulate and control the pressure in each effect. This system ensures a slight pressure reduction after each effect, causing the incoming streams $M_{d,[i-1]}$ and $M_{dv,[i-1]}$ to slightly flash evaporate upon entering the i^{th} flash-box and $M_{b,[i-1]}$ to slightly flash evaporate upon entering the i^{th} effect.

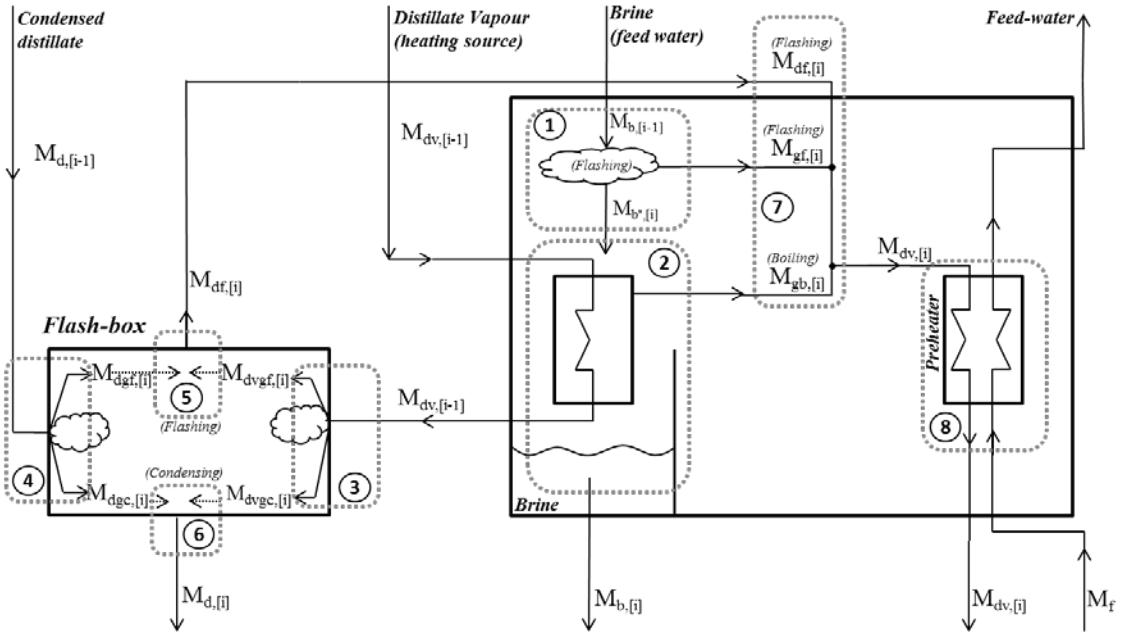

Figure 20: Schematic diagram of i^{th} effect

Stellenbosch University https://scholar.sun.ac.za

5.3.1 Flashing of brine (Control volume 1)

The brine formed in the previous effect ($M_{b,[i-1]}$) is carried over to the succeeding effect and acts as the incoming feed-water. As a result of the slight pressure reduction a small amount of the brine flash-evaporates, producing some distillate ($M_{gf,[i]}$).

Mass flow balance

$$M_{b,[i-1]}=M_{b",[i]}+M_{gf,[i]} \tag{15}$$

Salt balance

After the flashing process, the leftover brine's ($M_{b",[i]}$) salinity slightly increases to a value of $X_{b",[i]}$.

$$M_{b,[i-1]}\cdot X_{b,[i-1]}=M_{b",[i]}\cdot X_{b",[i]} \tag{16}$$

Energy balance

The following energy balance is used to govern the flashing process of the passed over brine:

$$M_{b,[i-1]}\cdot h_{b,[i-1]} = M_{b",[i]}\cdot h_{b",[i]} + M_{gf,[i]}\cdot h_{shv,[j]} \tag{17}$$

5.3.2 Boiling (Control volume 2)

The distillate produced in the previous effect ($M_{dv,[i-1]}$) flows into tube bundles entering the next effect and acts as the heating source. The distillate vapour inside the tube bundles exchanges all of its latent heat and reduces to fully saturated condensate. The incoming brine, after flashing, ($M_{b",[i]}$) falls onto tube bundles and is evaporated to produce the majority of the distillate ($M_{gb,[i]}$) and forms leftover brine ($M_{b,[i]}$) with an increased salt content to be carried over to the next effect.

Mass flow balance

$$M_{b",[i]}=M_{gb,[i]}+M_{b,[i]} \tag{18}$$

Stellenbosch University https://scholar.sun.ac.za

Salt balance

$$M_{b",[i]} \cdot X_{b",[i]} = M_{b,[i]} \cdot X_{b,[i]} \quad (19)$$

Energy balance

$$M_{dv,[i-1]} \cdot h_{dv,out,[i-1]} + M_{b",[i]} \cdot h_{b",[i]} = M_{dv,[i-1]} \cdot h_{dv,f,[i-1]} + M_{gb,[i]} \cdot h_{shv,[i]} + M_{b,[i]} \cdot h_{b,[i]} \quad (20)$$

5.3.3 Flash-box (Control volumes 3-6)

Once the distillate vapour from the previous effect ($M_{dv,[i-1]}$) has exchanged all of its latent heat to the succeeding effect, the fully saturated condensed distillate flows to a flash-box. All the condensed distillate accumulated in each flash box is then carried over to the next flash-box. The pressure in each flash-box corresponds to the pressure of its respective effect causing some of the condensed distillate entering to flash-evaporate.

The flash-evaporation occurs from the condensed distillate vapour ($M_{dv,[i-1]}$) and the condensate from the previous flash-box ($M_{d,[i-1]}$) entering control volume 7.

Mass flow balance (control volume 3)

Condensed distillate-vapour entering the flash-box is split up into distillate generated via flashing ($M_{dvgf,[i]}$) and condensed distillate ($M_{dvgc,[i]}$):

$$M_{dv,[i-1]} = M_{dv,gf,[i]} + M_{dv,gc,[i]} \quad (21)$$

Energy balance (control volume 3)

$$M_{dv,[i-1]} \cdot h_{dv,f,[i-1]} = M_{dv,gf,[i]} \cdot h_{dv,g,[i]} + M_{dv,gc,[i]} \cdot h_{dv,f,[i]} \quad (22)$$

Mass flow balance (control volume 4)

Distillate from the previous flash box is split up into distillate generated via flashing ($M_{dgf,[i]}$) and condensed distillate ($M_{dgc,[i]}$):

$$M_{d,[i-1]} = M_{dgf,[i]} + M_{dgc,[i]} \quad (23)$$

Stellenbosch University https://scholar.sun.ac.za

Energy balance (control volume 4)

$$M_{d,[i-1]} \cdot h_{dv,f,[i-1]} = M_{dgf,[i]} \cdot h_{dv,g,[i]} + M_{dgc,[i]} \cdot h_{dv,f,[i]} \quad (24)$$

Mass flow balance (control volume 5)

The distillate vapour formed in the i^{th} flash-box ($M_{df[i]}$) flows back to the i^{th} effect and forms part of the total distillate produced in the i^{th} effect.

$$M_{df,[i]} = M_{dgf,[i]} + M_{dvgf,[i]} \quad (25)$$

Mass flow balance (control volume 6)

The condensed distillate formed in the flash-box ($M_{d[i]}$) is carried over to the succeeding flash-box:

$$M_{d[i]} = M_{dgc[i]} + M_{dvgc[i]} \quad (26)$$

5.3.4 Distillate vapour produced (control volume 7)

The total distillate formed in the i^{th} effect ($M_{dv,[i]}$) is the sum of the distillate generated via boiling ($M_{gb,[i]}$), generated via the flashing of brine ($M_{gf,[i]}$) and some flashed distillate from the flash-box ($M_{df,[i]}$).

Mass flow balance

$$M_{dv[i]} = M_{gf[i]} + M_{gb[i]} + M_{df[i]} \quad (27)$$

Energy balance

$$M_{dv[i]} \cdot h_{dv,in[i]} = M_{gf[i]} \cdot h_{shv,[i]} + M_{gb[i]} \cdot h_{shv,[i]} + M_{df[i]} \cdot h_{dv,g,[i]} \quad (28)$$

Stellenbosch University https://scholar.sun.ac.za

5.3.5 Preheater (control volume 8)

The distillate vapour formed in the i^{th} effect ($M_{dv,[i]}$) passes through the counter flow preheater and slightly condenses before moving on to the next effect. In the counter flow direction the feed-water M_f gains a slight temperature rise across the preheater.

Energy balance

$$M_{dv[i]} \cdot (h_{dv,in[i]} - h_{dv,out,[i]}) = M_f \cdot (h_{f[i]} - h_{f[i+1]}) \quad (29)$$

5.4 Condenser

The total distillate vapour created in the last effect ($M_{dv,[N]}$) passes through the condenser (Figure 21) and is fully condensed to saturated vapour state in control volume 1, after which it accumulates with the distillate collected from the final flash-box ($M_{d,[N]}$). The cooling seawater (M_{sw}) is preheated in the condenser, absorbing all the latent heat from the incoming distillate vapour. A large fraction of the heated seawater is passed on as feed-water (M_f) and the remainder ($M_{rej,cw}$) is rejected along with the brine of the last effect ($M_{b,[N]}$).

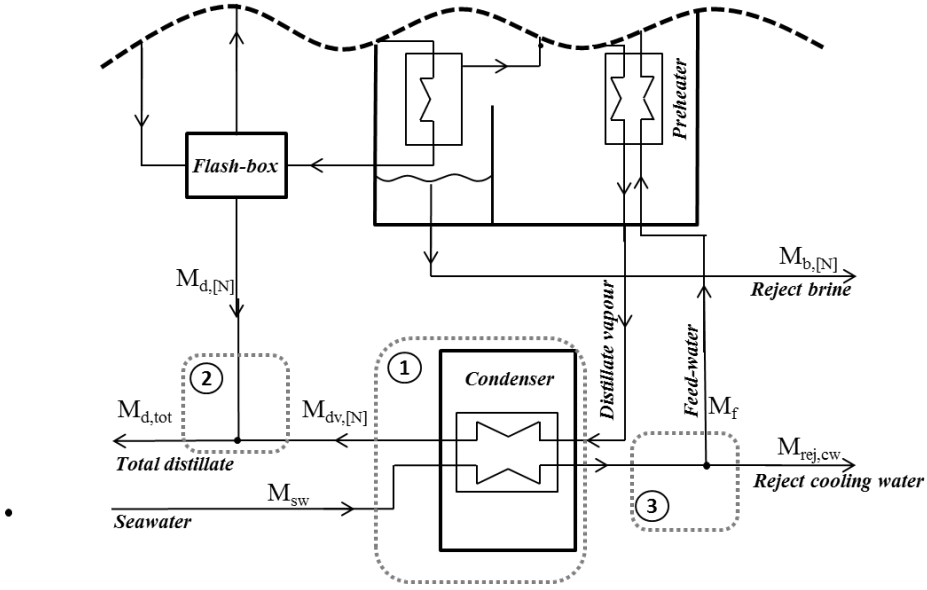

Figure 21: Schematic diagram of the final MES effect and condenser

Stellenbosch University https://scholar.sun.ac.za

Energy balance (control volume 1)

$$M_{dv,[N]} \cdot h_{dv,out,[N]} + M_{sw} \cdot h_{sw,in} = M_{dv,[N]} \cdot h_{dv,f,[N]} + M_{sw} \cdot h_{sw,out} \quad (30)$$

Mass flow balance (control volume 2)

After the distillate vapour of the last effect is condensed in the condenser it is added to the distillate accumulated in the last flash box. The total distillate produced in the MES system is calculated as the sum of the two streams:

$$M_{d,tot} = M_{d,[N]} + M_{dv,[N]} \quad (31)$$

Mass flow balance (control volume 3)

The seawater needed to fully condense the distillate vapour in the condenser usually exceeds the feed water required for the MES plant. The rejected seawater is simply the difference of the two streams:

$$M_{sw,rej} = M_{sw} - M_f \quad (32)$$

Temperature rise over condenser

The day-to-day ocean temperature at Swakopmund which matches the period (1 Nov. 2014 to 30 Oct. 2015) of the solar data obtained from GeoSun is used for this study. The monthly variation is seen in Figure 22, with the summer months being the hottest due to the Northern wind conditions pushing back on the cold Benguela stream, causing some degree of stagnation to occur and consequently increasing the ocean temperature.

An average annual temperature of 15 °C will be used for the sizing of the MED plant model. The temperature rise over the condenser will be constrained to a maximum of 15 °C in order to ensure that the condenser outlet temperature does not exceed 35 °C during summer conditions in order to minimise the amount of seawater required for the MES plant and consequently keeping pumping costs to a minimum.

Stellenbosch University https://scholar.sun.ac.za

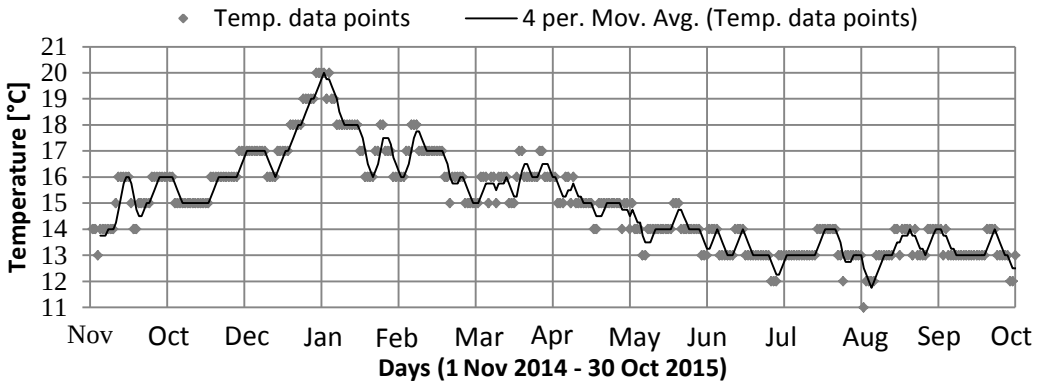

Figure 22: Ocean temperature at Swakopmund, Namibia (Seatemperature.info, 2016)

5.5 Heat transfer

5.5.1 Effects

The surface area on the condensing side must be sized sufficiently in order to ensure the distillate vapour from the previous effect condenses entirely while heating and evaporating the incoming feed-water. The rate of heat transfer is modelled sufficiently with Newton's Law of Cooling, Equation (33), since there is a phase change on both sides of the tubes (Mistry *et al.*, 2012). Equation (33) is written for the heat transfer of the first effect, but is applied to all other effects.

$$M_s\left(h_{s,in}-h_{s,out}\right) = A_{e,[1]}U_{e,[1]}\left(T_s - T_{b,[1]}\right) \tag{33}$$

The overall heat transfer coefficient in Equation (33) is approximated using the fouled evaporator correlation from (El-Dessouky & Ettouney, 2002: 596) which is a function of the temperature on the condensing side and described in Equation (34).

$$U_{e,[1]} = 1939.1 + 1.40562T_s - 0.0207525T_s^2 + 0.0023186T_s^3 \tag{34}$$

5.5.2 Preheaters and condenser

In order to calculate the heat transfer area of the preheaters and the condenser, an energy balance defined in Equation (35) and the log mean temperature difference (LMTD) method defined in Equation (36), are used.

Stellenbosch University https://scholar.sun.ac.za

$$M_f(h_{f,[i]}-h_{f,[i+1]}) = A_{ph,[i]}U_{ph,[i]}\left(LMTD_{ph,[i]}\right) \quad (35)$$

$$LMTD_{ph,[1]} = \frac{T_{f,[i+1]}-T_{f,[i]}}{Ln\left(\frac{T_{dv,[i]}-T_{f,[i]}}{T_{dv,[i]}-T_{f,[i+1]}}\right)} \quad (36)$$

The overall heat transfer coefficients of the preheaters and condenser are approximated using the fouled condenser correlation from (El-Dessouky & Ettouney, 2002: 596) and is defined in Equation (37) as a function of the temperature of the condensing distillate vapour.

$$U_{ph,[i]} = 1617.5 + 0.1537T_{dv,[i]} + 0.1825T_{dv,[i]}^2 - 0.00008026T_{dv,[i]}^3 \quad (37)$$

5.6 Control volume check-up

This MED-stacked desalination model is based on mass, salt and energy balances on component level with components linked to one another. As an additional assessment, the whole MED plant is taken as the control volume (Figure 23) in order to check whether the mass, salt and energy balances still add up.

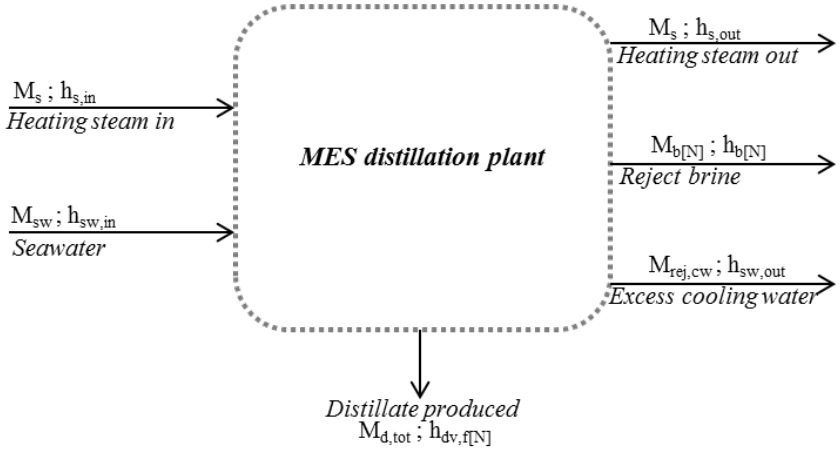

Figure 23: Check-up control volume of MES distillation plant

Stellenbosch University https://scholar.sun.ac.za

Mass balances

The heating steam and the total seawater streams are the only mass inflows into the MES system:

$$M_{mes,in} = M_s + M_{sw} \quad (38)$$

The heating steam, rejected seawater, total produced distillate and the rejected brine are the only mass outflows of the MES system:

$$M_{mes,out} = M_s + M_{rej,cw} + M_{d,total} + M_{b[N]} \quad (39)$$

Energy balances

Energy flow into MES control volume:

$$E_{mes,in} = M_s \cdot h_{s,in} + M_{sw} \cdot h_{sw,in} \quad (40)$$

Energy flow out the MES control volume

$$E_{mes,out} = M_s \cdot h_{s,out} + M_{sw,rej} \cdot h_{sw,out} + M_{d,tot[N]} \cdot h_{dv,[N]} + M_{b[N]} \cdot h_{b[N]} \quad (41)$$

5.7 Summary

The constraints under which the MED model is optimized for each configuration are summarized in Table 5. The methodology from (Mistry *et al.*, 2012) was used in developing the MED model, however some constraint values are different in order to fit the seawater conditions of the Namibian coast. The EES MED model is verified with the method from (Mistry *et al.*, 2012) by performing a parametric study in which the number of effects is varied, solving for the performance ratio. The MED model from this study slightly outperforms that from Mistry *et al* as illustrated in Figure 24. This is due to the fact that the BPE is calculated for each effect in the EES MES model, but in Mistry *et al*.'s model the BPE is assumed to be a conservative constant value of 1 °C.

Stellenbosch University https://scholar.sun.ac.za

Table 5: MED design constraints

Constraint	Value	References
Salinity of seawater	35 g/kg	(Martin, 2016)
Salinity of brine at N^{th} effect	60 g/kg	(Gebel, 2014)
Seawater temperature	15 °C	(Surf-Forecast.com, 2016)
Min TTD of 1^{st} effect	2.5 °C	(Gebel, 2014)
Min TTD of preheaters	5 °C	(Mistry *et al.*, 2012)
Min ΔT between effects	1.5 °C	(Ophir & Lokiec, 2005)
Temp. gain over condenser	15 °C	(-)
Brine temp. of N^{th} effect	40 °C	(Mistry *et al.*, 2012)
Spec. el. consumption	1.0 kWh/m^3	(ENTROPIE, 2014)

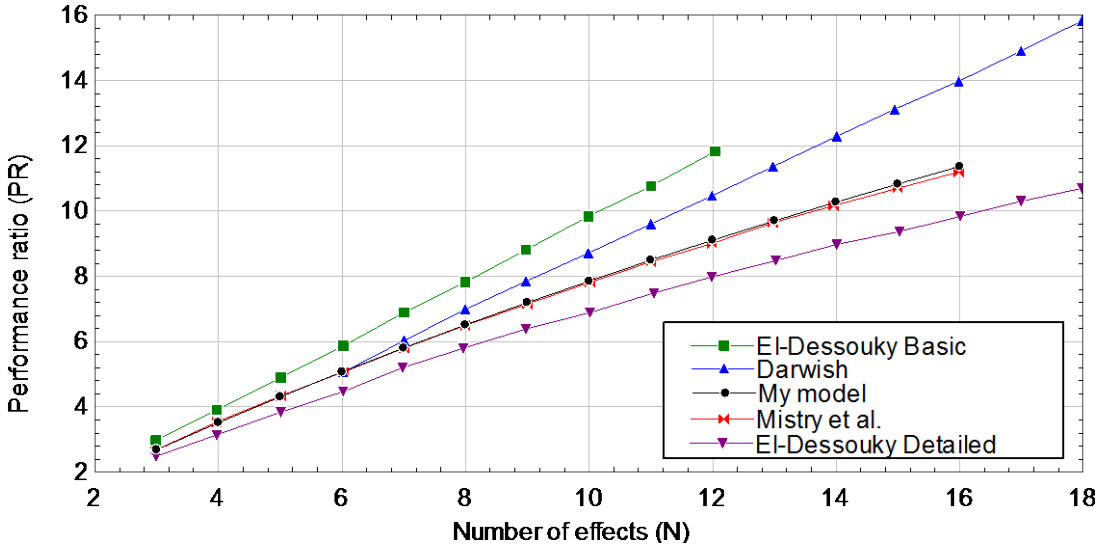

Figure 24: MED model performance ratio comparison

Stellenbosch University https://scholar.sun.ac.za

6. Bulk seawater pipeline

The seawater is desalinated at the CSP plant site and therefore has to be pumped 50 km inland from the coast to Arandis at an elevation of 580m, see Figure 25. A basic bulk water pipeline is modelled in order to estimate the potential electric pumping power requirements to supply feed-water to the MED plant at the reference design point conditions during full load operation. Pumping stations, wall thickness calculations, surge control, material selection, corrosion control, etc. are excluded in the scope of this model. The following assumptions are made in this model:

- Steady-state flow
- Turbulent flow
- Fluid properties of seawater (salinity of 35g/kg) at 15°C are used
- Losses due to bends are negligible

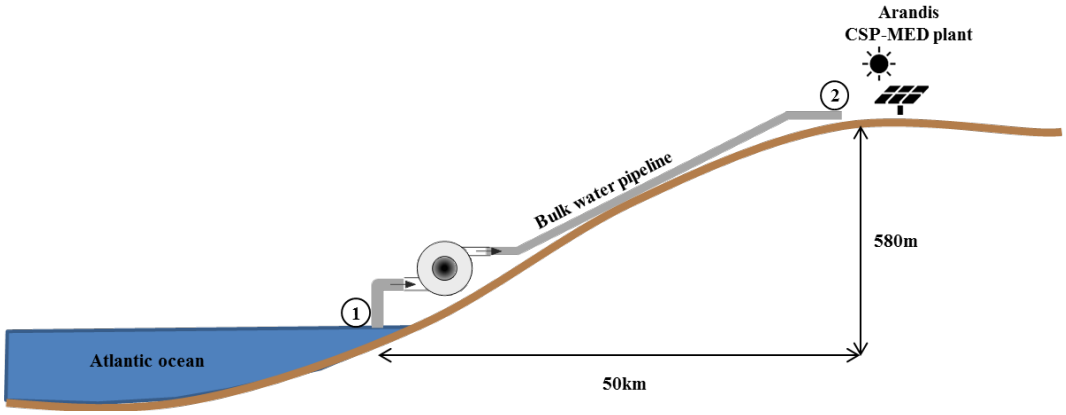

Figure 25: Bulk water pipeline schematic

After the MED plant is sized appropriately with its respective CSP plant, the required mass flow rate of seawater to be pumped inland at full load operation is known. Specifying the mean flow velocity and knowing the seawater mass flow rate, the diameter of the pipe is calculated using the continuity equation for steady flow:

$$\dot{m}_{sw}=\rho_{sw} v_m \left(\frac{\pi}{4}\right) D^2 \quad (42)$$

Stellenbosch University https://scholar.sun.ac.za

Where $\dot{m}_{sw}$ is the seawater mass flow rate, ρ_{sw} the seawater density, v_m the mean velocity and D the diameter of the piping used. Thresh (1901) suggested that the mean velocity for pumping mains should be between 0.6 m/s and 0.75 m/s. A CSP-MED study done by (Servert *et al.*, 2016) chose a mean velocity of 2 m/s and examining the bulk water pipeline database from NamWater, Namibia's water utility, the rated mean velocity values varies between 0.2 m/s and 1.8 m/s as shown in Figure 26. A mean velocity of 1 m/s has been decided for this study. Figure 27 illustrates the effect that the design mean-velocity has on the pumping requirements as well as the diameter of the bulk water pipeline.

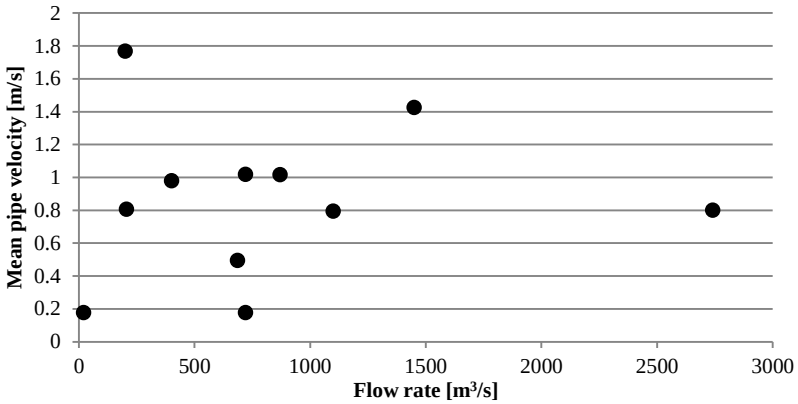

Figure 26: Mean pipe velocities adapted from NamWater's database, (NamWater, 2016)

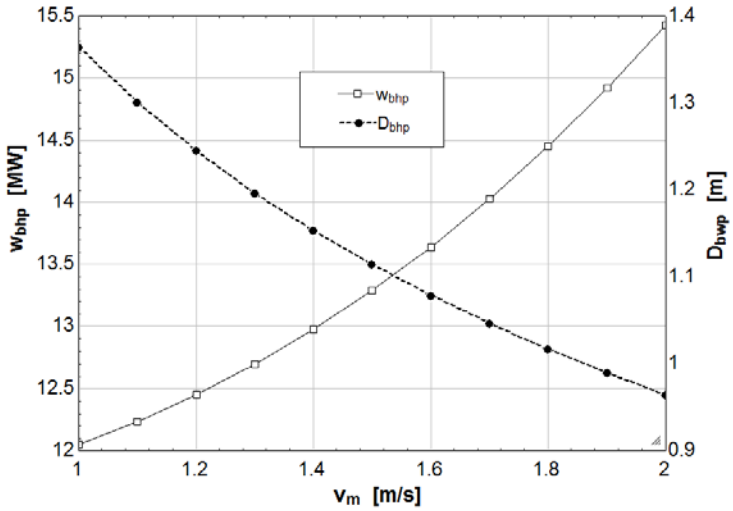

Figure 27: Effects of mean pipe velocity specification

Stellenbosch University https://scholar.sun.ac.za

Assuming a constant cross section of the pipeline, the velocity terms in Bernoulli's equation for incompressible steady flow can be cancelled out and can be rewritten as:

$$(\Delta h)=z_1-z_2-h_L \tag{43}$$

where (Δh) is the required head to be delivered from the pump, $z_1$and z_2 are the elevations of points 1 and 2 measured from the centre line of the pipe and h_L the total head loss over the pipeline. Head losses due to bends, valves, etc. are negligible in long transmission lines having no take-offs and have therefore been excluded in the pumping calculations (Swamee & Sharma, 2008: 16). Friction losses are accounted for using the Darcy-Weisbach equation:

$$h_f=\frac{8fLQ^2}{\pi^2 gD^5} \tag{44}$$

Where f is the coefficient of resistance, L the length of the pipeline and Q the volume flow rate of the seawater. The friction coefficient in turbulent flows ($Re > 4000$) is a function of the average height roughness of the pipe surface ε_{ps} and is calculated using the implicit Colebrook equation:

$$f = 1.325\left[\ln\left(\frac{\varepsilon_{ps}}{3.7D}+\frac{2.51}{Re\sqrt{f}}\right)\right]^{-2} \tag{45}$$

Typical materials selected for seawater pipelines depending on the availability and application include copper alloys, carbon steel, galvanized steel, stainless steel, plastics and titanium. A conservative roughness of 0.15 mm for galvanized steel has been chosen, however a minimum roughness of 0.0015 mm for copper could also be used considering the abovementioned materials (Cengel & Cimbala, 2006). Knowing the total head that needs to be delivered by the pump and the pump efficiency, the pumping requirements can be calculated with the following equation:

$$W_{bhp}=\frac{\dot{m}_{sw}\Delta h\, g}{\eta_{pump}} \tag{46}$$

Once an appropriate pipe diameter has been determined, it becomes a fixed input value in the model with the pumping power requirement varying as the seawater mass flow rate fluctuates. The effects of the material choices for the pipeline on the pumping requirements can be seen in Figure 28. A summary of the key constraints for the bulk water pipeline model is made in Table 6.

Stellenbosch University https://scholar.sun.ac.za

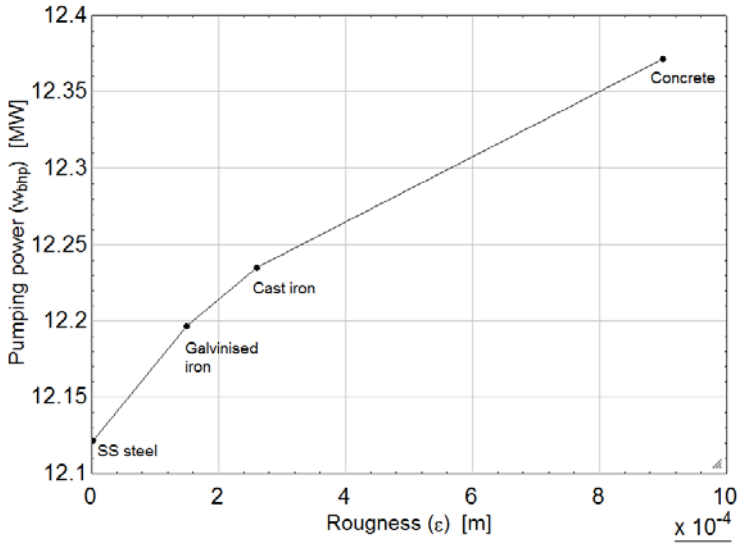

Figure 28: Effects of pipe materials on pumping requirements

Table 6: Seawater pipeline design constraints and considerations

Constraint	**Symbol**	**Value**
Pipeline length	L_{BWP}	50 km
Elevation	H_{elev}	580 m
Mean velocity	v_m	1 m/s
Pipe roughness	ε	0.0015-0.15 mm
Pump efficiency	η_{pump}	75 %

Stellenbosch University https://scholar.sun.ac.za

7. Economics

7.1 CSP plant

The economics of the CSP plant is based on data made available from the National Renewable Energy Laboratory (NREL). Using SAM's Excel Exchange spread sheet, more detailed cost categories for a CSP tower model can be accessed.

7.1.1 Direct installed costs

The direct capital cost values represent the costs of equipment or installation service that is applicable to year zero.

Site preparation

Depending on the site location and the heliostat field layout, some degree of land preparation would be required in order install the solar field and construct the rest of the CSP plant. A linear cost correlation value of 16 $/m^2 is used (Turchi & Heath, 2013).

Heliostat field

An overall heliostat cost of 170 $/m^2 (Turchi & Heath, 2013) is chosen and is multiplied by the total required field aperture area to obtain the heliostat capital costs. There have been some advances in the reduction of heliostat costs by SBP's Stellio product achieving 100 €/m^2 (schlaich bergermann und partner, 2015). However, Stellio's costs are not used in this study as the field efficiency is based on the 144 m^2 size heliostats which are at this stage more commercially mature as well as being conservative with the costs.

Tower

The cost of the tower is a function of its height and material used as well as the added downcomer piping and insulation. The scope of this study does not include the optimisation of the height of the tower which for a 100 MW plant can have a height of 150 m to 200 m (Eskom, 2015). A fixed height of 180 m is assumed with the tower capital costs given by Equation (47) where FTC is the fixed tower cost ($ 3000000), TCSE the tower cost scaling exponent (0.0113), H_T the tower height, H_{Rec} the

Stellenbosch University https://scholar.sun.ac.za

receiver height (20.4 m) and H_{helio} the heliostat height (12 m) (Turchi & Heath, 2013; NREL, 2015).

$$C_{T,tot}=FTC\times e^{(TCSE)\times(H_T-0.5H_{Rec}+0.5H_{helio})} \quad (47)$$

Receiver

An external type receiver is chosen with its main costs being the component costs and is a function of the receiver tube surface area. Other costs include insulation, cold salt pumps, controls and instrumentation as well as spare parts as the receiver is a critical component of CSP plant. The receiver capital costs are calculated using Equation (48), where RRC is the receiver reference cost ($ 110400000), A_{Rec} the outside surface area of the receiver (1100 m^2), $A_{Rec,ref}$ the receiver reference area (1571 m^2) and RSE the receiver scaling exponent (0.7) (Turchi & Heath, 2013; NREL, 2015).

$$C_{Rec}=RRC\left(\frac{A_{Rec}}{A_{Rec,ref}}\right)^{RSE} \quad (48)$$

Thermal energy storage system

A two-tank molten salt TES system is chosen and a linear system cost correlation of 26 $/kWh$_t$ is used (Turchi & Heath, 2013).

Balance of plant

The linear "balancing of the plant" cost correlation of 340 $/kW$_e$ is used (Turchi & Heath, 2013) and is a function of the name plate capacity.

Power plant

The cost of the power plant is calculated as 1190 $/kW$_e$ (Turchi & Heath, 2013). The integration of a MED plant to serve as the condenser of the power block would certainly influence the conventional capital expenses that associated with the power plant. The "auxiliary cooling water system" and the "water treatment system" is essentially replaced by the MED desalination plant, however being conservative, these costs are still included in the economic models of the CSP+MED plant configurations.

Stellenbosch University https://scholar.sun.ac.za

Contingency

In order to account for unforeseen cost uncertainties related to the installed equipment, a 7 % contingency of the sum of all the capital costs is included in the economic model. This is a value that SAM uses and it is assumed that this is an industry standard used by engineering procurement and construction (EPC) companies.

7.1.2 Indirect installed costs

All the expenses that cannot be attributed to a specific component or equipment fall under the following indirect installed costs.

Land cost

Reliable sources for the cost of large areas of land in Arandis are relatively limited. A 47 acre plot in Usakos costs approximately 5200 $/acre (Usci & Diane Properties, 2016a) and a 72 acre plot 10 km from Swakopmund costs about 4200 $/acre (Usci & Diane Properties, 2016b). Given the uncertainty and being conservative, the default 10000 $/acre value from SAM is used for this study (Turchi & Heath, 2013).

EPC and owner costs

The engineering, procurement and construction (EPC) and owner costs are related to the design and construction of the project. A value of 11% of the total direct installed costs is used as the EPC and owner costs.

Sales tax

The sales tax value in Namibia currently stands at 15 % (Trading economics, 2016). The United States (US) makes use of a federal policy mechanism called the Solar Investment Tax Credit. This policy enables solar power utilities to have up to 30 % of its taxes exempted as an incentive to drive the market solar power in the US. SAM uses 5 % as a default value for the sales tax and is applied to 80 % of the total direct installed costs (Turchi & Heath, 2013: 9). Namibia currently has no official sales tax exemption incentives for CSP and may follow a similar approach as in South Africa providing 17 % tax return on equity (Eberhard, Kolker & Leighland, 2014).

Stellenbosch University https://scholar.sun.ac.za

7.2 MES plant

As MED desalination plants make up the minority of the commercial global installed desalination capacity, there are limited in-depth cost correlations available in the literature. Almost all the literature concerning the economics of MED desalination expresses the capital cost of a plant in terms of $\$/m^3/day$. Such a correlation is not sufficient for detailed techno-economic studies, especially in the case of this study when the TBT of the plant is varied significantly (85 °C – 55 °C).

According to (Loutatidou & Arafat, 2015) 71-81 % of the direct capital cost of an MED plant is attributed to direct material and equipment expenses. The MED desalination plant cost breakdown of (Loutatidou & Arafat) however did not include or mention the cost relationship between the total heat transfer area and the capital costs. Instead a cost breakdown in terms of installed capacity ($\$/m^3/day$) was assumed. The cost breakdown is summarised in Appendix C. MED plant economics and is calculated as 2326 $\$/m^3/day$.

Using a cost database of more than 300 desalination plants, a study done by (Wittholz, Neill, Colby & Lewis, 2008) developed cost correlations for large-scale desalination plants . A correlation between plant capacity and cost was used, also known as the power law, in order to capture the effect of economies of scale. A power law exponent of 0.83 is suggested for MED desalination technologies.

(Hall, Ahmad & Smith, 1990) suggested various cost correlations for heat exchangers as a function of the materials used in which the all network exchangers obey a single cost law. The cost law correlation for a shell-in-tube heat exchanger made from a combination of titanium and stainless steel is given in Equation (49).

$$C_{HX,Ti/SS}=30800+3749A^{0.81} \quad (49)$$

Figure 29 is a comparative illustration of the discussed economic correlations that are considered. The correlations from Loutatidou & Arafat and Wittholz *et al.* follow the the same trend with a strong relationship between the two curve values. Hall's correlation is illustrated by performing a parametric analysis with the MED plant model in EES. The plant capacityis varied as an input parameter to calculate the total heat transfer area of the plant. Hall's correlation is very conservative at a TBT of 55 °C while it underestimates the investment costs at a TBT value of 85 °C. The TBT value of 70 °C still overestimates the investment costs compared to Loutatidou and Wittholtz, but follows their correlation the clost compared to the other two TBT values. Hall's correlation will be used in this study due to the fact that a cost value

Stellenbosch University https://scholar.sun.ac.za

can be related to the physical size of the plant, irrespective of the output (m^3/day) of the plant.

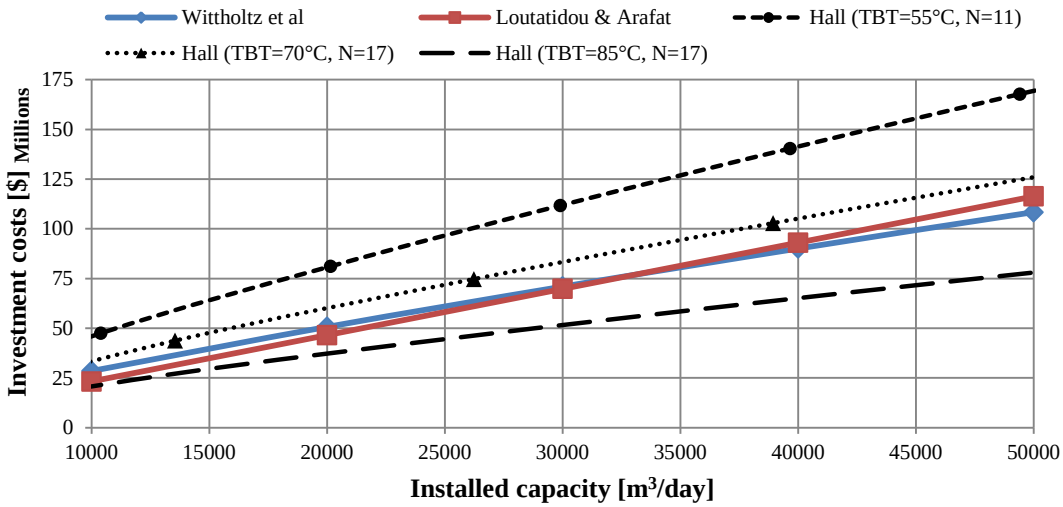

Figure 29: MED literature cost comparison

7.3 Pipeline

In the case of the CSP+MED scenario, a pipeline would be required to pump feed seawater inland to Arandis to the desalination plant. The reject brine is assumed to be pumped to solar stills/ salt pans in Arandis. There are several variables that influence the design of a bulk seawater pipeline including pumps, pumping stations, pipe material selection, pipe diameter sizing, repeated energy costs and operation and maintenance costs.

Choosing the suitable diameter of a pipeline is essentially a trade-off between operating costs and capital investment costs as shown by Figure 30(a). The costing function in Figure 30(b) for cast iron pipe diameters indicate that the investment costs rise steeply as the diameter increases. It is also important to keep in mind that a pipeline has a potential life time between 60 to 90 years (Swamee & Sharma, 2008: 88). Therefore the sizing of a pipeline is crucial in order to balance the capital and O&M costs in order to arrive at an optimal system configuration as shown in Figure 30(a).

Stellenbosch University https://scholar.sun.ac.za

Conversely, this model's simplicity of the pipeline model overlooks the details of all the components attributing to pipeline costs. A fixed overall cost in 3 million N$/km is used instead (NamWater, 2016).

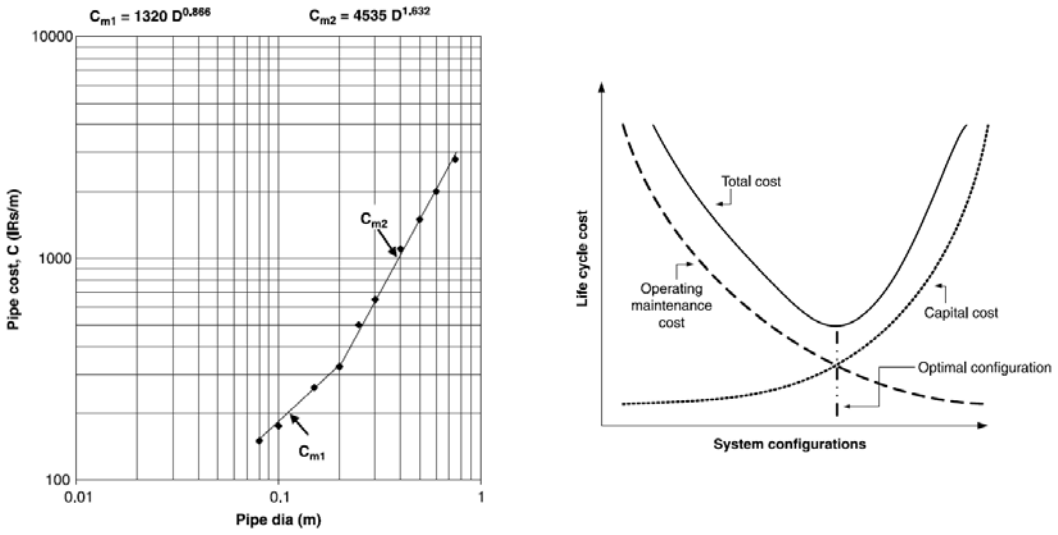

(a) (b)

Figure 30: (a) Costing of cast iron piping as a function of diameter, (b) variation of total cost with system configuration, (Swamee & Sharma, 2008: 88)

7.4 Levelized cost of electricity and water

A simplified constant dollar method, Equation (50),is used for calculating the LCOE and LCOW values (Walter Short, Daniel J. Packey & Thomas Holt, 1995: 57). This method makes the following assumptions:

- Constant annual output
- Constant O&M

$$LCOE = \frac{CAPEX_{tot} \times UCRF}{P_{annual}} + \frac{O\&M}{P_{annual}} \quad (50)$$

Where $CAPEX_{tot}$ is the total initial investment of the project, O&M the annual operation and maintenance done at the plant, P_{annual} the annual product output from the plant (kWh or m^3) and UCRF the uniform capital recovery factor.

Stellenbosch University https://scholar.sun.ac.za

The URCF is used to calculate the annual payment due to the lender by multiplying it with the initial capital investment and is calculated using Equation (51), with DR_n the nominal discount rate and n the plant life time cycle (25 years). The project nominal discount rates are 8.17% for NamPower and 11.41% for an independent power producer (IPP) investor (WSP, 2013). A conservative value of 11.41% is used.

$$\text{UCRF} = \frac{DR_n}{1-\left(\frac{1}{1+DR_n}\right)^n} \tag{51}$$

7.5 Summary

Given the high-level nature of this cogeneration study, the accuracy of the costing data used in the economic model should be sufficient to capture the relative difference between the CSP+MED plant configuration case studies.

The fixed investment cost values for the bulk water pipeline used in this study may not necessarily accurately reflect the actual costs as the costing data from NamWater does not consider seawater transportation.

Using Hall's correlation for the MED costs do follow other costs in the literature, but depending on the TBT results in either a conservative or optimistic deviation. The greatest level of uncertainty lies with the MED economics. It is recommended that further work be done in the economic modelling MED desalination plants and the relationships between the capital costs and the required heat transfer area for a variety of selected materials.

Stellenbosch University https://scholar.sun.ac.za

8. Results

In this section the results of the dry-cooled reference plant and the five CSP+MED cases are discussed. The optimization of the dry-cooled Rankine cycle is done, followed by the sizing of the heliostat field and TES to deliver the minimum LCOE. The Excel CSP model is verified with a parametric study done in SAM by comparing the CF values of each model. The five CSP+MED configuration results also includes the sizing of the MED plant effects in order to achieve the minimum LCOW for each configuration. The performance ratio of the MED model in EES is also verified against known models in literature.

8.1 Sizing of dry-cooled CSP plant

8.1.1 Power block

The single difference between the Rankine cycles of each configuration is that the condensing temperature is altered. Each Rankine cycle is optimized using the procedure mentioned in Chapter 4; delivering the design point specifications used to size the MED desalination plant, heliostat field and storage. Figure 31, Figure 32 and Figure 33 illustrate the final results of the parametric studies performed until the Rankine efficiency reached convergence with a value of 43.49 %.

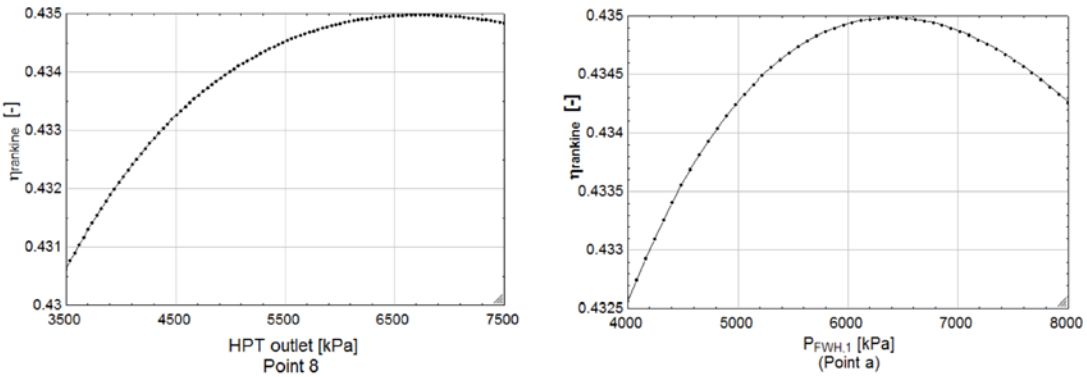

(a) (b)

Figure 31: Parametric study to determine the optimal (a) pressure outlet for the HPT and (b) the bleeding pressure for the first closed FWH

Stellenbosch University https://scholar.sun.ac.za

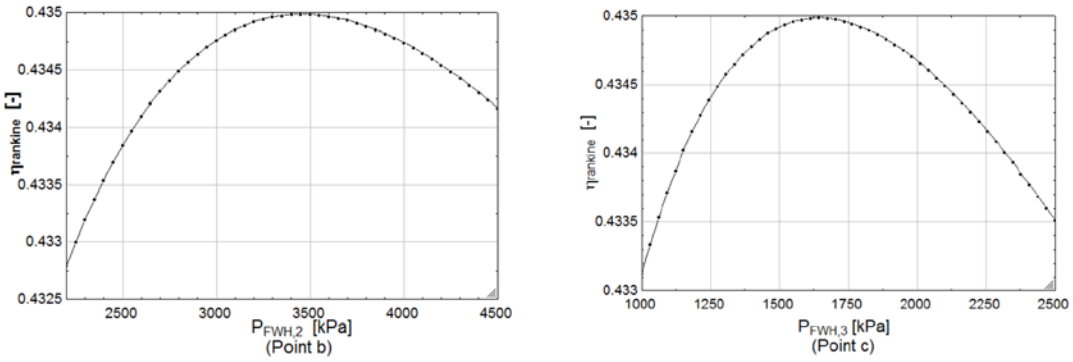

(a) (b)

Figure 32: Parametric study to determine the optimal bleeding pressures for (a) the second closed FWH and (b) the direct contact FWH (deaerator)

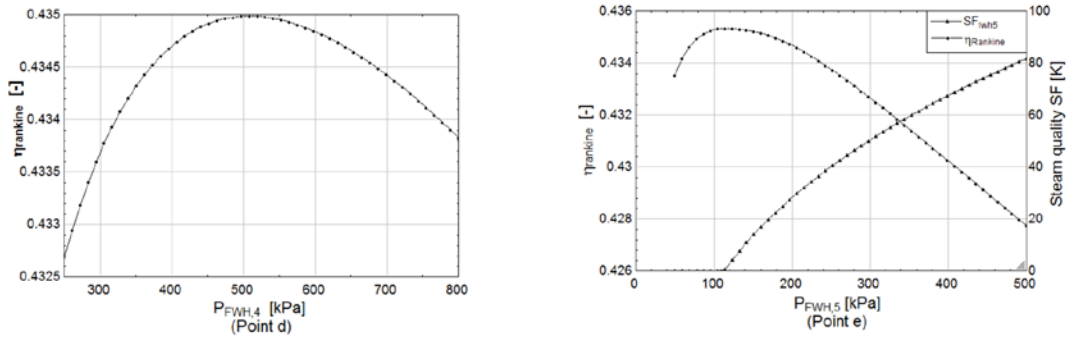

(a) (b)

Figure 33: Parametric study to determine the optimal bleeding pressures for (a) the third closed FWH and (b) the fourth closed FWH

The outlet pressure of the HPT and the feed water heating pressures along with the steam mass flow fractions are summarized in Table 17 in Appendix D. Results. Refer back to the Rankine cycle diagram (Figure 16) regarding the numbering locations of the parameters in Table 17. The two main outputs required from the power block model is the saturated steam mass flow rate exiting the low pressure turbine as well as Rankine cycle efficiency which defines the required heat input. The key outputs of the dry-cooled Rankine cycle are summarized in Table 7. As the ambient dry-bulb temperature varies during operation, the cycle efficiency varies and the required heat input also changes.

Stellenbosch University https://scholar.sun.ac.za

Table 7: Dry-cooled Rankine cycle at design point conditions

Parameter	Value
Condensing temperature, design point [°C]	58.9
Rankine efficiency, design point [%]	43.49
Total steam mass flow rate [kg/s]	89.26

Using linear regression, the second order polynomial in Equation 42 was derived and relates the cycle efficiency to the changing dry bulb temperature. The linear regression fit correlates very well as seen in Figure 34 and has a coefficient of determination value (R^2) of 98.28 %. This polynomial is incorporated into the Excel CSP model to calculate the hourly heat input requirement to run the power block at full load.

$$\eta_{Rankine} = 0.640017 - 0.0000983578T_{db} - 0.00000184328T_{db}^2 \quad (52)$$

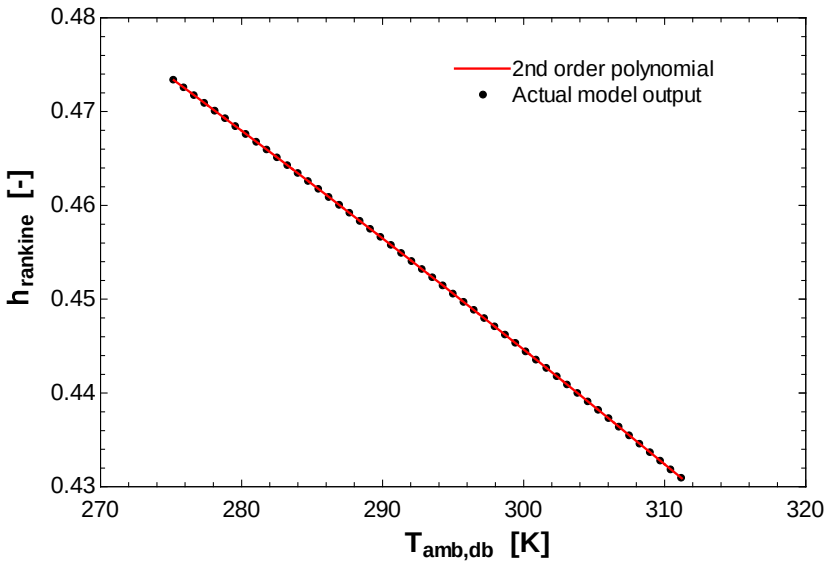

Figure 34: Linear regression fit for dry-cooled Rankine cycle efficiency

Stellenbosch University https://scholar.sun.ac.za

8.1.2 Heliostat field and storage

The "Data Table" function in Excel is used to run a parametric study in which the heliostat field SM and full load hours of TES are varied as inputs, solving for the LCOE as the output parameter. The hours of TES are incremented by 0.5 between 0 and 24, while the SM values are incremented by 0.2 between 1 and 4. In Figure 35 below the drastic reduction in LCOE is observed when storage is implemented for a given SM.

There is however an optimal configuration in terms of TES and SM that will deliver the minimum LCOE value. A SM of 3.3 and 13.5 hours of TES gives the absolute minimum LCOE for the dry-cooling plant given the resolution of the parametric study.

Using the same parametric study to determine the minimum LCOE, the capacity factor (CF) is also a selected output parameter and is illustrated in Figure 36. The results of the plant CF are not used for the sizing of the plant in this study. It merely gives some insight to how the SM and a TES influences the annual plant performance.

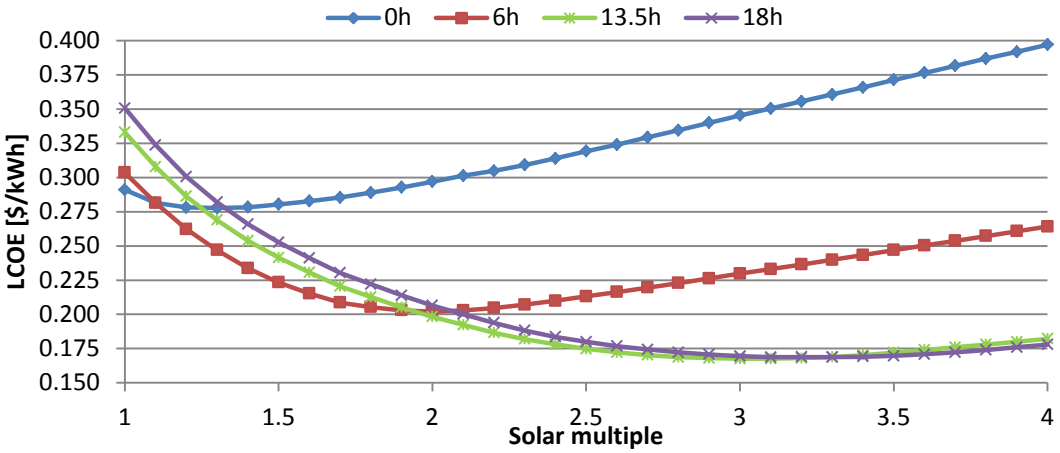

Figure 35: Dry-cooled parametric study results, levelized cost of electricity

Stellenbosch University https://scholar.sun.ac.za

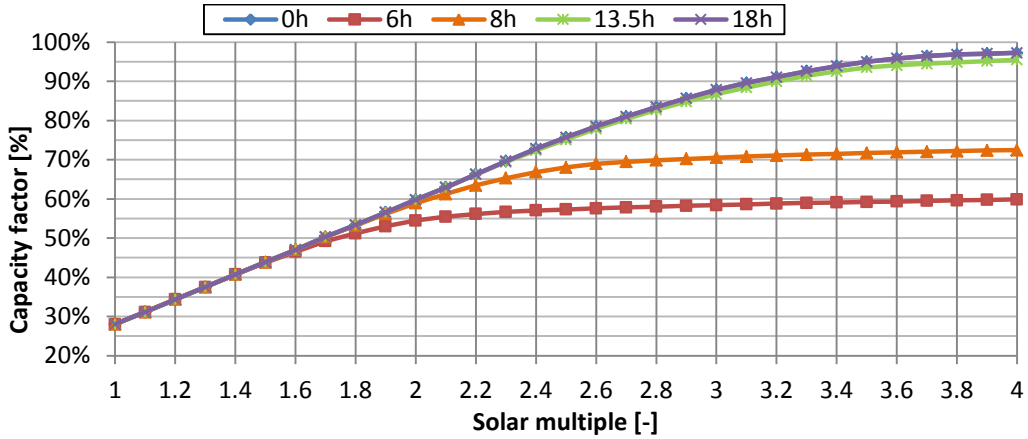

Figure 36: Dry-cooled parametric study results, capacity factor

8.2 Sizing of CSP+MED plant configurations

8.2.1 Power block

A MED desalination plant is integrated into the power block to serve as the condenser for the steam exiting the LPT. In each CSP+MED case the steam exiting the LPT condenses at the saturation temperature equal to the sum of MED plant's top brine temperature (TBT) and the terminal temperature difference (TTD). The optimization procedure described in Chapter 4 is used to optimize each Rankine cycle case.

In Appendix D. Results, the HPT outlet pressures and the bleed-off pressure locations for the open and closed feed-water heating are summarized Table 18, while Table 19 summarizes the steam mass flow rate fractions defining the amount of steam bled for each feed-water heating location.

The key output parameters of the CSP+MED Rankine cycles are summarized in Table 8 and are used as input values in the Excel CSP model. The quality of the steam exiting the LPT is not fully saturated steam. It is assumed that only the remaining saturated steam is sent to the MED plant, serving as the heating source of the first effect. As the Rankine efficiency decreases, a greater steam mass flow rate is required to produce an equal gross electricity output.

Stellenbosch University https://scholar.sun.ac.za

Table 8: Once-through cooled Rankine cycle outputs

Parameter	TBT= 55 °C	TBT= 62.5 °C	TBT= 70 °C	TBT= 77.5 °C	TBT= 85 °C
Condensing temperature [°C]	57.5	65	72.5	80	87.5
Rankine efficiency [%]	43.68	42.73	41.78	40.81	39.84
Steam quality exiting LPT [%]	93.14	94.25	95.42	96.49	97.46
Total steam mass flow rate [kg/s]	87.43	89.41	91.13	93.95	96.59
Saturated steam exiting LPT [kg/s]	54.3	57.1	60.1	63.25	66.37

8.2.2 Heliostat field and storage

Similar as with the dry-cooled case, the heliostat field SM and TES is sized by performing a parametric study. The resulting configuration that produces the minimum LCOE values for all the CSP+MED cases is a SM of 3.3 and a TES system of 14 hours. Similar trends are observed in the parametric study results, the LCOE curves slightly shifts down as the TBT is lowered. Lowering the TBT slightly shifts each curve on the LCOE graph downwards as a consequence of the slight increase in the CF. The sizing results of the heliostat field and TES for the CSP+MED configurations are summarized in Table 9. It can be seen that although the SM and TES values for each configuration are the same, the amount of heliostats and TES storage volume increase. This is due to every configuration having a different thermal energy input requirement, because of varying condensing conditions.

Table 9: Heliostat field and TES sizing for CSP+MED plant configurations

Parameter	Dry-cooled	TBT= 55 °C	TBT= 62.5 °C	TBT= 70 °C	TBT= 77.5 °C	TBT= 85 °C
SM [-]	3.3	3.3	3.3	3.3	3.3	3.3
Heliostat field aperture area [mil m^2]	1.492	1.485	1.518	1.553	1.590	1.628
TES [hours]	13.5	14	14	14	14	14
TES [GWh_{th}]	3.103	3.205	3.276	3.350	3.430	3.513
CF [%]	91.4	89.5	89.5	89.5	89.5	89.5
LCOE [$/kWh]	0.166	0.170	0.172	0.175	0.177	0.180

Stellenbosch University https://scholar.sun.ac.za

8.2.3 MED plant and pipeline sizing

After the SM and TES values have been optimized for the CSP plant, the MED plants need to be sized in terms of the number of effects used. The performance ratio increases with the number of effects, however so does the specific area. Consequently, there is a trade-off that needs to be made in terms of performance and capital cost in order to reach the minimum LCOW.

Top brine temperature at 55 °C

Considering a top brine temperature of 55 °C and limiting the minimum temperature difference between effects to be 1.5 °C, restricts the maximum amount of effects in this configuration to be 11 as illustrated in Figure 37. Consequently the lowest LCOW is reached at the maximum number of effects in this case as shown in Figure 38.

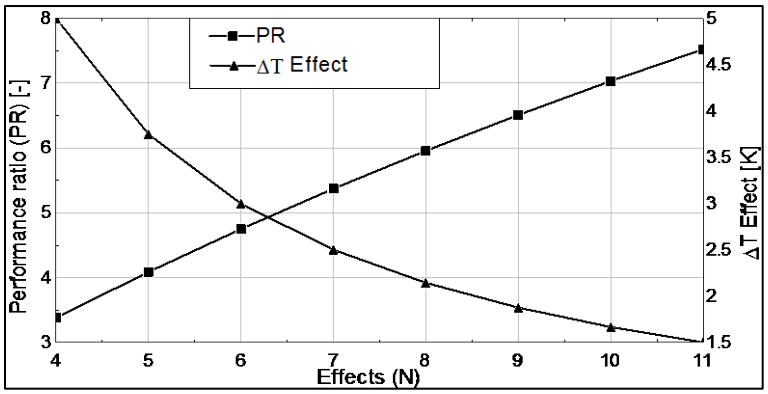

Figure 37: Parametric results of PR vs. effects, TBT = 55 °C

Stellenbosch University https://scholar.sun.ac.za

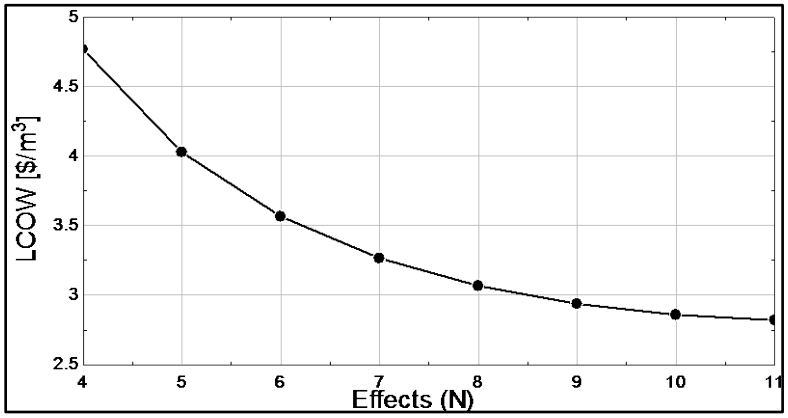

Figure 38: Parametric results of LCOW vs. effects, TBT = 55 °C

Top brine temperature at 62.5 °C

Considering a top brine temperature of 62.5 °C and limiting the minimum temperature difference between effects to be 1.5 °C, restricts the maximum amount of effects in this configuration to be 16. The minimum LCOW is achieved using 14 effects as illustrated in Figure 39. The PR could be increased further by adding additional effects as illustrated in Figure 40; however the exponential increase in specific area (SA) outweighs the economic benefits of additional water production.

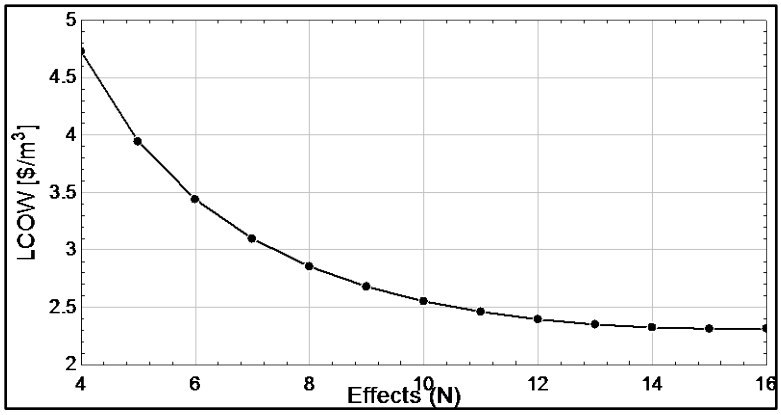

Figure 39: Parametric results of LCOW vs. effects, TBT = 62.5 °C

Stellenbosch University https://scholar.sun.ac.za

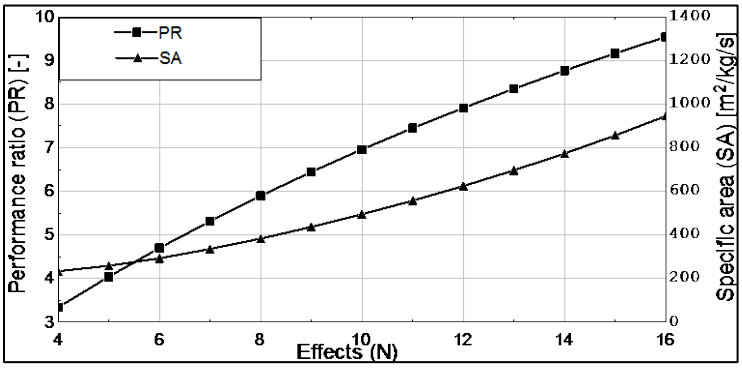

Figure 40: Parametric results of PR and SA vs. effects, TBT = 62.5 °C

Top brine temperature at 70 °C

A top brine temperature of 70 °C has a limit of 21 effects if the minimum temperature difference between each effect is restricted at 1.5 °C. However, in the case of a 15 °C temperature rise over the condenser (Fig 38) the usability ratio (UR) approaches a value over 1 at 18 effects. This implies more feed water enters the MED plant than is actually available, therefore the amount of effects in this case are restricted by the UR. Even if more water was pumped to address this issue, the preheating of seawater through the condenser would not be sufficient and additional heating would need to be supplied.

Decreasing the temperature rise over the condenser to 10 °C requires more heat from the preheating process leaving less available heat for the evaporating processes and consequently lowers the PR as seen in Figure 41. In this case the effects are not restricted by the UR, but the system delivers a less efficient process at a higher cost. The lowest LCOW is attained at 17 effects with a 15 °C temperature rise over the condenser.

Stellenbosch University https://scholar.sun.ac.za

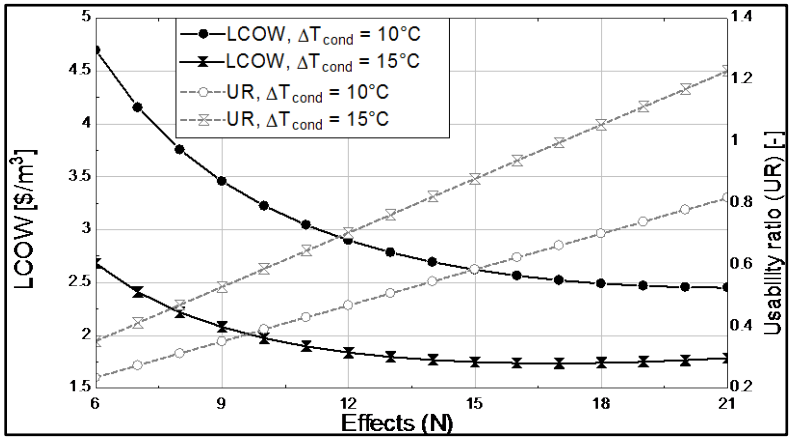

Figure 41: Parametric results of LCOW and UR vs. effects, TBT = 70 °C with various temperature rises over the condenser

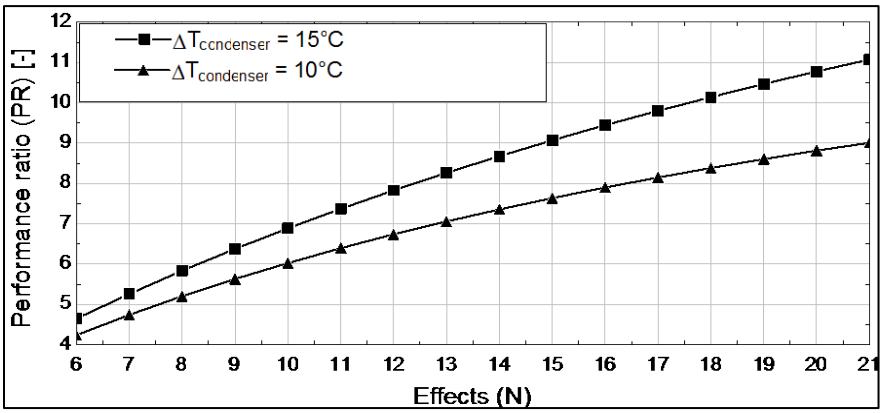

Figure 42: Parametric results of PR vs. effects, TBT = 70 °C with various temperature rises over the condenser

Top brine temperature at 77.5 °C

In this case the maximum number of effects that can be included in the MED system is also restricted by the UR as in the case where the TBT = 70 °C. The lowest LCOW for this scenario is found with 17 effects and has a UR approaching a value of 1, consequently minimizing the pumping costs. The highlighted area in Figure 43 and Figure 44 indicates the region where the design is not feasible.

Stellenbosch University https://scholar.sun.ac.za

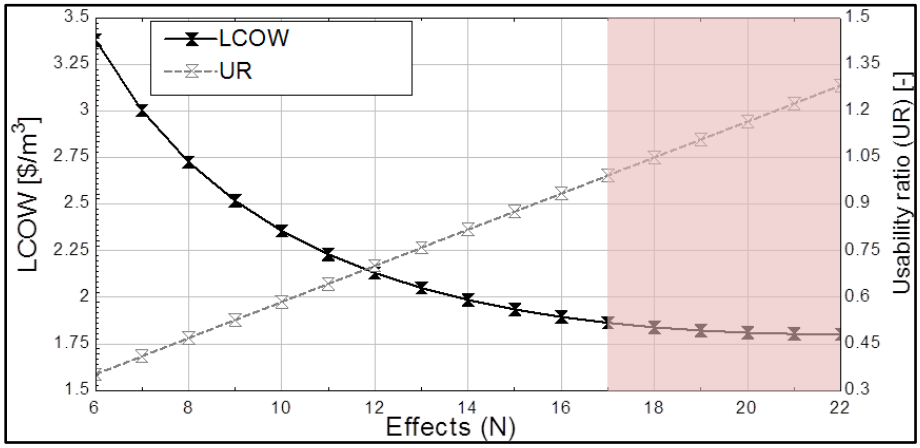

Figure 43: Parametric results of LCOW and UR vs. effects, TBT = 77.5 °C

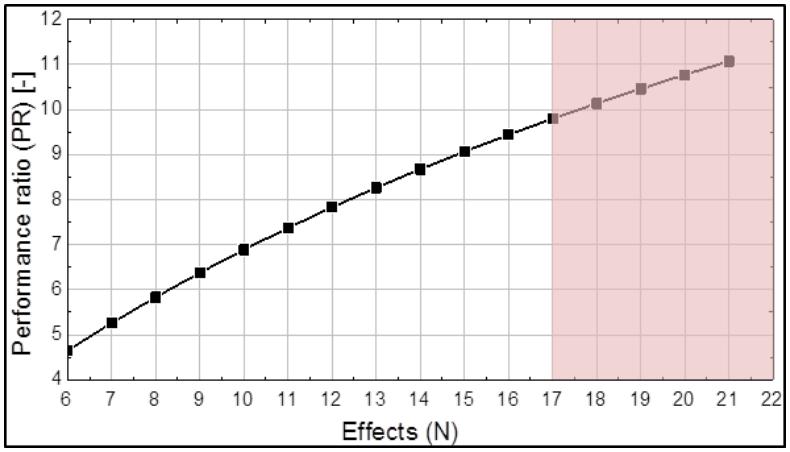

Figure 44: Parametric results of PR vs. effects, TBT = 77.5 °C

Top brine temperature at 85 °C

As with the TBT = 70 °C and TBT = 77.5 °C cases the restriction of the number of effects in this scenario is 17 as illustrated in Figure 45 by the UR correlation. The PR in this scenario experiences a slight decline compared to the previous two scenarios having an equal number of effects. It is deduced that this configuration is slightly less efficient compared to the two previous scenarios.

Stellenbosch University https://scholar.sun.ac.za

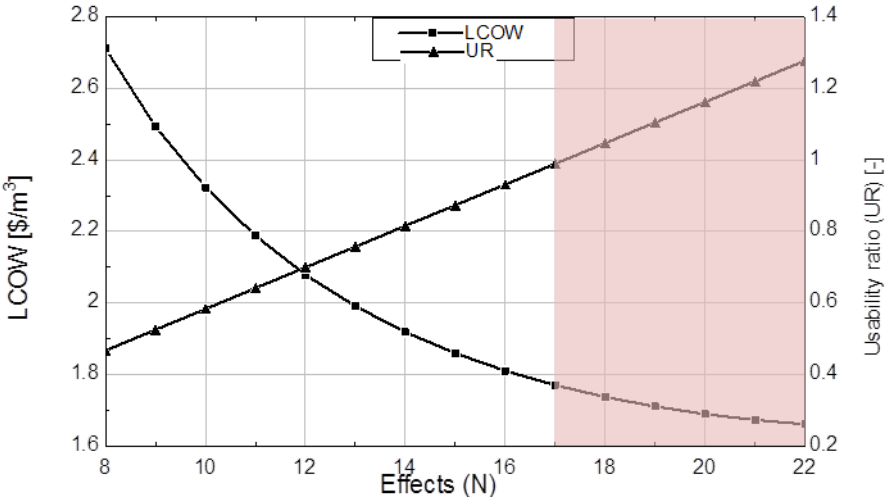

Figure 45: Parametric results of LCOW and UR vs. effects, TBT = 85 °C

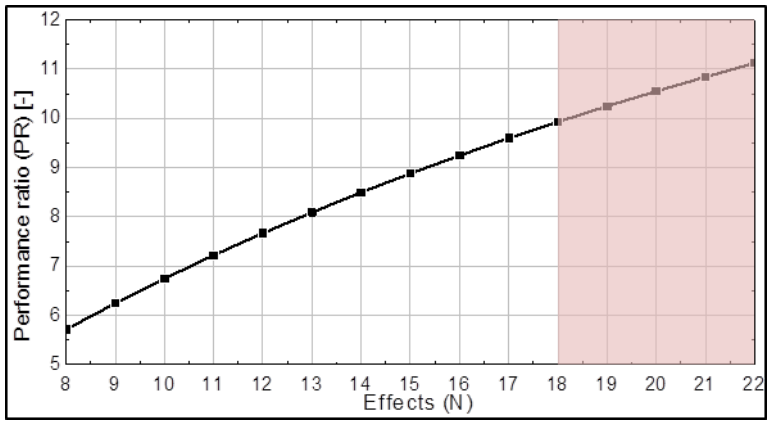

Figure 46: Parametric results of PR vs. effects, TBT = 85 °C

Table 10 is a summary of the performance parameters of each optimized MED configuration investigated. Case 1 is the least efficient configuration in terms of desalination having the lowest PR value. Also, the UR value indicates that 35% of the seawater pumped inland is only used for cooling purposes and rejected without entering the MED plant for desalination. Further investigation would be necessary to justify whether the gain in the cycle efficiency is worth the increased pumping costs. Case 3 at a TBT of 70 °C is the most efficient configuration having the highest PR and UR, while case 5 at a TBT of 85°C is the most economical using the least amount

Stellenbosch University https://scholar.sun.ac.za

of heat transfer area per unit distillate produced. Table 11 is a summary of the technical specifications of each CSP+MED plant configuration.

Table 10: MED configurations performance parameter summary

Parameter	**TBT = 55 °C**	**TBT = 62.5 °C**	**TBT = 70 °C**	**TBT = 77.5 °C**	**TBT = 85 °C**
Performance ratio [-]	7.52	8.76	9.79	9.69	9.59
Specific area [m^2/kg/s]	964.7	773.6	669.1	482.5	370.3
Usability ratio [-]	0.651	0.824	0.996	0.992	0.988

Table 11: MED configurations technical specifications summary

Parameter	**TBT = 55 °C**	**TBT = 62.5 °C**	**TBT = 70 °C**	**TBT = 77.5 °C**	**TBT = 85 °C**
Heating steam required [kg/s]	54.3	57.1	60.1	63.25	66.37
Effects [-]	11	14	17	17	17
Effect temp. difference [°C]	1.5	1.7	1.87	2.3	2.8
Heat transfer area (× 10^5) [m^2]	3.94	3.87	3.93	2.95	2.35
Pumping at full load [MW]	12.1	11.7	11.4	11.9	12.4
Seawater required [m^3/s]	1.508	1.458	1.418	1.483	1.546

8.3 CSP+MED plant performance summary

Figure 47 illustrates the trade-off that has to be made between the levelized cost of electricity and water. When the TBT of the MED plant is increased, the LCOE will increase linearly. Conversely, the LCOW will decrease with a steeper gradient, especially at lower TBT's. Varying the TBT between 55 °C and 85 °C the maximum increase in LCOE is only 5.5 % compared to a maximum 63.5% increase in LCOW. The LCOE and LCOW cost breakdown graphs in Figure 48 and Figure 49 illustrates why the LCOW is influenced considerably more than the LCOE with respect to the TBT.

Stellenbosch University https://scholar.sun.ac.za

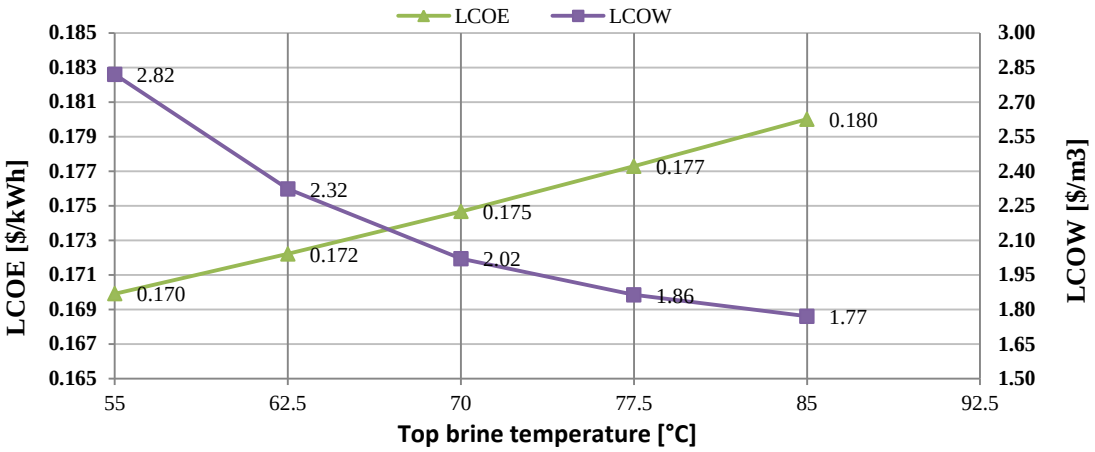

Figure 47: CSP+MED plant LCOE vs. LCOW value curves

Increasing the TBT of the MED plant essentially increases the outlet pressure of the LPT and consequently reduces the cycle efficiency which in turn requires additional thermal energy to run the CSP plant at the desired 100 MW_e capacity. A decrease in cycle efficiency requires the size of the heliostat field and TES capacity to increase, thereby increasing the LCOE as illustrated in Figure 48. The "Remaining CAPEX" also increases due to the 7 % contingency, 15 % sales tax and the 11 % EPC costs that are all a function of the direct capital costs.

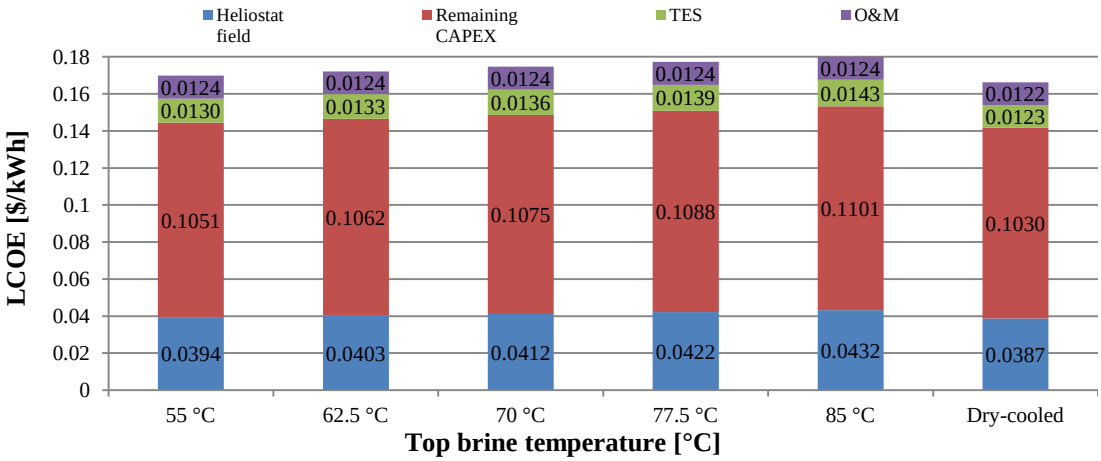

Figure 48: LCOE cost breakdown for CSP+MED vs. dry-cooled

Stellenbosch University https://scholar.sun.ac.za

Figure 49 depicts the LCOW cost breakdown for each respective CSP+MED case in terms of the set TBT. It is noted that the pumping of the required seawater contributes a significant amount of the total LCOW, varying between 40-49 %. A TBT of 85 °C delivers the lowest LCOW mostly due to the reduced capital cost required. However, the TBT of 70 °C entails the lowest pumping costs and can be attributed to this configuration having the highest UR and therefore pumping the least excess cooling-water.

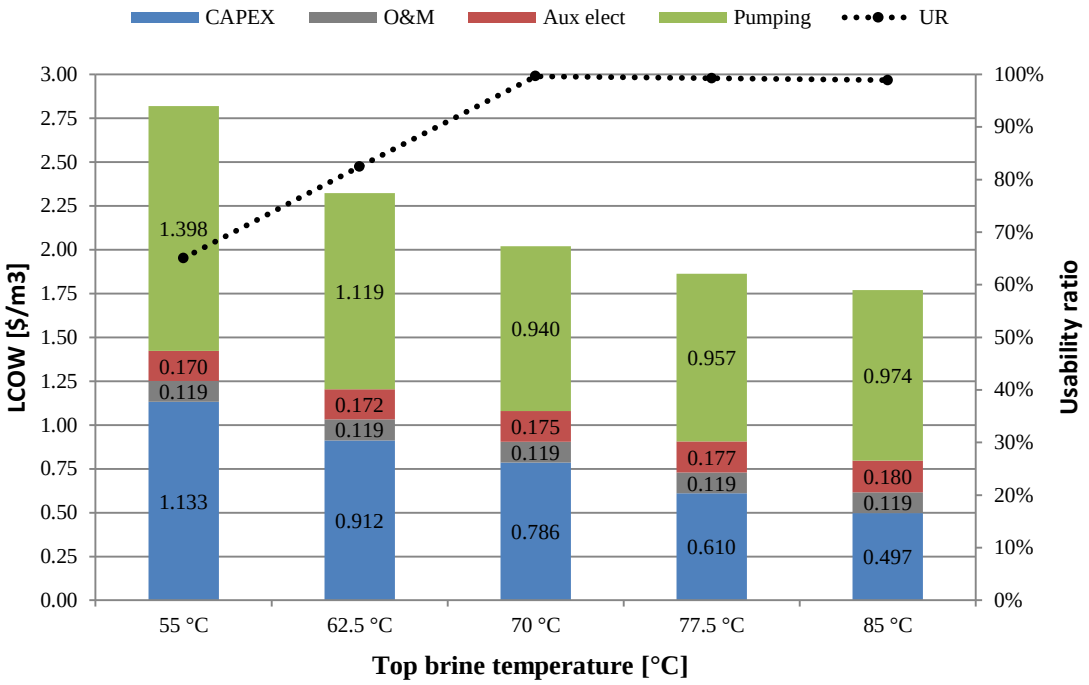

Figure 49: LCOW cost breakdown for CSP+MED configurations

The electricity consumption of the MED plant scenarios are compared to the electricity consumption of the existing Trekkoppje RO plant in Figure 50. The MED pumping power consumption excludes pumping the distillate inland to Arandis. It is noted that the TBT cases 70-85 °C seem to be comparable and would require slightly less electricity (<3.5 %) from the CSP plant. However, the integrated CSP+MED plant configuration also produces less electricity (<2 %) than the dry-cooled CSP plant as seen in Figure 51.

Stellenbosch University https://scholar.sun.ac.za

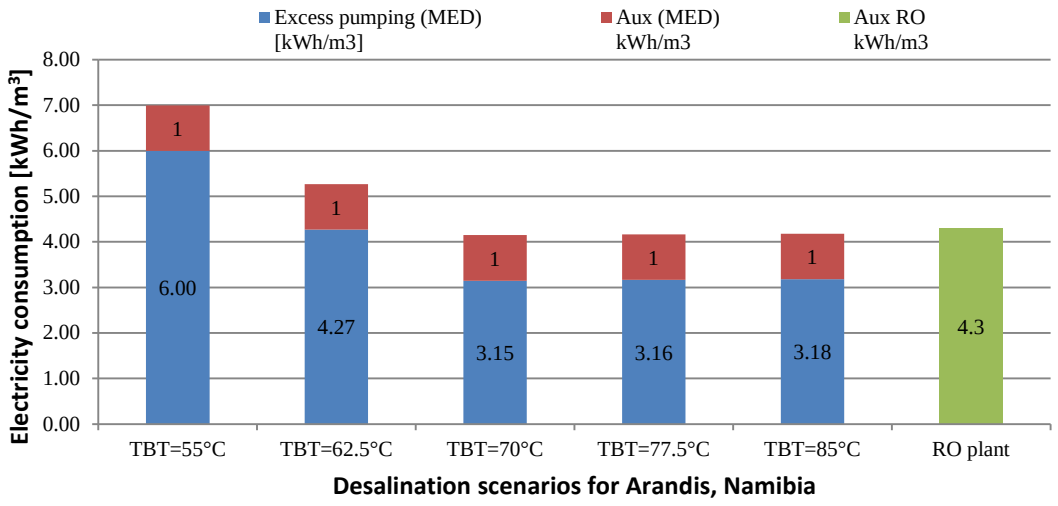

Figure 50: Electricity consumption scenarios for desalination for Arandis, Namibia

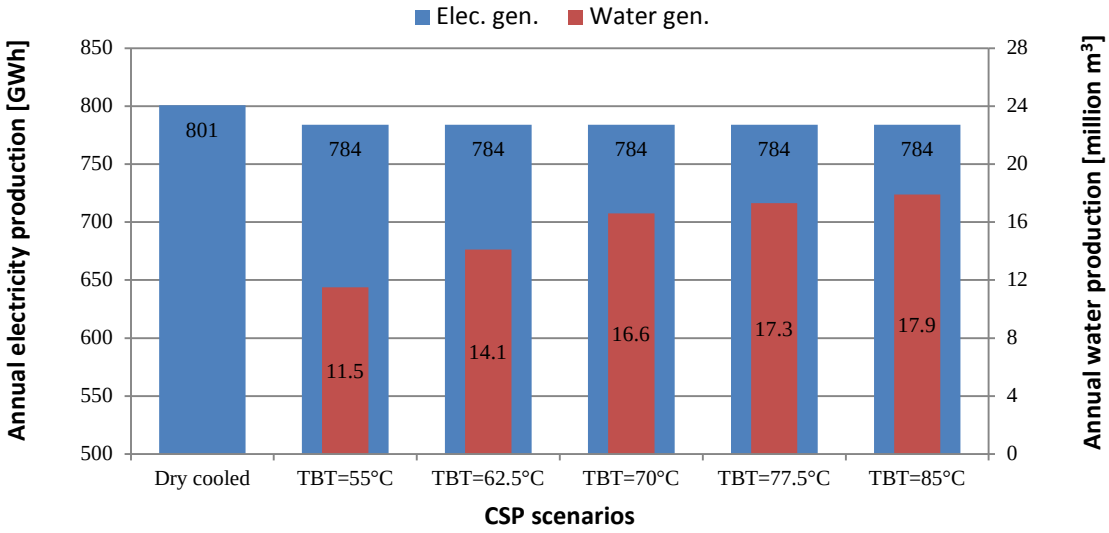

Figure 51: Electricity and water production of possible CSP scenarios in Arandis, Namibia

Stellenbosch University https://scholar.sun.ac.za

8.4 Sensitivity analysis

Due the uncertainty of some values in the model such as the discount rate, sales tax, capital investment costs, etc. it is necessary to identify the impact of these values within the model. A sensitivity analysis is performed to address this issue. In Figure 52 it is noted that the variability of the discount rate has a greater influence than the heliostat costs which can attribute over 40 % of the plant cost. What should also be kept in mind is that the discount rate variability may not change as much; however sales tax values between Namibia and the US differ by approximately 60 % and would therefore have a much greater variability impact on the LCOE.

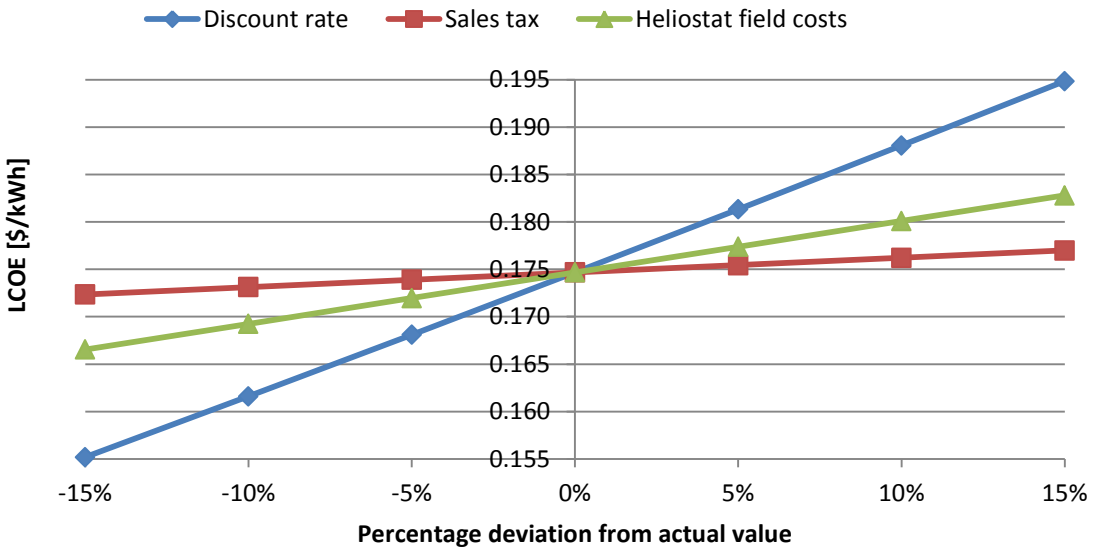

Figure 52: Sensitivity analysis on LCOE, TBT=70 °C

Stellenbosch University https://scholar.sun.ac.za

Due to the high pumping requirements of the CSP+MED plant, the LCOW is greatly dependent on the LCOE as can be seen in the sensitivity results in Figure 53. In this study it is assumed that the MED plant "buys" the electricity from the CSP plant at the LCOE cost. If revenue would be added the LCOW gradient in the sensitivity study would increase even further. MED plants are essentially very large heat exchangers made from expensive materials such as titanium, copper-nickel alloys, stainless steel etc. and the prices of these commodities can fluctuate aggressively with time. This is a risk that needs to be evaluated in the planning of MED plant projects. The cost of the pipeline is based on fresh water pipeline costs from NamWater and is expected to be more expensive due to corrosion that needs to be addressed. However, even if the cost doubles, the impact thereof is not as significant as the LCOE and capital investment.

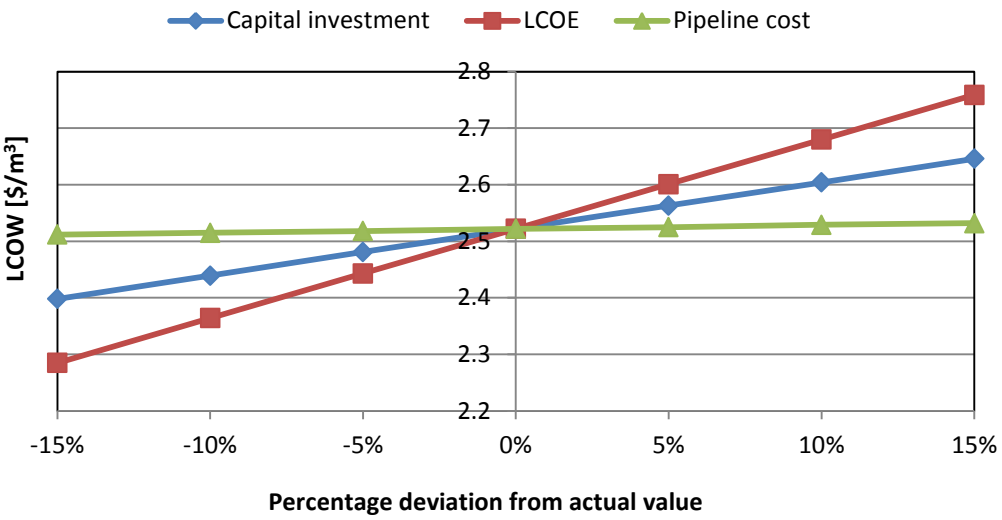

Figure 53: Sensitivity analysis on LCOW, TBT=70 °C

Stellenbosch University https://scholar.sun.ac.za

9. Conclusion

9.1 Summary

A steady-state MED desalination plant has successfully been modelled, closely following the approach of Mistry *et al.* (2012). The desalination plant was incorporated into the simplified CSP plant model, serving as the condenser as opposed to a dry-cooled scenario. A sensitivity analyses study was done in which the top brine temperature was varied between 55 °C and 85 °C in order to investigate the performance and economic implications of an integrated CSP+MED cogeneration plant. The LCOE and LCOW values were metrics to evaluate each top brine temperature scenario.

9.2 Conclusion

Given the assumptions of this model, the CSP+MED cogeneration plant appears to be a viable prospect relative to the dry-cooled reference case as the reduction on LCOE is relatively low. Choosing the optimal plant configuration is a compromise between the LCOE and LCOW values and will depend on the allocated price structures for water- and electricity sales, to generate the maximum possible revenue. The feasibility of such a plant would hinge on the CSP tariff structures to incentivise base load production.

Integrating a low-temperature thermal desalination plant with a CSP plant does affect the power block performance unfavourably in relation to the dry-cooled configuration. This might not always be the case as seen in from the study done in the Literature review chapter by CEIMAT-PSA where the CSP+MED configuration #1 illustrated higher cycle efficiencies as the dry cooled system configuration #4. The Rankine cycle efficiency impacts the number of heliostats required as well as the size of the TES, which in turn will affect the levelized cost of electricity. It is therefore suggested that one study cannot serve as a “template” for future CSP desalination studies. Each location will have different geographical, climate and RE policy conditions and will influence the optimal plant configuration for that specific site.

The high cost of pumping the seawater inland is considered the main disadvantage of this system. In contrast, locating the CSP+MED plant closer to the coastline will see a reduction in DNI and could have adverse effects on lifespan of plant components due to rust corrosion. Considering sustainability, additional desalination (solar ponds) and

Stellenbosch University https://scholar.sun.ac.za

the extraction of salt from the reject brine could potentially add value to such a cogeneration plant. Additionally, revision of the desalination plant capital cost approximation is recommended to ensure that overestimated costs at lower TBT's do not occur.

9.3 Recommendations

There is very little transparency regarding the cost breakdown of desalination plants with room for further investigation if further more detailed economic studies were to be done with less uncertainty. It is suggested that more work is to be done in order to capture the relationship between the increased costs of large heat exchangers for a variety of materials. A conservative approach has been followed in this study in which a titanium-stainless steel cost correlation from (Hall *et al.*, 1990) was used. As the temperature decreases in each effect, scaling and corrosion becomes less prominent and cheaper materials could be investigated.

The cost assumptions for the economic model of the CSP plant are predominantly reliant on values used in SAM. Discount, sales tax and land cost values were adapted for the Namibian context, however it is recommended that for further more detailed studies the cost assumptions should be scrutinized with care to provide more reliable results regarding the LCOE of the plant.

Integrating desalination directly with CSP for cogeneration makes the system dependent on a electricity source which may be prone to intermittency and therefore increased start-ups as opposed to be connected to the grid. In this study large SM's and ample storage has been used to reduce the amount of start-ups per year. It is suggested that a more dynamic model be used when investigating CSP systems with lower SM's and TES.

Although the combination of CSP and RO cannot technically be seen as cogeneration, as the RO desalination plant is not making use of waste energy from the CSP plant, a detailed study focusing on such a combination within the context of Namibia would add value to the work done in this study. Other less conservative alternatives such as CSP+RO+MED and even the addition of PV would also be approaches that could be worthwhile investigating.

Stellenbosch University https://scholar.sun.ac.za

Appendices

Stellenbosch University https://scholar.sun.ac.za

A. Literature review

A.1 Cogeneration studies

CSP+MED vs. CSP+RO (CEIMAT-PSA)

The four different integrations of CSP+D plants that were evaluated are:

- MED unit integrated into a PT-CSP plant: Configuration #1
- MED+TVC unit integrated into a PT-CSP plant: Configuration #2
- TVC-MED unit integrated into a PT-CSP plant: Configuration #3
- RO unit connected to a PT-CSP plant: Configuration #4

In configuration #1 (Figure 54) all the steam exiting the low pressure turbine is condensed in the first effect of the MED plant. Essentially the MED plant replaces the condenser of the power block. Instead of condensing all the steam from the low pressure turbine, configurations #2 and #3 merely makes use of extracting part of the steam; leaving the rest of the steam to pass through to the power block condenser. Configuration #4 is the combination of a RO plant receiving its electricity requirements from a conventional CSP plant.

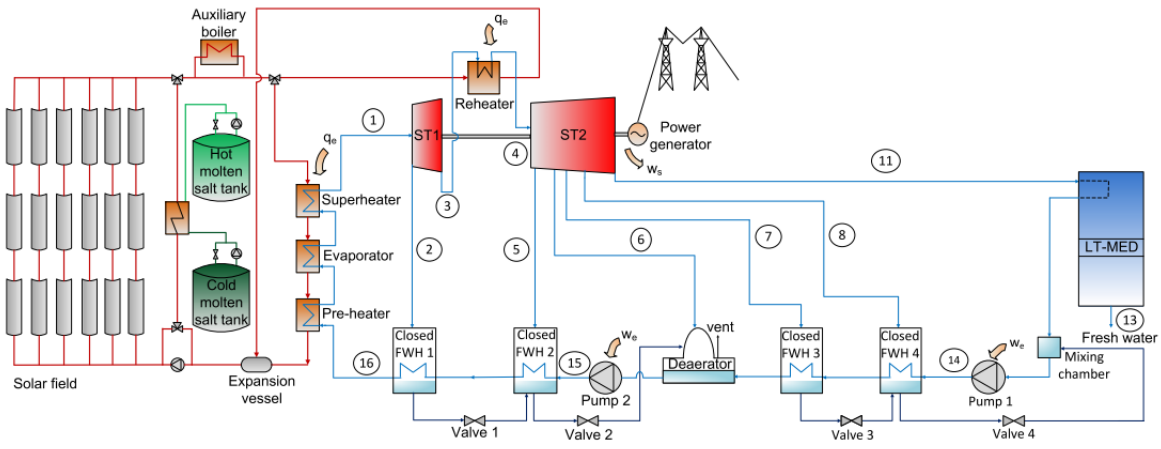

Figure 54: Flow diagram of configuration #1

Stellenbosch University https://scholar.sun.ac.za

The techno-economic analysis of each configuration was carried out for two locations, namely Abu Dhabi (United Arab Emirates) and Almería (Spain). The design point for both locations was set at the 21st of September at solar noon with the weather and geographical information of the selected sites is shown in Table 12. The analyses for all configurations except configuration #1 were performed for three different cooling technologies: once-through, evaporative water cooling and dry air cooling.

The thermodynamic analyses comprised of three main model components. The power cycle was modelled in EES and largely based on the operating conditions of the Andasol-1 CSP plant in Spain. The solar field and MED plant modelling were done separately in MATLAB and incorporated as required with the power cycle to run the simulations for each respective configuration. The MED plant model used was developed by (Palenzuela, Hassan, Zaragoza & Alarcón-padilla, 2014) and based on the design and operational characteristics of the vertical stacked MED pilot plant at Plataforma Solar de Almería (PSA), Spain. The main design constraints of the CSP+D plants are shown in Table 13. The economic analysis was performed for a plant life span of 20 years to determine the levelized cost of electricity and water respectively. The main input figures for the cost model are shown in Table 14.

Table 12: Weather and geographical information of Abu Dhabi and Almería

Parameter	**Abu Dhabi**	**Almeria**
DNI [kWh/m^2/year]	1925	1990
Seawater temperature [°C]	35	25
Elevation [m]	150	150
Distance from coast [km]	60	60

Table 13: CSP+D plant technical specifications

Parameter	**Abu Dhabi**	**Almeria**
CSP net electricity output [MW$_e$]	50	50
CSP thermal storage [hours]	6.5	6.5
CSP+D plant availability [%]	0.96	0.96
MED number of effects [-]	12	14
MED spec elec. cons. [kWh/m^3]	1.5	1.5
RO spec elec. cons. [kWh/m^3]	4	3

Stellenbosch University https://scholar.sun.ac.za

Table 14: CSP and desalination plant cost figures

Parameter	Value
Land preparation and infrastructure	15 $/m^2
Solar collector	150 $/m^2
Heat transfer fluid and hydraulic circuit	90 $/m^2
Thermal storage system	35 $/kWh$_{th}$
Power block	1000 $/MW$_{gross}$
Auxiliary gas burner	60 $/kW$_{th}$
Reverse Osmosis plant	1207 $/(m^3/day)
Multi-effect Distillation plant	1230 $/(m^3/day)

The plant thermal efficiencies, levelized electricity costs and levelized water costs of each configuration are illustrated in Figure 55 to Figure 57. In Abu Dhabi, plant configuration #1 has the highest thermal efficiency along with the lowest levelized electricity cost. However it has a higher levelized water cost compared to configuration #4, mainly due to the increased capital costs of MED compared to RO technologies. In Almeria, configuration #4 has the highest thermal efficiency along with the lowest levelized water cost. Nonetheless, configuration #1 indicates a lower levelized electricity cost due to the higher gross power required in configuration #4; 62.42 MW_e against 56.08 MW_e. The drawback of reduced power production due to higher pressure of the exhaust steam at the LPT is less of a disadvantage than the additional electricity required in configuration #4 for the RO plant and condenser system.

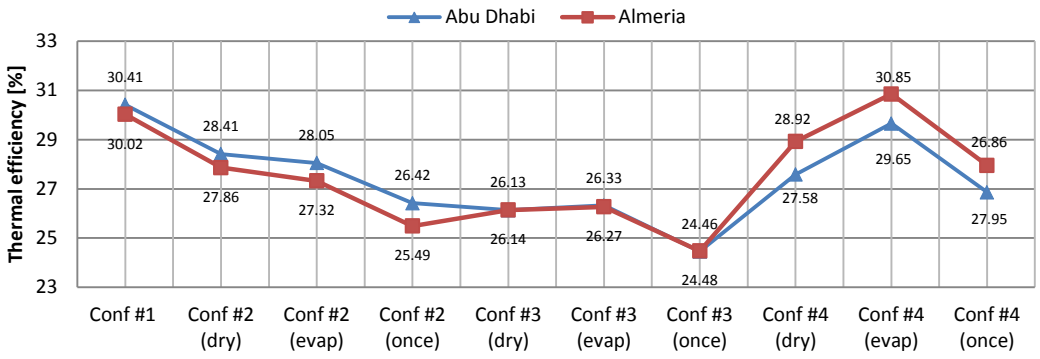

Figure 55: Thermal efficiency results of configurations #1 to #4

Stellenbosch University https://scholar.sun.ac.za

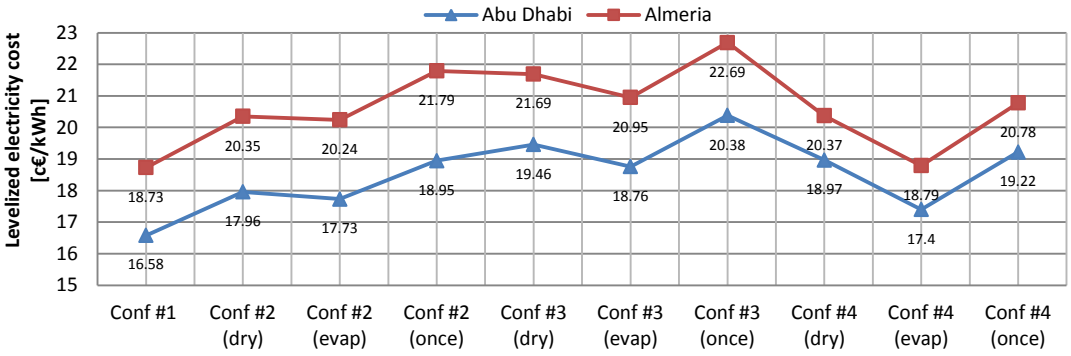

Figure 56: Levelized electricity cost results of configurations #1 to #4

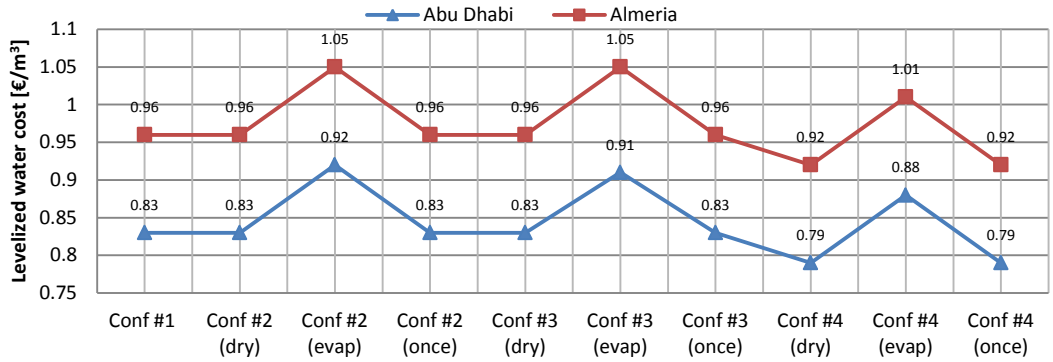

Figure 57: Levelized water cost results of configurations #1 to #4

CSP+MED vs. CSP+RO (DLR)

A methodology was developed in order to find the most suitable areas for a CSP+D plant. Suitable locations were not just based on the site DNI potential and were excluded if any one of the following criteria was met:

- Terrain slope > 2.1 % or Shifting sands and dunes
- Irrigated cropland, forests or protected areas
- Water bodies or permanently flooded areas
- Urban areas or infrastructure

Stellenbosch University https://scholar.sun.ac.za

The data derived from the assessment criteria were utilized to generate the map in Figure 58 that illustrate the potentially suitable sites for the CSP+D plants as well as the DNI.

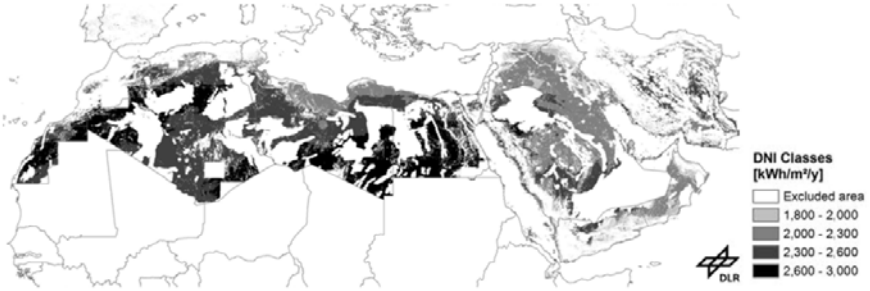

Figure 58: Potential of concentrating power in the MENA region, (Moser *et al.*, 2013)

Another condition that had to be met for the CSP+D plant location was that the site had to be within 5km from the shore with an elevation not exceeding 20m above sea level. The study focus is on the prospective consideration of integrated CSP and desalination plants for the entire MENA region. Four possible configurations are investigated, namely:

12. CSP-MED located at the coast, Figure 59(a)
13. CSP-RO plant at the coast with once-through cooling located near desalination plant, Figure 59(b)
14. Decoupled combination of RO at coast and dry cooled CSP plant located inland
15. RO at the coast with dry cooled CSP plant and solar only operation (no fossil fuel backup)

The CSP+D plant configurations were designed for a base load operation of 8000 hours per year assuming that if no energy is available from the solar field or storage, that the deficit would be filled with fossil fuels. A two-tank molten salt storage system with a capacity of 7.5 hours at full load operation is added to the power cycle. The desalination capacity is 100000 m^3/day with a net power production of 90 MW_e for all four configurations. The four configurations are evaluated at the following two different DNI classes:

- Medium irradiance: 2000kWh/m^2/year on the coast and 2400kWh/m2/year inland
- Excellent irradiance: 2400kWh/m2/year on the coast and 2800 kWh/m2/year inland

Stellenbosch University https://scholar.sun.ac.za

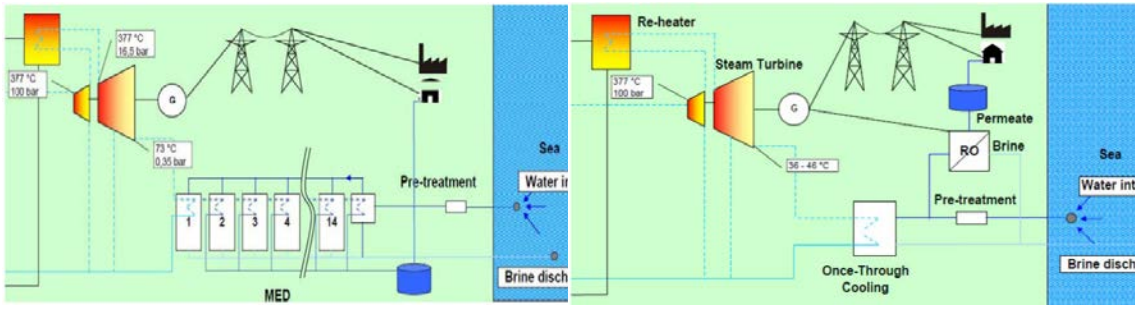

(a) (b)

Figure 59: (a) CSP-MED plant scheme and (b) CSP-RO plant scheme

The levelized electricity and water costs were done based on the assumption of a 25 year plant life cycle period. The cost of steam from the MED plant is also taken into account, and the energy associated with the extracted steam is considered with respect to the loss of electric power that would otherwise be used for further electricity generation.

The LCOE results in Figure 60(a), using heavy fuel oil as the back-up fuel, found that the CSP-RO with once-through cooling has a lower LCOE than the equivalent CSP-MED plant. Case 4 can be seen to be more sensitive to DNI variations and is attributed to its solar-only operation.

Figure 60(b) illustrates the variance in LCOW for different seawater properties and using natural gas as the back-up fuel. Seawater RO is cheaper in the Red Sea than in the Arabian Gulf. MED is the cheaper option in the Arabian Gulf due to its robust behaviour against higher seawater salinity and temperature. During high fluctuations in seawater quality, temperature and the presence of algae bloom, MED could appear preferable to RO.

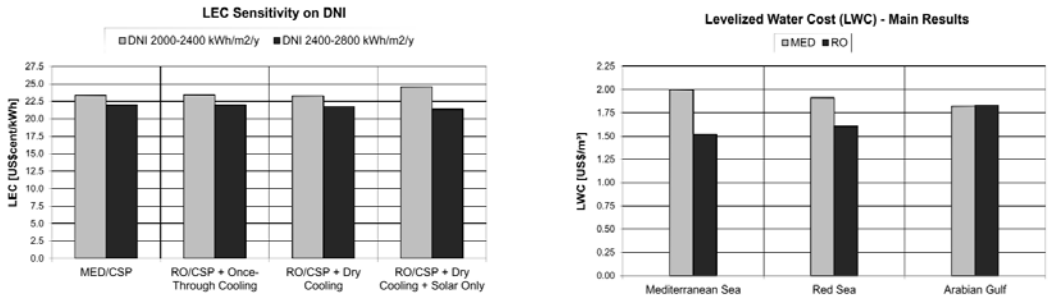

(a) (b)

Figure 60: (a) LCOE as a function of DNI and (b) LCOW of RO

Stellenbosch University https://scholar.sun.ac.za

Solar desalination in Chile

In the conventional RO + grid configuration, water is desalinated via reverse osmosis at the coastline and pumped inland to the consumer location using electricity from the grid for all processes. The first alternative is using a combination of RO + PV where sea water is pumped up to the consumer location using grid electricity and then desalinated via reverse osmosis driven by the PV plant. A second alternative is a cogeneration plant by integrating a MED plant and CSP tower with 15 hours of thermal storage. In this scenario all the electricity and heat requirements for the pumping and desalination plant are provided by the CSP tower plant. The rationale for placing the solar facilities at a high altitude nearby the consumer facility is that the solar resource in terms of direct normal irradiation (DNI) significantly improves from the coast moving inland.

A high-level modelling methodology is used for the simplified technical and business models of each configuration. The key technical aspects of each desalination configuration are summarized in Table 15 while the detailed list of all the assumptions and restrictions can be found in (Servert *et al.*, 2016). The pumping requirements are included in the electricity consumption and as a result of the slight excess electricity production of the CSP plant; the electricity consumption value is negative.

Table 15: Key technical and economic aspects of the compared solutions

Parameter	**RO + grid**	**RO + PV**	**MED + CSP**
Capacity factor, %	91	33	70
Solar investment cost, US$/($m^3$/year)	-	3	30
Desalination investment cost, US$/($m^3$/year)	4.5	13	5
Pumping investment cost, US$/($m^3$/year)	16	80	40
Operation and maintenance costs, US$/($m^3$/year)	2.4	3.7	1.6
Required land, m^2/(m^3/year)	n/a	<0.1	0.4
Desalinated water production, 10^6 m^3/year	7	3	6
Electricity consumption, kWh/m^3	9	18	-2

Stellenbosch University https://scholar.sun.ac.za

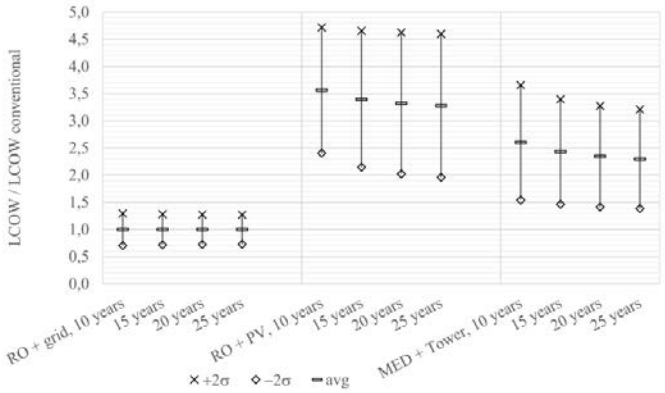

Figure 61: Estimated levelized cost of water for each configuration with varying lifetime scenarios

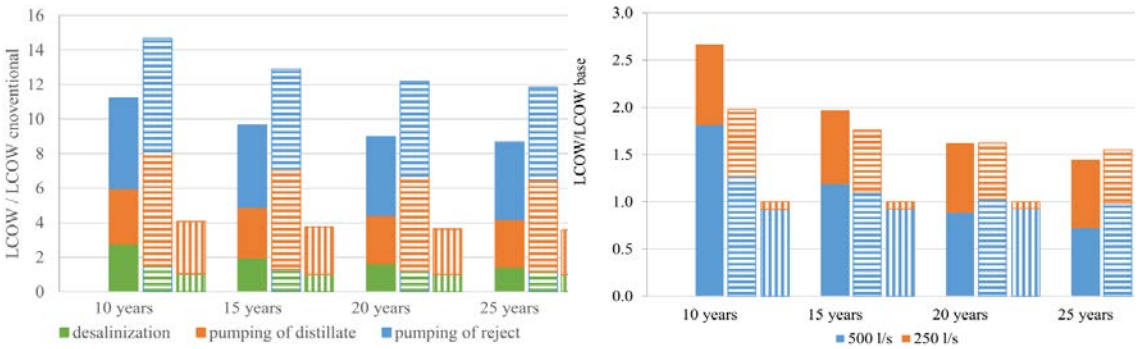

(a) (b)

Figure 62: (a) LCOW breakdown and (b) LCOW comparison when plant size is doubled for: MED + CSP tower (solid), RO + PV (horizontal) and RO + grid (vertical)

The study determined that solar desalination in the Atacama Desert in Chile could technically be feasible with MED + CSP being the most favourable option. The main issues being the high pumping requirements due to the high elevation of the site from the coast and could be compensated for by putting use to the leftover brine, i.e. extraction of salt. It should also be kept in mind that CSP tower technologies are still a new commercial technology and experiences annual cost reductions as CSP technologies advance and becomes more efficient and may become the preferable configuration in the near future.

Stellenbosch University https://scholar.sun.ac.za

Central receiver and MED

A parallel/cross flow configuration is chosen because of its higher performance ratio (PR) compared to other MED plant configurations. The plant components are modelled using mass and energy conservation laws.

A central receiver CSP plant with a two-tank molten salt storage system is also modelled in Scilab©. The heliostat field efficiency is modelled using the ray tracing software SolTrace© with the receiver efficiency characterised as a function of DNI, azimuth and elevation angles and wind velocity. The small scale power block comprises of a Rankine cycle without reheat or regenerative feed water preheating. The layout of the integrated CSP+D system is illustrated in Figure 63.

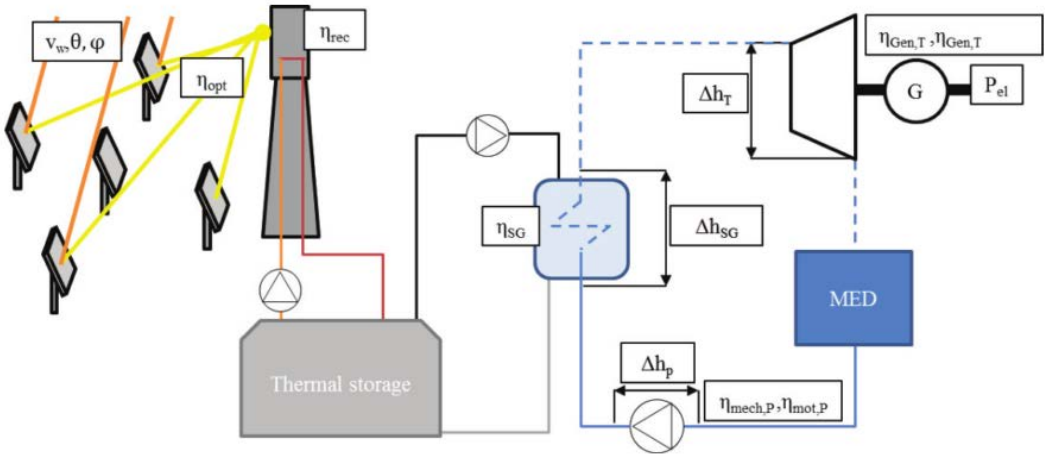

Figure 63: Schematic of CSP tower and MED cogeneration plant, (Frantz & Seifert, 2015)

The results of this study demonstrate the trade-off dynamics between the production of electricity and water in a cogeneration CSP+D plant. It found that the annual water production can be more than doubled when a higher heating steam temperature of 90°C is used as opposed to 65°C. The disadvantage of that approach is that 11% of the annual electricity production is lost. Alternatively, when increasing the total heat transfer area of the MED plant by 30%, the annual water production is increased by more than 50% and the electricity production is only reduced by 1%.

Stellenbosch University https://scholar.sun.ac.za

A.2 Central receiver plant modelling

Heliostat field

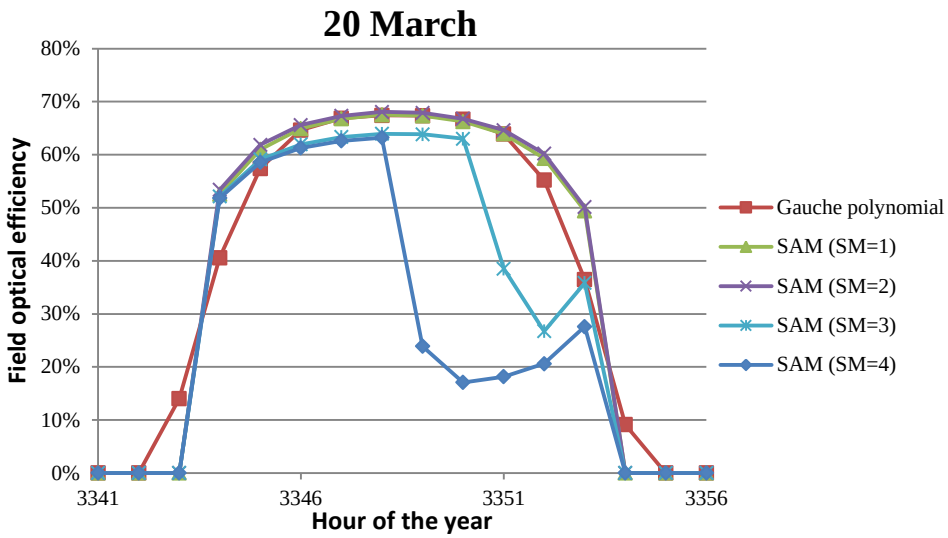

Figure 64: Field efficiency comparison at vernal equinox

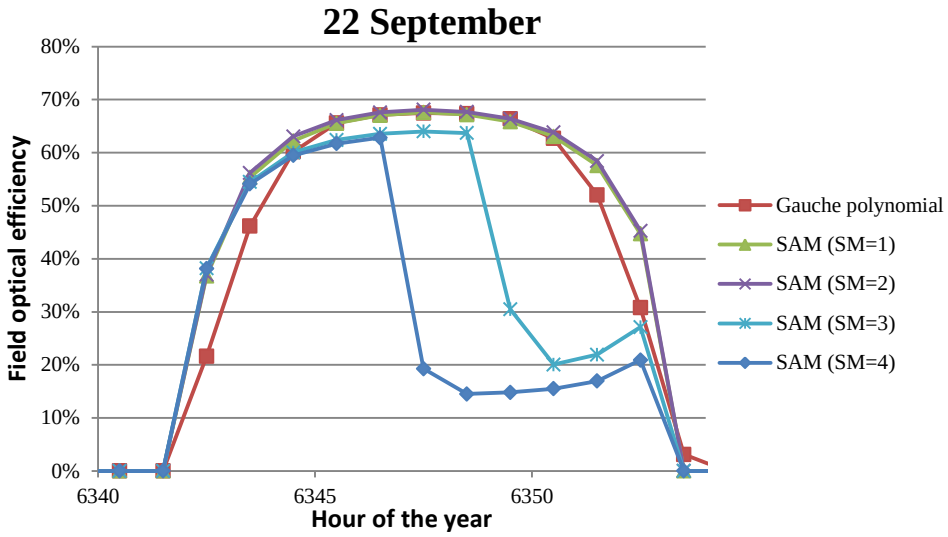

Figure 65: Field efficiency comparison at autumnal equinox (Dagget, CA)

Stellenbosch University https://scholar.sun.ac.za

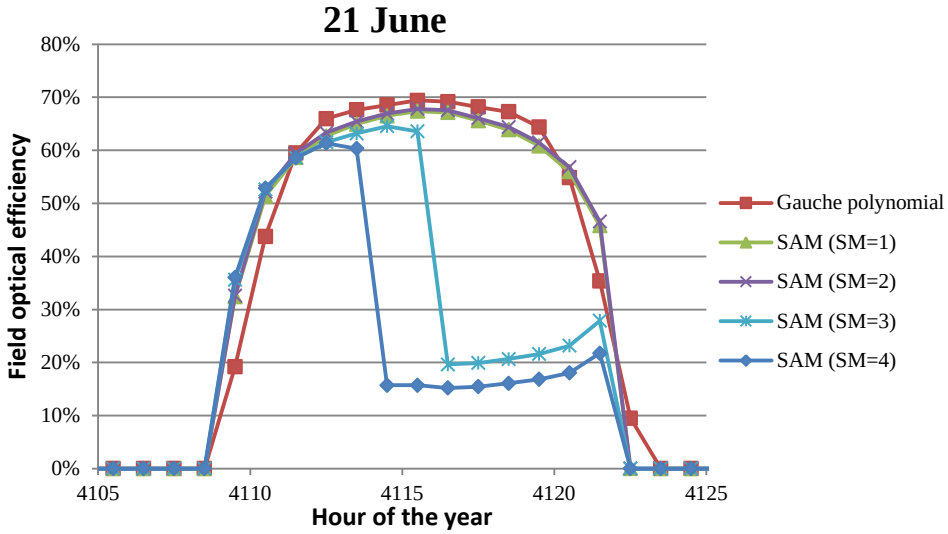

Figure 66: Field efficiency comparison at summer solstice (Dagget, CA)

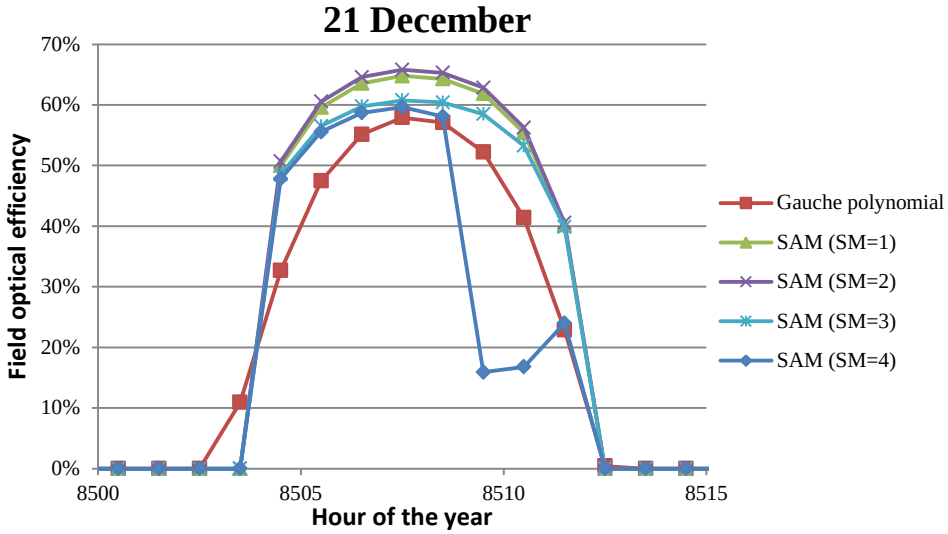

Figure 67: Field efficiency comparison at winter solstice (Dagget, CA)

Stellenbosch University https://scholar.sun.ac.za

A.3 MED model comparisons

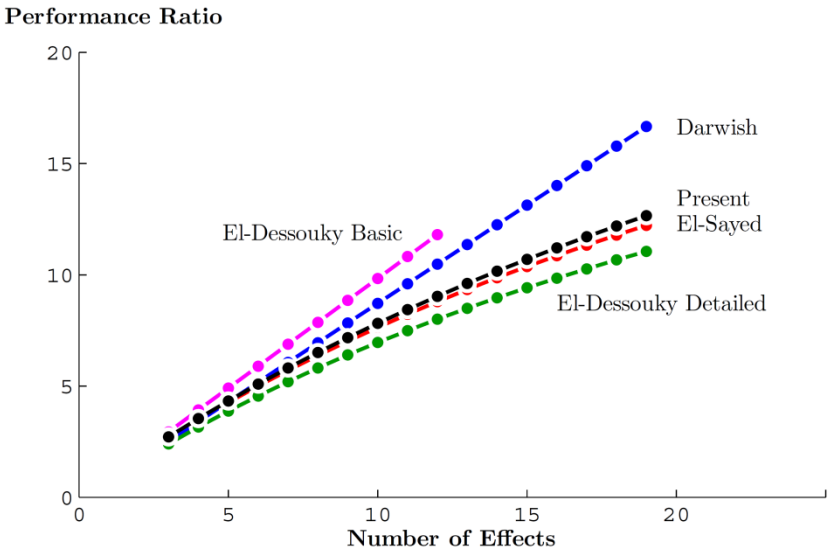

Figure 68: MED model comparison for PR vs. N

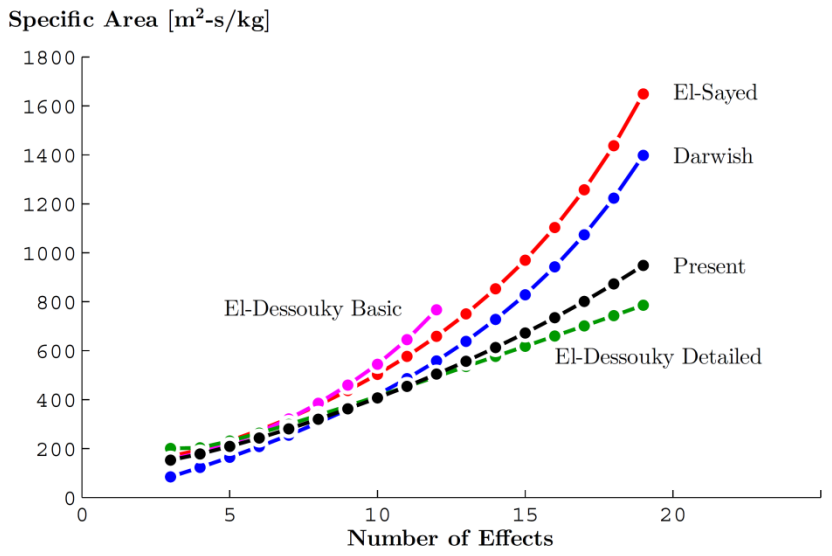

Figure 69: MED model comparison for SA vs. N

Stellenbosch University https://scholar.sun.ac.za

A.4 Heat transfer coefficient correlations

Fouled condenser, (El-Dessouky *et al.*, 1998)

$$U_c=1\times10^{-3}\left(16175+0.1537T+0.1825T^2-0.00008026T^3\right) \quad (53)$$

Fouled evaporator, (El-Dessouky *et al.*, 1998)

$$U_e=1\times10^{-3}\ (1939.4+\ 1.40562\ T\ -\ 0.0207525\ T^2\ +\ 0.0023186\ T^3) \quad (54)$$

Fouled condenser, (Takada & Drake, 1983)

$$U_c\ =0.8\ (3+0.05\ (T\ -\ 60)) \quad (55)$$

Clean drop-wise condenser, (Bromley & Read, 1970)

$$U_c=1\times10^{-3}\ (5186\ -\ 90.82\ T\ +\ 0.5566\ T^2\ -\ 0.0009159\ T^3)/0.17612 \quad (56)$$

Clean film-wise condenser, (Bromley & Read, 1970)

$$U_c\ =\ 1\times10^{-3}\ (-316.2\ +\ 6.62\ T)/0.17612 \quad (57)$$

Oxidized film-wise condenser, (Bromley & Read, 1970)

$$Uc\ =\ 1\times10^{-3}\ (-\ 64.37+4.625\ T)/0.17612 \quad (58)$$

Stellenbosch University https://scholar.sun.ac.za

B Central receiver plant model

B.1 SAM set-up

1. The solar resource data of Arandis obtained from GeoSUN™ Africa (Pty) Ltd is saved as a "Comma Separated Values" file in a format so that it is readable to SAM.
2. Under the "Heliostat Field" tab:
   2.1. "Always optimize" box is ticked
   2.2. the design-point DNI value is changed to 820 W/m^2
   2.3. "Heliostat start-up energy" set to 0 kW_e-hr
   2.4. "Heliostat tracking energy" set to 0 kW_e
   2.5. the atmospheric attenuation polynomial coefficients are set to 0
3. Under the "Tower and Receiver" tab:
   3.1. "Minimum receiver turndown fraction" set to 0
   3.2. "Maximum receiver operation fraction" set to 1
   3.3. "Receiver start-up delay time" set to 0 hours
   3.4. "Receiver start-up delay energy fraction" set to 0
   3.5. "Maximum receiver flux" set to 1100 kW_t/m^2
4. Under the "Power cycle" tab:
   4.1. "Design turbine gross output" set to 100 MW_e
   4.2. "Estimated gross to net conversion Factor" set to 1
   4.3. "Constant losses" set to 0%
   4.4. "Rated cycle conversion efficiency" set to 0.434986
   4.5. "Low resource standby period" set to 0
   4.6. "Fraction of thermal power needed for standby" set to 0
   4.7. "Power block start-up time" set to 1 hour
   4.8. "Fraction of thermal power needed for start-up" set to 1
   4.9. "Maximum turbine over design operation" set to 1
   4.10. "Boiler operating pressure" set to 165 Bar
   4.11. "Steam cycle blowdown fraction" set to 0.016

Stellenbosch University https://scholar.sun.ac.za

4.12. “Ambient temperature at design” set to 34.9 °C

4.13. “ITD at design point” set to 24 °C

5. Under “Parasitics” tab:

5.1. “Receiver HTF pump efficiency” set to 1

5.2. All other parasitic losses are set to 0

Stellenbosch University https://scholar.sun.ac.za

C. MED plant economics

Table 16: MED capital cost breakdown, (Loutatidou & Arafat, 2015)

Parameter	Value [$/m^3/day]
Direct capital costs	
Main investment	1394
Main investment	1394
Post treatment	55
Open seawater intake	217
ERD for discharge pipeline	29
Indirect capital costs	
Freight and insurance rate during construction	84.75
Owners cost rate	169.5
Contingency rate	169.5
Construction overhead	207.47
Total	2326.22

Stellenbosch University https://scholar.sun.ac.za

D. Results

Table 17: Dry-cooled Rankine bleed-off optimization results

Parameter	**Pressure [kPa]**	**Steam mass flow rate fraction [-]**
HPT outlet (Point 8)	6724	1
Closed FWH (Point a)	6393	0.08129
Closed FWH (Point b)	3461	0.06178
Direct contact FWH (Point c)	1644	0.06465
Closed FWH (Point d)	507.5	0.05339
Closed FWH (Point e)	177.3	0.08080

Table 18: CSP+MED bleed-off optimization results

Pressure [kPa]	**TBT= 55°C**	**TBT= 62.5°C**	**TBT= 70°C**	**TBT= 77.5°C**	**TBT= 85°C**
HPT outlet (Point 8)	6509	6536	6512	6600	6737
Closed FWH (Point a)	5800	5800	5659	5908	5973
Closed FWH (Point b)]	2947	2948	2893	3113	3232
Direct contact FWH (Point c)	1300	1300	1380	1475	1577
Closed FWH (Point d)	434.3	442.4	457	477.4	545.4
Closed FWH (Point e)	164.1	164.1	160.2	160.2	210.7

Stellenbosch University https://scholar.sun.ac.za

Table 19: CSP+MED bleed-off optimization results

Steam mass flow rate fraction [-]	**TBT= 55°C**	**TBT= 62.5°C**	**TBT= 70°C**	**TBT= 77.5°C**	**TBT= 85°C**
Closed FWH (Point a)	0.08500	0.08506	0.0836	0.08171	0.07926
Closed FWH (Point b)]	0.06374	0.06377	0.05662	0.05928	0.05802
Direct contact FWH (Point c)	0.05566	0.05462	0.05912	0.06098	0.05951
Closed FWH (Point d)	0.04872	0.04944	0.05255	0.05486	0.05017
Closed FWH (Point e)	0.07983	0.06931	0.05703	0.04541	0.04798

Stellenbosch University https://scholar.sun.ac.za

E. Model code

B.1 Rankine EES code

```
{Rankine cycle: Dry-cooled

    {Input parameters: Design point conditions}
"Turbine inlet steam temperature"
    T_max = (565 + 273) [K]
"Turbine inlet steam pressure"
    P_max = 16500 [kPa]
"Terminal temperature difference between steam and MED plant"
    TTD_s = 2.5
"Top brine temperature of MED plant"
    TBT = (55+273)

    {Isentropic efficiencies}
"Pumps"
Eta_FWP = 0.75
Eta_HPT = 0.85
Eta_LPT = 0.85

{Point1}
"Condenser outlet - FWP 1 inlet"
T_cond = TBT + TTD_s
T[1] = T_cond
P[1] = P_sat(Water,T=T[1])
x[1] = 0
s[1] = Entropy(Water,T=T[1],x=x[1])
h[1] = Enthalpy(Water,T=T[1],x=x[1])
    "Energy rejected at condenser (specific)"
    Q_101 = ((h[10]-h[29])*(1-m_1-m_2-m_3-m_4-m_5)) + ((h[29]-h[1])*(1-m_1-m_2-m_3))

{Point2 actual}
"FWP 1 outlet - FWP 2 inlet"
eta_FWP = (h_acs[2]-h[1])/(h[2]-h[1])
P_FWP1 = P[19]
P[2] = P_FWP1
s[2] = Entropy(Water,P=P[2],h=h[2])
T[2] = Temperature(Water,P=P[2],h=h[2])
    "Pump work (specific)"
    W_12 = ((h[2] - h[1])*(1-m_1-m_2-m_3))

{Point2 Ideal}
"FWP 1 outlet - FWP 2 inlet"
s_acs[2] = s[1]
```

Stellenbosch University https://scholar.sun.ac.za

```
T_acs[2] = Temperature(Water,P=P[2],s=s_acs[2])
h_acs[2] = Enthalpy(Water,P=P[2],s=s_acs[2])

{Point3}
"1st Preheating stage outlet -  FWP 2 inlet"
P[3] = P[2]
x[3] = 0
T[3] = Temperature(Water,P=P[3],x=x[3])
s[3] = Entropy(Water,P=P[3],x=x[3])
h[3] = Enthalpy(Water,P=P[3],x=x[3])
    "Preheating heat input (specific)"
    Q_23 = h[3] - (h[2]*(1-m_1-m_2-m_3))

{Point4 - Actual}
"FWP 2 outlet - 2nd stage preheating inlet"
eta_FWP = (h_acs[4]-h[3])/(h[4]-h[3])
P[4] = P_max
s[4] = Entropy(Water,P=P[4],h=h[4])
T[4] = Temperature(Water,P=P[4],h=h[4])
    "Pump work (specific)"
    W_34 = (h[4]-h[3])*(1)

{Point4 - Ideal}
"FWP 2 outlet - 2nd stage preheating inlet"
s_acs[4] = s[3]
T_acs[4] = Temperature(Water,P=P[4],s=s_acs[4])
h_acs[4] = Enthalpy(Water,P=P[4],s=s_acs[4])

{Point5}
"2nd stage preheating outlet - evaporation inlet"
P[5] = P[4]
x[5] = 0
T[5] = Temperature(Water,P=P[5],x=x[5])
s[5] = Entropy(Water,P=P[5],x=x[5])
h[5] = Enthalpy(Water,P=P[5],x=x[5])
    "Preheating heat input (specific)"
    Q_413 = h[13]-h[4]
    "Preheating external heat input (specific)"
    Q_135 = (h[5]-h[13])
    "Total preheating"
    Q_45 = h[5]-h[4]

{Point6}
"evaporation outlet - superheating inlet"
P[6] = P[5]
x[6] = 1
T[6] = T[5]
s[6] = Entropy(Water,P=P[6],x=x[6])
h[6] = Enthalpy(Water,P=P[6],x=x[6])
    "Evaporation heat input (specific)"
    Q_56 = (h[6]-h[5])
```

Stellenbosch University https://scholar.sun.ac.za

```
{Point7}
"Superheating outlet - HPT inlet"
P[7] = P[6]
T[7] = T_max
s[7] = Entropy(Water,P=P[7],T=T[7])
h[7] = Enthalpy(Water,P=P[7],T=T[7])
    "Superheating heat input (specific)"
    Q_67 = (h[7]-h[6])

{Point8 - Actual}
"HPT outlet - Reheat inlet"
Eta_HPT = (h[7]-h[8])/(h[7]-h_acs[8])
P[8] = 6509 [kPa] "Optimised value"
s[8] = Entropy(Water,P=P[8],h=h[8])
T[8] = Temperature(Water,P=P[8],h=h[8])
    "HPT work output (specific)"
    W_78 = (h[7]-h[8])

{Point8 - Ideal}
"HPT outlet - Reheat inlet"
s_acs[8] = s[7]
T_acs[8] = Temperature(Water,P=P[8],s=s_acs[8])
h_acs[8] = Enthalpy(Water,P=P[8],s=s_acs[8])

{Point9}
"Reheat outlet - LPT inlet"
T[9] = T_max
P[9] = P[8]
h[9] = Enthalpy(Water,P=P[9],T=T[9])
s[9] = Entropy(Water,P=P[9],T=T[9])
    "Reheating heat input (specific)"
     Q_89 = (h[9]-h[8])

{Point10}
"LPT outlet - condenser inlet - Actual"
Eta_LPT = (h[26]-h[10])/(h[26]-h_acs[10])
P[10] = P[1]
T[10] = Temperature(Water,P=P[10],h=h[10])
s[10] = Entropy(Water,P=P[10],h=h[10])
x[10] = Quality(Water,P=P[10],h=h[10])
    "LPT work output (specific)"
    W_910 = ((h[9]-h[11])*(1))+((h[11]-h[15])*(1-m_1))+((h[15]-h[19])*(1-m_1-m_2))+((h[19]-
h[22])*(1-m_1-m_2-m_3))+((h[22]-h[26])*(1-m_1-m_2-m_3-m_4))+((h[26]-h[10])*(1-m_1-m_2-
m_3-m_4-m_5))

"LPT outlet - condenser inlet - Ideal"
s_acs[10] = s[26]
T_acs[10] = T[1]
h_acs[10] = Enthalpy(Water,P=P[10],s=s_acs[10])
"x_acs[10] = Quality(Water,P=P[10],s=s_acs[10])"
```

Stellenbosch University https://scholar.sun.ac.za

```
{Feed water heater 1 - Closed_____________________________________________________}
{Point 11 -Actual}
"Bleeding point"
Eta_LPT = (h[9]-h[11])/(h[9]-h_acs[11])
P_FWH_1 = 5800 [kPa]
P[11] = P_FWH_1
s[11] = Entropy(Water,P=P[11],h=h[11])
T[11] = Temperature(Water,P=P[11],h=h[11])

{Point 11 -  Ideal}
"Bleeding point"
s_acs[11] = s[9]
T_acs[11] = Temperature(Water,P=P[11],s=s_acs[11])
h_acs[11] = Enthalpy(Water,P=P[11],s=s_acs[11])

{Point 12}
"Saturated vapour point"
P[12] = P[11]
x[12] = 1
T[12] = T_sat(Water,P=P[12])
h[12] = Enthalpy(Water,P=P[12],x=x[12])
s[12] = Entropy(Water,P=P[12],x=x[12])

{Point 13}
"Saturated fluid point"
P[13] = P[12]
x[13] = 0
T[13] = T[12]
h[13] = Enthalpy(Water,P=P[13],x=x[13])
s[13] = Entropy(Water,P=P[13],x=x[13])

{Point 14}
"Flashing to next feedwater heater"
P[14] = P[15]
h[14] = h[13]
T[14] = T[16]
x[14] = Quality(Water,P=P[14],h=h[14])
s[14] = Entropy(Water,P=P[14],h=h[14])

{Feed water heater 2 - Closed_____________________________________________________}
{Point 15 - Actual}
"Bleeding point"
Eta_LPT = (h[11]-h[15])/(h[11]-h_acs[15])
P_FWH_2 = 2948[kPa]
P[15] = P_FWH_2
s[15] = Entropy(Water,P=P[15],h=h[15])
T[15] = Temperature(Water,P=P[15],h=h[15])

{Point 15 - Ideal}
"Bleeding point"
s_acs[15] = s[11]
```

Stellenbosch University https://scholar.sun.ac.za

```
T_acs[15] = Temperature(Water,P=P[15],s=s_acs[15])
h_acs[15] = Enthalpy(Water,P=P[15],s=s_acs[15])

{Point 16}
"Saturated vapour point"
P[16] = P[15]
x[16] = 1
T[16] = T_sat(Water,P=P[16])
h[16] = Enthalpy(Water,P=P[16],x=x[16])
s[16] = Entropy(Water,P=P[16],x=x[16])

{Point 17}
"Saturated fluid point"
P[17] = P[16]
x[17] = 0
T[17] = T[16]
h[17] = Enthalpy(Water,P=P[17],x=x[17])
s[17] = Entropy(Water,P=P[17],x=x[17])

{Point 18}
"Flashing to next feedwater heater"
P[18] = P[19]
h[18] = h[17]
T[18] = T[20]
x[18] = Quality(Water,P=P[18],h=h[18])
s[18] = Entropy(Water,P=P[18],h=h[18])

{Feed water heater 3 - Contact_____________________________________________}
{Point 19}
"Bleeding point - Actual"
Eta_LPT = (h[15]-h[19])/(h[15]-h_acs[19])
P_FWH_3 = 1300 [kPa]
P[19] = P_FWH_3
s[19] = Entropy(Water,P=P[19],h=h[19])
T[19] = Temperature(Water,P=P[19],h=h[19])

"Bleeding point - Ideal"
s_acs[19] = s[15]
T_acs[19] = Temperature(Water,P=P[19],s=s_acs[19])
h_acs[19] = Enthalpy(Water,P=P[19],s=s_acs[19])

{Point 20}
"Saturated vapour point"
P[20] = P[19]
x[20] = 1
T[20] = T_sat(Water,P=P[20])
h[20] = Enthalpy(Water,P=P[20],x=x[20])
s[20] = Entropy(Water,P=P[20],x=x[20])
```

Stellenbosch University https://scholar.sun.ac.za

```
{Point 21}
"Saturated fluid point"
P[21] = P[20]
x[21] = 0
T[21] = T[20]
h[21] = Enthalpy(Water,P=P[21],x=x[21])
s[21] = Entropy(Water,P=P[21],x=x[21])

{Feed water heater 4 -
Closed_____________________________________________________________________}
{Point 22}
"Bleeding point - Actual"
Eta_LPT = (h[19]-h[22])/(h[19]-h_acs[22])
P_FWH_4 = 433.2 [kPa]
P[22] = P_FWH_4
s[22] = Entropy(Water,P=P[22],h=h[22])
T[22] = Temperature(Water,P=P[22],h=h[22])
T_sat[22] = T_sat(Water,P=P[22])
SF_fwh4 = T[22] - T_sat[22]

"Bleeding point - Ideal"
s_acs[22] = s[19]
T_acs[22] = Temperature(Water,P=P[22],s=s_acs[22])
h_acs[22] = Enthalpy(Water,P=P[22],s=s_acs[22])

{Point 23}
"Saturated vapour point"
P[23] = P[22]
x[23] = 1
T[23] = T_sat(Water,P=P[23])
h[23] = Enthalpy(Water,P=P[23],x=x[23])
s[23] = Entropy(Water,P=P[23],x=x[23])

{Point 24}
"Saturated fluid point"
P[24] = P[23]
x[24] = 0
T[24] = T[23]
h[24] = Enthalpy(Water,P=P[24],x=x[24])
s[24] = Entropy(Water,P=P[24],x=x[24])

{Point 25}
"Flashing to next feedwater heater"
P[25] = P[26]
h[25] = h[24]
T[25] = T[27]
x[25] = Quality(Water,P=P[25],h=h[25])
s[25] = Entropy(Water,P=P[25],h=h[25])
```

Stellenbosch University https://scholar.sun.ac.za

```
"Energy balance"
{Feed water heater 5 Closed_____________________________________________________}
{Point 26}
"Bleeding point -  Actual"
Eta_LPT = (h[22]-h[26])/(h[22]-h_acs[26])
P_FWH_5 = 162.3 [kPa]
P[26] = P_FWH_5
s[26] = Entropy(Water,P=P[26],h=h[26])
T[26] = Temperature(Water,P=P[26],h=h[26])
x[26] = Quality(Water,P=P[26],s=s[26])
T_sat[26] = T_sat(Water,P=P[26])
SF_fwh5 =T[26] - T_sat[26]

"Bleeding point - Ideal"
s_acs[26] = s[22]
T_acs[26] = Temperature(Water,P=P[26],s=s_acs[26])
h_acs[26] = Enthalpy(Water,P=P[26],s=s_acs[26])

{Point 27}
"Saturated vapour point"
P[27] = P[26]
x[27] = 1
T[27] = T_sat(Water,P=P[27])
h[27] = Enthalpy(Water,P=P[27],x=x[27])
s[27] = Entropy(Water,P=P[27],x=x[27])

{Point 28}
"Saturated fluid point"
P[28] = P[27]
x[28] = 0
T[28] = T[27]
h[28] = Enthalpy(Water,P=P[28],x=x[28])
s[28] = Entropy(Water,P=P[28],x=x[28])

{Point 29}
"Flashing to next feedwater heater"
P[29] = P[10]
h[29] = h[28]
T[29] = T[10]
x[29] = Quality(Water,P=P[29],h=h[29])
s[29] = Entropy(Water,P=P[29],h=h[29])

{_____________________________________________________________________________}
{Feed water heater energy balances}
"FWH1"
h[17] + m_1*h[11] = m_1*h[13] + h[13]
"FWH2"
h[4] + h[14]*m_1 + h[15]*m_2 = h[17] + (m_1+m_2)*h[17]
"FWH3"
h[3] = h[19]*m_3 + h[18]*(m_2+m_1) + h[24]*(1-m_1-m_2-m_3)
```

Stellenbosch University https://scholar.sun.ac.za

```
"FWH4"
((1-m_1-m_2-m_3)*(h[24]-h[28])) = ((m_4)*(h[22]-h[24]))
"FWH5"
h[2]*(1-m_1-m_2-m_3) + h[26]*(m_5) + h[25]*m_4 = h[28]*(1-m_1-m_2-m_3) +
h[28]*(m_5+m_4)

"Rankine cycle energy balance"
E_rankine_in = W_12 + W_34 + Q_135 + Q_56 + Q_67 + Q_89
E_rankine_out = W_78 + W_910 + Q_101

"Rankine cycle efficiency"
eta_rankine = (W_78+W_910)/(Q_135 + Q_56 + Q_67 + Q_89)

eta_CN = 1 - sqrt(T_cond/T_max)

m_steam = 100000000/(W_78+W_910)

{CSP link}
"Heat required from receiver/ storage for full load"
Q_PB_full = m_steam*(Q_135+Q_56+Q_67+Q_89)

{MES Link }
"Steam going to MES plant"
((1-m_1-m_2-m_3-m_4-m_5)*m_steam) = m_steam_f + m_steam_g
((1-m_1-m_2-m_3-m_4-m_5)*m_steam)*h[10] = m_steam_f*h_steam_f +
m_steam_g*h_steam_g

"Enthalpy of saturated steam condensate"
h_steam_f = Enthalpy(Steam,P=P[10],x=0)

"Enthalpy of saturated steam vapour"
h_steam_g = Enthalpy(Steam,P=P[10],x=1)
```

B.2 MED desalination EES code

```
"MES mass and energy balance and heat transfer model"
{=================================================================}
{-----------------------High level MES input specifications----------------------}
"Number of effects"
    N=17
"Top brine temperature"
    TBT = 70
"Bottom brine temperature"
    BBT = 40
"Mass flow rate of steam entering MES system"
    M_s = 60.091822784
```

Stellenbosch University https://scholar.sun.ac.za

```
"Salt content of raw seawater"
    X_f = 35 [g/kg]
"Maximum salinity restriction"
    X_b[N] = 60 [g/kg]
"Sea water temperature"
    T_sw = 15 [C]

{----------------------------Heating steam properties----------------------------------------------------------------}
"Assuming temperature stays constant for now"
"Heating steam heat exchanger TTD"
    TTD_s = 2.5
"Steam temperature"
    T_s = TBT + TTD_s
"Enthalpy of vaporization of steam entering"
    h_s_in = Enthalpy(Water,T=T_s,x=1)
"Enthalpy of vaporization of steam exiting"
    h_s_out = Enthalpy(Water,T=T_s,x=0)

{-------------------------System temperature differences-----------------------------------------------------------}
"Temperature difference between effects"
    Delta_T_mes = (TBT-BBT)/(N-1)
"Preheater TTD"
    TTD_Hx = T_dv[N] - T_f[N+1]

{-----------------------------------------------------Effect 1-----------------------------------------------------}
    "Effect number"
Effect[1] = 1

"------------Temperatures---------------------------------"
    "Brine temperature"
T_b[1] = TBT
    "Temperature of saturated distillate vapour"
T_dv[1] = T_b[1] - BPE[1]
    "Feed water temperature entering effect"
T_f[1] = T_dv[1] - TTD_f[1]
    "TTD feed heater"
TTD_f[1] = TTD_Hx
    "Boiling point elevation"
BPE[1] = SW_BPE(T_dv[1],X_f)

"---------Pressures-------------------------------------------"
    "Effect pressure"
P_e[1] = P_sat(Water,T=T_dv[1])

"---------Enthalpy values-------------------------------"
    "Enthalpy of superheated vapour"
h_shv[1] = Enthalpy(Water,T=T_b[1],P=P_e[1])
    "Enthalpy of distillate vapour - sat fluid"
h_dv_f[1] = Enthalpy(Water,T=T_dv[1],x=0)
    "Enthalpy of distillate vapour - sat steam"
h_dv_g[1] = Enthalpy(Water,T=T_dv[1],x=1)
```

Stellenbosch University https://scholar.sun.ac.za

```
    "Enthalpy of brine entering effect"
h_b_acs[1] = SW_Enthalpy(T_f[1],X_f)
    "Enthalpy of brine generated"
h_b[1] = SW_Enthalpy(T_b[1],X_b[1])
    "Enthalpy of feed-water exiting preheater"
h_f[1] = SW_Enthalpy(T_f[1],X_f)

"---------Governing equations-----------------------"
"Mass balances"
"Brine entering effect"
    M_f = M_b[0]
"Brine entering after flashing"
    M_b_acs[1] = M_b[0] - M_gf[1]
    "No flashing in 1st effect"
    M_gf[1] = 0
"Boiling of brine"
    M_b_acs[1] = M_gb[1] + M_b[1]
"Distillate vapour formed in effect"
    M_dv[1] = M_gf[1] + M_gb[1] + M_df[1]

"Salt balance"
    x_f*M_f = X_b[1]*M_b[1]

"Energy balances"
"Flashing of brine - No flashing in 1st effect"
"Effect heat source"
    M_s*h_s_in + M_b_acs[1]*h_b_acs[1] = M_s*h_s_out + M_gb[1]*h_shv[1]+ M_b[1]*h_b[1]

"Heat transfer area"
    M_s*(h_s_in-h_s_out) = A_effect[1]*U_effect[1]*(T_s - T_b[1])
"Overall heat transfer coefficient"
    U_effect[1] = (10^(-3)*(1939.1 + 1.40562*T_s - 0.0207525*T_s^2 +
0.0023186*T_s^3))*1000

"Heat transfer"
    Q_eff[1] = M_s*(h_s_in-h_s_out)
"Heat transfer requirement/duty"
    Q_duty[1] = Q_eff[1]/A_effect[1]

"Heat exchanger effectiveness"
epsilon[1] = (T_b[1]-T_f[1])/((T_b[1]-T_f[1])+TTD_s)

"---------------------------------Preheater---------------------------------"
"Energy balance"
    M_dv[1]*(h_shv[1]-h_dv_fg_out[1]) = M_f*(h_f[1]-h_f[2])

"Preheater heat transfer area"
m_f*(h_f[1]-h_f[2]) = A_ph[1]*U_ph[1]*(LMTD_ph[1])
"Log mean temperature difference"
LMTD_ph[1] = (T_f[2]-T_f[1])/(Ln((T_dv[1]-T_f[1])/(T_dv[1]-T_f[2])))
"Overall heat transfer coefficient"
```

Stellenbosch University https://scholar.sun.ac.za

```
U_ph[1] = (10^(-3)*(1617.5 + 0.1537*(T_dv[1])+0.1825*T_dv[1]^2 -
0.00008026*T_dv[1]^3))*1000

"----------------------------Flash box-------------------------"
"Flash box - 1st effect has no flash box"
"Distillate generated by flashing"
    M_df[1] = 0
"Distillate condensed"
    M_d[1] = 0

{--------------------------------MES effects 2 to N-1-----------------------------------------------------------------}
DUPLICATE j= 2,N-1

    "Effect labelling"
Effect[j] = j

"---------Temperatures--------"
    "Effect brine temperature"
T_b[j] = TBT - (j-1)*Delta_T_mes
    "Temperature of distillate vapour"
T_dv[j] = T_b[j] -  BPE[j]
    "Feed water exiting preheater"
T_f[j] = T_dv[j] - TTD_f[j]
    "TTD feed heaters"
TTD_f[j] = TTD_Hx
    "Boiling point elevation"
BPE[j] = SW_BPE(T_dv[j],X_b_acs[j])

"---------Pressures--------"
    "Effect pressure"
P_e[j] = P_sat(Water,T=T_dv[j])

"---------Enthalpy values--------"
    "Enthalpy of superheated vapour"
h_shv[j] = Enthalpy(Water,T=T_b[j],P=P_e[j])
    "Enthalpy of distillate vapour - sat fluid"
h_dv_f[j] = Enthalpy(Water,T=T_dv[j],x=0)
    "Enthalpy of distillate vapour - sat steam"
h_dv_g[j] = Enthalpy(Water,T=T_dv[j],x=1)
    "Enthalpy of brine entering effect"
h_b_acs[j] = SW_Enthalpy(T_b[j],X_b_acs[j])
    "Enthalpy of brine generated"
h_b[j] = SW_Enthalpy(T_b[j],X_b[j])
    "Enthalpy of feed-water exiting preheater"
h_f[j] = SW_Enthalpy(T_f[j],X_f)

"---------Governing equations---------"
"Mass balances"
"Brine entering after flashing"
    M_b_acs[j] = M_b[j-1] - M_gf[j]
```

Stellenbosch University https://scholar.sun.ac.za

```
"Boiling of brine"
    M_b_acs[j] = M_gb[j] + M_b[j]
"Distillate vapour formed in effect"
    M_dv[j] = M_gf[j] + M_gb[j] + M_df[j]

"Salt balance"
    "Flashing of brine"
    X_b[j-1]*m_b[j-1] = x_b_acs[j]*M_b_acs[j]
    "Boiling over tubes"
    x_b_acs[j]*M_b_acs[j] = X_b[j]*M_b[j]

"Energy balances"
"Flashing of brine"
    M_b[j-1]*h_b[j-1] = M_b_acs[j]*h_b_acs[j] + M_gf[j]*h_shv[j]
"Distillate vapour formed in effect"
    M_dv[j]*h_dv_fg_in[j] = M_gf[j]*h_shv[j] + M_gb[j]*h_shv[j] + M_df[j]*h_dv_g[j]
"Effect heat source"
    M_dv[j-1]*h_dv_fg_out[j-1] + M_b_acs[j]*h_b_acs[j] = M_dv[j-1]*h_dv_f[j-1] +
M_gb[j]*h_shv[j]+ M_b[j]*h_b[j]

"Effect Heat transfer area"
    M_dv[j-1]*(h_dv_fg_out[j-1]-h_dv_f[j-1]) = A_effect[j]*U_effect[j]*(T_dv[j-1] - T_b[j])
"Overall heat transfer coefficient"
    U_effect[j] = (10^(-3)*(1939.1 + 1.40562*T_dv[j-1] - 0.0207525*T_dv[j-1]^2 +
0.0023186*T_dv[j-1]^3))*1000
"Heat transfer"
    Q_eff[j] =  M_dv[j-1]*(h_dv_fg_out[j-1]-h_dv_f[j-1])
"Heat transfer requirement/duty"
    Q_duty[j] = Q_eff[j]/A_effect[j]
"Heat exchanger effectiveness"

"----------------------------------Preheater----------------------------------"
"Energy balance"
    M_dv[j]*(h_dv_fg_in[j]-h_dv_fg_out[j]) = M_f*(h_f[j]-h_f[j+1])
"Quality of heating steam leaving preheater"
    x_dv_fg[j] = Quality(Water,T=T_dv[j],h=h_dv_fg_out[j])

"Preheater heat transfer area"
m_f*(h_f[j]-h_f[j+1]) = A_ph[j]*U_ph[j]*(LMTD_ph[j])
"Log mean temperature difference"
LMTD_ph[j] = (T_f[j+1]-T_f[j])/(Ln((T_dv[j]-T_f[j])/(T_dv[j]-T_f[j+1])))
"Overall heat transfer coefficient"
U_ph[j] = (10^(-3)*(1617.5 + 0.1537*(T_dv[j])+0.1825*T_dv[j]^2 -
0.00008026*T_dv[j]^3))*1000

"----------------------------------Flash box----------------------------------"
"Mass balances"
    "Mass flow into flash box"
"Flashing of previous flashbox distillate"
    M_d[j-1] = M_dgf[j] + M_dgc[j]
```

Stellenbosch University https://scholar.sun.ac.za

```
"Flashing of condensed distillate vapour heat source"
    M_dv[j-1] = M_dvgf[j] + M_dvgc[j]
    "Mass flow out of flash box"
"Distillate generated by flashing"
    M_df[j] = M_dgf[j] + M_dvgf[j]
"Distillate gernerated by condensation"
    M_d[j] = M_dgc[j] + M_dvgc[j]

"Energy balances"
"Flashing of distillate from previous flash box"
    M_d[j-1]*h_dv_f[j-1] = M_dgf[j]*h_dv_g[j] + M_dgc[j]*h_dv_f[j]
"Flashing of condensed distillate vapour heat source"
    M_dv[j-1]*h_dv_f[j-1] = M_dvgf[j]*h_dv_g[j] + M_dvgc[j]*h_dv_f[j]
END

{-----------------------------------------------------N-th effect -----------------------------------------------------}
    "Effect labelling"
Effect[N] = N

"---------Temperatures-----------------------"
    "Effect brine temperature"
T_b[N] = TBT - (N-1)*Delta_T_mes
    "Temperature of distillate vapour"
T_dv[N] = T_b[N] -  BPE[N]
    "Feed water exiting preheater"
T_f[N] = T_dv[N] - TTD_f[N]
    "TTD feed heaters"
TTD_f[N] = TTD_Hx
    "Boiling point elevation"
BPE[N] = SW_BPE(T_dv[N],X_b_acs[N])

"-------------Pressures--------------------------"
    "Effect pressure"
P_e[N] = P_sat(Water,T=T_dv[N])

"---------Enthalpy values-----------------------"
    "Enthalpy of superheated vapour"
h_shv[N] = Enthalpy(Water,T=T_b[N],P=P_e[N])
    "Enthalpy of distillate vapour - sat fluid"
h_dv_f[N] = Enthalpy(Water,T=T_dv[N],x=0)
    "Enthalpy of distillate vapour - sat steam"
h_dv_g[N] = Enthalpy(Water,T=T_dv[N],x=1)
    "Enthalpy of brine entering effect"
h_b_acs[N] = SW_Enthalpy(T_b[N],X_b_acs[N])
    "Enthalpy of brine generated"
h_b[N] = SW_Enthalpy(T_b[N],X_b[N])
    "Enthalpy of feed-water exiting preheater"
h_f[N] = SW_Enthalpy(T_f[N],X_f)
```

Stellenbosch University https://scholar.sun.ac.za

```
"---------Governing equations-----------------"
"Mass balances"
"Brine entering after flashing"
    M_b_acs[N] = M_b[N-1] - M_gf[N]
"Boiling of brine"
    M_b_acs[N] = M_gb[N] + M_b[N]
"Distillate vapour formed in effect"
    M_dv[N] = M_gf[N] + M_gb[N] + M_df[N]

"Salt balance"
    "Flashing of brine"
    X_b[N-1]*m_b[N-1] = x_b_acs[N]*M_b_acs[N]
    "Boiling over tubes"
    x_b_acs[N]*M_b_acs[N] = X_b[N]*M_b[N]

"Energy balances"
"Flashing of brine"
    M_b[N-1]*h_b[N-1] = M_b_acs[N]*h_b_acs[N] + M_gf[N]*h_shv[N]
"Distillate vapour formed in effect"
    M_dv[N]*h_dv_fg_in[N] = M_gf[N]*h_shv[N] + M_gb[N]*h_shv[N] + M_df[N]*h_dv_g[N]
"Effect heat source"
    M_dv[N-1]*h_dv_fg_out[N-1] + M_b_acs[N]*h_b_acs[N] = M_dv[N-1]*h_dv_f[N-1] +
M_gb[N]*h_shv[N]+ M_b[N]*h_b[N]

"Effect Heat transfer area"
    M_dv[N-1]*(h_dv_fg_out[N-1]-h_dv_f[N-1]) = A_effect[N]*U_effect[N]*(T_dv[N-1] - T_b[N])
"Overall heat transfer coefficient"
    U_effect[N] = (10^(-3)*(1939.1 + 1.40562*T_dv[N-1] - 0.0207525*T_dv[N-1]^2 +
0.0023186*T_dv[N-1]^3))*1000
"Heat transfer"
    Q_eff[N] =  M_dv[N-1]*(h_dv_fg_out[N-1]-h_dv_f[N-1])
"Heat transfer requirement/duty"
    Q_duty[N] = Q_eff[N]/A_effect[N]

"------------------------Flash box-----------------"
"Mass balances"
    "Mass flow into flash box"
"Flashing of previous flashbox distillate"
    M_d[N-1] = M_dgf[N] + M_dgc[N]
"Flashing of condensed distillate vapour heat source"
    M_dv[N-1] = M_dvgf[N] + M_dvgc[N]
    "Mass flow out of flash box"
"Distillate generated by flashing"
    M_df[N] = M_dgf[N] + M_dvgf[N]
"Distillate gernerated by condensation"
    M_d[N] = M_dgc[N] + M_dvgc[N]

"Energy balances"
"Flashing of distillate from previous flash box"
    M_d[N-1]*h_dv_f[N-1] = M_dgf[N]*h_dv_g[N] + M_dgc[N]*h_dv_f[N]
```

Stellenbosch University https://scholar.sun.ac.za

```
"Flashing of condensed distillate vapour heat source"
    M_dv[N-1]*h_dv_f[N-1] = M_dvgf[N]*h_dv_g[N] + M_dvgc[N]*h_dv_f[N]

{-----------------------------------------------------Condenser-----------------------------------------------------}
"First preheater inlet temperature"
    T_f[N+1] =  T_sw + 14.41

    "Seawater enthalpy values"
"Seawater entering condenser"
    h_sw_in = SW_Enthalpy(T_sw,X_f)
"Seawater exiting condenser"
    h_sw_out = SW_Enthalpy(T_f[N+1],X_f)
"Seawater exiting condenser is inlet of first preheater"
    h_f[N+1] = h_sw_out

"Distillate mass balance"
    M_d_tot = M_d[N] + M_dv[N]

"Condenser energy balance"
    M_dv[N]*h_dv_fg_in[N] + M_sw*h_sw_in = M_dv[N]*h_dv_f[N] + (M_sw)*h_sw_out

"Seawater streams"
    M_sw = M_sw_rej + M_f

"Overall heat transfer coefficient"
U_condenser = 1617.5 + 0.1537*T_dv[N] + 0.1825*T_dv[N]^2 - 0.00008026*T_dv[N]^3

"Log mean temperature difference"
LMTD_condenser = (T_f[N+1]-T_sw)/(Ln((T_dv[N]-T_sw)/(T_dv[N]-T_f[N+1])))

"Heat transfer area"
m_sw*(h_sw_out-h_sw_in) = A_condenser*U_condenser*LMTD_condenser

"Heat exchanger effectiveness"
epsilon[N] = (T_f[N+1]-T_sw)/((T_f[N+1]-T_sw)+(T_dv[N] - T_f[N+1]))


"---------------------------------Total energy and mass balance check---------------------------------"
"Mass flow into MES control volume"
    M_mes_in = M_s + M_sw
"Mass flow out of MES control volume"
    M_mes_out = M_s + M_sw_rej + M_d[N] + M_dv[N] + M_b[N]

"Energy into MES control volume"
    E_mes_in = M_s*h_s_in + M_sw*h_sw_in
"Energy out of MES control volume"
    E_mes_out = M_s*h_s_out + M_sw_rej*h_sw_out +  M_d[N]*h_dv_f[N]  +
M_dv[N]*h_dv_f[N] + M_b[N]*h_b[N]

"Energy balance error"
Err = (1-(E_mes_in/E_mes_out))*100
```

Stellenbosch University https://scholar.sun.ac.za

```
"----------------------------------Performance ratio----------------------------------"

PR = m_d_tot/m_s

"----------------------------------Recovery ratio----------------------------------"

RR = m_d_tot/m_sw

"----------------------------------Usefulness ratio----------------------------------"

UR = m_f/m_sw

"----------------------------------Gained output ratio----------------------------------"

GOR = m_f/m_d_tot

"Distillate per megawatt pumping power"

DM = m_d_tot/w_bhp

"----------------------------------Specific area----------------------------------"
"Effects total area"
A_effects_tot = sum(A_effect[j],j=1,N)
"Average effect area"
A_effects_avg = A_effects_tot /n

"Preheaters total area"
A_ph_tot = sum(A_ph[j],j=1,N-1)
"Total heat transfer area"
A_MES_tot = A_condenser+A_effects_tot + A_ph_tot

"Specific area"
SA = (A_MES_tot)/m_d_tot

"Polynomial for predicting the specific area based on the top brine temperature and the
number of effects"
SA_poly=1.08384095E+05-7.33118466E+03*TBT+1.84393470E+02*TBT^2-
2.04419531E+00*TBT^3+8.43851902E-03*TBT^4+8.64871431E+03*N-
9.42947124E+02*N^2+5.82612676E+01*N^3+9.93401390E-03*N^4-
3.92298905E+02*TBT*N+4.39570339E+01*TBT*N^2-
2.67815900E+00*TBT*N^3+5.93069871E+00*TBT^2*N-6.76057185E-
01*TBT^2*N^2+4.07622778E-02*TBT^2*N^3-2.99675572E-02*TBT^3*N+3.45964887E-
03*TBT^3*N^2-2.06888871E-04*TBT^3*N^3

"MES economics and power requirements"
{=====================================================================}
"Capital investment costs (Using Titanium alloys)"
C_capital = 30800+3749*(A_condenser+A_effects_tot + A_ph_tot)^0.81

"Electrical power consumption of MES plant"
P_e_MES = (7.2*(M_d_tot)/1000)
```

Stellenbosch University https://scholar.sun.ac.za

```
"Seawater pipeline mass flow and electricity calculations"
{=====================================================================}
"Sea water properties"
"Density"
    rho_sw = SW_Density(T_sw,X_f) * 1 [kg/m^3]
"Dynamic viscosity"
    mu_sw = SW_Viscosity(T_sw,X_f) * 1 [kg/m s]

"Elevation of water to be pumped"
    h_elev = 580 [m]
"Gravitational constant"
    g = 9.81 [m/s^2]
"Pump efficiency"
    eta_pump = 0.75

"Design velocity"
    "v_m = 2 [m/s]"
"Bulk water pipe lenght"
    L_bwp = 50000 [m]
"Bulk water pipe diameter"
    D_bwp^2 = ((4*m_sw)/(rho_sw*v_m*Pi))
    D_bwp = 2
"Bulk water pipe roughness"
    Epsilon = (0.9/1000) [m]

"Reynolds number"
    Re_D = (rho_sw*v_m*D_bwp)/mu_sw

"Friction factor"
    1/SQRT(f_fric) = -2*Log10(((Epsilon/D_bwp)/3.7)+(2.51/(Re_D*sqrt(f_fric))))

"Wall shear stress"
    Tau_s = (f_fric/8)*(rho_sw*v_m^2)

"Pressure gradient"
    Delta_Px = (4*Tau_s)/D_bwp

"Pressure loss over length of pipe"
    Delta_P_bwp = Delta_Px*L_bwp

"Headloss over pipeline"
    h_loss = Delta_P_bwp/(rho_sw*g)

"Total head required by pump"
    h_tot = h_elev + h_loss

"Water horse power"
    W_whp = m_sw*g*h_tot

"Brake horse power"
    w_bhp = (W_whp/eta_pump)/1000000
```

Stellenbosch University https://scholar.sun.ac.za

```
r = 0.0814/(1-(1/(1+0.0814))^25)

LCOW = ((((C_cap_tot)*r)+(OAM))/(W_ann))
OAM = OAM_pump+OAM_aux+OAM_maint
OAM_aux = LCOE*W_ann
OAM_pump = (W_bhp*1000)*24*365*CF*LCOE
OAM_maint = 39*( (M_d_tot/1000)*3600*24)
LCOE = 0.221

C_pipe = (3000000/15)*50
C_cap_tot = C_pipe + C_capital
CF = 1
W_ann = (M_d_tot/1000)*3600*24*365*CF

Inst_cap = m_d_tot/1000*3600*24

P_aux = W_ann
P_pump = (W_bhp*1000)*24*365*CF
P_pump_excl_dist = (W_bhp*1000)*24*365*CF*((m_sw_rej+m_b[N])/(m_sw))
```

B.3 Pumping EES code

```
{Pumping of seawater calcs}

"Sea water properties"
"Temperature"
    T_sw = 15 [C]
"Pressure"
    "P_amb = 101000 [Pa]"
"Salinity"
    X_sw = 35 [g/kg]
"Density"
    rho_sw = SW_Density(T_sw,X_sw) * 1 [kg/m^3]
"Dynamic viscosity"
    mu_sw = SW_Viscosity(T_sw,X_sw) * 1 [kg/m s]

"Elevation of water to be pumped"
    h_elev = 580 [m]
"Gravitational constant"
    g = 9.81 [m/s^2]
"Pump efficiency"
    eta_pump = 0.75

"Design velocity"
    "v_m = 1 [m/s]"
"Design mass flow rate"
```

Stellenbosch University https://scholar.sun.ac.za

```
    "m_dot_sw = 1542 [kg/s]"
"Bulk water pipe lenght"
    L_bwp = 50000 [m]
"Bulk water pipe diameter"
    m_dot_sw = rho_sw*v_m*(Pi*(D_bwp/2)^2)
    D_bwp=1.383
"Bulk water pipe roughness"
    Epsilon = (0.9/1000) [m]

"Reynolds number"
    Re_D = (rho_sw*v_m*D_bwp)/mu_sw

"Friction factor"
    1/SQRT(f_fric) = -2*Log10(((Epsilon/D_bwp)/3.7)+(2.51/(Re_D*sqrt(f_fric))))

"Wall shear stress"
    Tau_s = (f_fric/8)*(rho_sw*v_m^2)

"Pressure gradient"
    Delta_Px = (4*Tau_s)/D_bwp

"Pressure loss over length of pipe"
    Delta_P_bwp = Delta_Px*L_bwp

"Headloss over pipeline"
    h_loss = Delta_P_bwp/(rho_sw*g)

"Total head required by pump"
    h_tot = h_elev + h_loss

"Water horse power"
    W_whp = m_dot_sw*g*h_tot

"Brake horse power"
    w_bhp = (W_whp/eta_pump)/1000000
```

Stellenbosch University https://scholar.sun.ac.za

References

2030 Water Resources Group. 2009. *Charting Our Water Future - Economic frameworks to inform decision-making*.

ABENGOA SOLAR. 2016. *Khi Solar One*. [Online], Available: http://www.abengoasolar.com/web/en/acerca_de_nosotros/sala_de_prensa/noticias/2016/abg_20160205.html [2016, November 14].

Al-Karaghouli, A. & Kazmerski, L.L. 2013. Energy consumption and water production cost of conventional and renewable-energy-powered desalination processes. *Renewable and Sustainable Energy Reviews*. 24:343–356.

AUSTELA. 2013. *New Tools for Economic Assessment of Australian CSP Projects New Tools for Economic Assessment of Australian CSP Projects*. [Online], Available: http://www.austela.com.au/newsletter/129-new-tools-for-economic-assessment-of-australian-csp-projects.

AUSTELA. 2016. *The NREL System Advisor Model for Australian CSP Stakeholders ﴾ SAM ﴿*. [Online], Available: http://austela.com.au/newsletter/133-the-nrel-system-advisor-model-for-australian-csp-stakeholders-sam [2016, November 13].

Bergan, N.E. 1986.

Biomass Technology Group. 2016. *Torrefaction -*. [Online], Available: http://www.btgworld.com/en/rtd/technologies/torrefaction [2016, November 15].

Bromley, L.A. & Read, S.M. 1970. Multiple effect flash (MEF) evaporator. *Desalination*. 7(3):343–391.

Cengel, Y.A. & Cimbala, J.M. 2006. *Fluid Mechanics, Fundamentals and Applications*. S. Jeans, D.D. Matteson, & K. Sheinman (eds.). New York: McGraw-Hill.

Christian, J., Moya, A., Ho, C., Andraka, C. & Yuan, J. 2016. Probabilistic Analysis to Quantify Optical Performance and Error Budgets for Next Generation Heliostats. *Journal of Solar Energy Engineering*. 137(June 2015):1–8.

Collado, F.J. & Guallar, J. 2013. A review of optimized design layouts for solar power tower plants with campo code. *Renewable and Sustainable Energy Reviews*. 20:142–154.

CSP Today. 2015. *Namibia tenders for up to 200 MW ; Abengoa starts insolvency*. [Online], Available: http://social.csptoday.com/markets/namibia-tenders-200-mw-abengoa-starts-insolvency [2016, January 29].

Stellenbosch University https://scholar.sun.ac.za

Darwish, M.A., Al-Juwayhel, F. & Abdulraheim, H.K. 2006. Multi-effect boiling systems from an energy viewpoint. *Desalination*. 194(1–3):22–39.

Duvenhage, W. 2014. *Rio Tinto, Rossing Uruanium Employee Brief*. Swakopmund.

Eberhard, A., Kolker, J. & Leighland, J. 2014. *South Africa's REIPPPP: Success Factors and Lessons*. Washington DC.

El-Dessouky, H.T. & Ettouney, H.M. 2002. *Fundamentals of Salt Water Desalination*. 2002nd ed. Amsterdam: Elsevier.

El-Dessouky, H., Alatiqi, I., Bingulac, S. & Ettouney, H. 1998. Steady-state analysis of the multiple eff *Chemical Engineering* desalination process. *Technology*. 21:15–29.

El-Sayed, Y.M. & Silver, R.S. 1980. Fundamentals of. In 1st ed. Elsevier *Principles of Desalination*. 55–109.

ENTROPIE, V. 2014. *Multiple Effect Distillation (MED)*. [Online], Available: http://www.entropie.com/en/services/desalination/MED/ [2016, July 18].

Eskom. 2015. *Concentrating Solar Power*. [Online], Available: http://www.eskom.co.za/AboutElectricity/FactsFigures/Documents/RW_0003ConsentratingSolarPowerRev5.pdf [2016, November 24].

Frantz, C. & Seifert, B. 2015. Thermal analysis of a multi effect distillation plant powered by a solar tower plant. *Energy Procedia*. 69:1928–1937.

Gauché, P., Backström, T.W. Von & Brent, A.C. 2011. Csp Modeling Methodology for Macro Decision Making - Emphasis on the Central Receiver Type. *Proceedings of Solar Power and Chemical Energy Systems conference (SolarPACES 2011)*. 1–8.

GEA. 2012. *Air Cooled Condensers (ACC) engineering for a better world*. Bochum, Germany.

Gebel, J. 2014. Thermal Desalination Processes. In 1st ed. J. Kucera (ed.). Beverly: Scrivener Publishing LLC. *Desalination, water from water*. 41–154.

German Aerospace Center (DLR). 2007. *Concentrating Solar Power for Seawater Desalination*. Stuttgart. [Online], Available: www.dlr.de/tt/Portaldata/41/...csp/AQUA-CSP-Full-Report-Final.pdf.

Ghobeity, A., Noone, C.J., Papanicolas, C.N. & Mitsos, A. 2011. Optimal time-invariant operation of a power and water cogeneration solar-thermal plant. *Solar Energy*. 85(9):2295–2320.

Stellenbosch University https://scholar.sun.ac.za

Gleick, P.H. 1996. *Water Resources in Encyclepedia of Climate and Weather*. vol. 2 ed. S.H. Schneider (ed.). New York: University Press.

Greenlee, L.F., Lawler, D.F., Freeman, B.D., Marrot, B., Moulin, P. & Ce, P. 2009. Reverse osmosis desalination : Water sources , technology , and today ' s challenges. *Water Research*. 43(9):2317–2348.

Hall, S.G., Ahmad, S. & Smith, R. 1990. FOR HEAT EXCHANGER. *Computers chem. Engng*. 14(3):319–335.

Hartman, A. 2016. Namibia : Xaris Says Is Ready for NamPower Talks. *The Namibian* (Windhoek). 18 January. [Online], Available: http://allafrica.com/stories/201601180237.html.

Ho, C.K. & Iverson, B.D. 2014. Review of high-temperature central receiver designs for concentrating solar power. *Renewable and Sustainable Energy Reviews*. 29:835–846.

International Energy Agency. 2011. *Co-generation and Renewables: Solutions for a low-carbon energy future*. Paris. [Online], Available: https://www.iea.org/publications/freepublications/publication/CoGeneration_RenewablesSolutionsforaLowCarbonEnergyFuture.pdf.

International Energy Agency. 2015. *World Energy Outlook 2015 Factsheet*. Paris.

Isaka, M. 2012. *Water Desalination Using Renewable Energy*. [Online], Available: https://www.irena.org/DocumentDownloads/Publications/IRENA-ETSAP Tech Brief I12 Water-Desalination.pdf.

Kalogirou, S. 1997. Survey of solar desalination systems and system selection. *Energy*. 22(1):69–81.

Kalogirou, S.A. 2005. Seawater desalination using renewable energy sources. *Progress in Energy and Combustion Science*. 31(3):242–281.

Kröger, D.G. 2002. Convection heat transfer between a horizontal surface and the natural environment. 18(3).

Lee, K.P., Arnot, T.C. & Mattia, D. 2011. A review of reverse osmosis membrane materials for desalination — Development to date and future potential. *Journal of Membrane Science*. 370(1–2):1–22.

Loutatidou, S. & Arafat, H.A. 2015. Techno-economic analysis of MED and RO desalination powered by low-enthalpy geothermal energy. *Desalination*. 365:277–292.

Stellenbosch University https://scholar.sun.ac.za

Lovegrove, K. & Stein, W. 2012. *Concentrating Solar Power Technology*. K. Lovegrove & W. Stein (eds.). Cambridge: Woodmead Publishing.

Martin, M.J. 2016. Suitability of satellite sea surface salinity data for use in assessing and correcting ocean forecasts. *Remote Sensing of Environment*. 180:305–319.

MBH Energy. 2016. *A New Lease of Life for NamPower's Van Eck Power Station*. [Online], Available: http://www.power-technology.com/contractors/boilers/mbh/pressnampower-van-eck.html [2016, November 15].

Michael J., W. & Gilman, P. 2011. *Technical manual for the SAM physical trough model*. Colorado. [Online], Available: http://www.nrel.gov/docs/fy11osti/51825.pdf.

Mistry, K.H., Antar, M.A. & Lienhard, J.H. 2012. An improved model for multiple effect distillation. *DESALINATION AND WATER TREATMENT*. 51(4):1–15. [Online], Available: https://www.researchgate.net/publication/254225595_An_improved_model_for_multiple_effect_distillation.

Moser, M., Trieb, F. & Fichter, T. 2013. Potential of Concentrating Solar Power Plants for the Combined Production of Water and Electricity in MENA Countries. *Journal of Sustainable Development of Energy, WAter and Environment Systems*. 1(2):122–141.

NamPower. 2011a. *ANIXAS power station*. [Online], Available: http://www.nampower.com.na/Page.aspx?p=220 [2016, November 15].

NamPower. 2011b. *Paratus Power Station*. [Online], Available: http://www.nampower.com.na/Page.aspx?p=186 [2016, November 15].

NamPower. 2016a. *Baynes Hydropower Project*. [Online], Available: http://www.nampower.com.na/Page.aspx?p=222 [2016, November 15].

NamPower. 2016b. *Van Eck Power Station*. [Online], Available: http://www.nampower.com.na/Page.aspx?p=185.

NamWater. 2016. *Main Menu*. [Online], Available: http://www.namwater.com.na/index.php?option=com_content&view=article&layout=edit&id=65 [2016, March 02].

Nasal, J. 2003. *Boiler Feed Pump Performance Assessment Method Using Pump Affinity Laws Reduces Unceartanty*. [Online], Available: http://www.power-eng.com/articles/print/volume-107/issue-11/features/boiler-feed-pump-performance-assessment-method-using-pump-affinity-laws-reduces-uncertainty.html [2016, November 23].

Stellenbosch University https://scholar.sun.ac.za

NREL. 2015.

Ophir, A. & Lokiec, F. 2005. Advanced MED process for most economical sea water desalination. *Desalination*. 182(1–3):187–198.

Palenzuela, P., Hassan, A.S., Zaragoza, G. & Alarcón-padilla, D. 2014. Steady state model for multi-effect distillation case study : Plataforma Solar de Almería MED pilot plant. *Desalination*. 337:31–42.

Palenzuela, P., Alarcon-Padilla, D.C., Zaragoza, G. & Blanco, J. 2015. Comparison between CSP+MED and CSP+RO in Mediterranean Area and MENA Region: Techno-economic Analysis. In Vol. 69. Elsevier B.V. *Energy Procedia*. 1938–1947.

Papanicolas, C.N., Bonanos, A.M., Georgiou, M.C., Guillen, E., Jarraud, N., Marakkos, C., Montenon, A., Stiliaris, E., et al. 2015. CSP cogeneration of electricity and desalinated water at the Pentakomo field facility. In Vol. 1734. Nicosia: American Institute of Physics *SolarPaces 2015*.

Pennsylvania State University. 2014. *Fluid storage*. [Online], Available: https://www.e-education.psu.edu/eme812/node/704 [2016, November 23].

Pitz-Paal, R., Dersch, J. & Milow, B. 2005. *European concentrated solar thermal road- mapping – roadmap document*.

Pryor, M. & Blanco, B. 2010. Trekkoppje desalination plant. *Imiesa*. (July):25–28. [Online], Available: http://reference.sabinet.co.za/webx/access/electronic_journals/imiesa/imiesa_v35_n7_a11.pdf.

Pugsley, A., Zacharopoulos, A., Mondol, J.D. & Smyth, M. 2016. Global applicability of solar desalination. *Renewable Energy*. 88:200–219.

Purohit, I., Purohit, P. & Shekhar, S. 2013. Evaluating the potential of concentrating solar power generation in Northwestern India. *Energy Policy*. 62:157–175.

REEEI. 2012. *Pre-feasibility study for the establishment of a pre-commercial concentrated solar power plant in namibia*. Windhoek. [Online], Available: http://nei.nust.na/sites/default/files/projects/NA.2012.R.005.2.pdf.

Roelf, W. 2015. *Final decision on Namibia's Kudu gas to - power project seen mid - 2016*. Cape Town. [Online], Available: http://www.reuters.com/article/africa-oil-namibia-idUSL8N12T3D620151029 [2016, November 15].

Samanes, J., García-Barberena, J. & Zaversky, F. 2015. Modeling Solar Cavity Receivers: A Review and Comparison of Natural Convection Heat Loss Correlations. *Energy Procedia*. 69:543–552.

Stellenbosch University https://scholar.sun.ac.za

Sandia. 2003. *Desalination and Water Purification Roadmap - A Report of the Exceutive Committee. DWPR Program Report #95*.

Sargent, L. 2003. Assessment of Parabolic Trough and Power Tower Solar Technology Cost and Performance Forecasts Assessment of Parabolic Trough and Power Tower Solar Technology Cost and Performance Forecasts. *Report No. NREL/SR-550-34440*. (October):47.

Sawin, J.L., Seyboth, K., Sverrisson, F. & Martinot, E. 2016. *Renewables 2016: Global status report*. Paris.

Schell, S. 2011. Design and evaluation of esolar's heliostat fields. *Solar Energy*. 85(4):614–619.

schlaich bergermann und partner. 2015. *Point-focusing Solar Energy Technology: Stellio Heliostat confirms unprecedented optical and economic performance*. Stuttgart. [Online], Available: http://www.sbp.de/fileadmin/sbp.de/Presse/Downloads/150819_Stellio_Heliostat_Press_Release_2.pdf.

Seatemperature.info. 2016. *Water temparature at Swakopmund*. [Online], Available: http://seatemperature.info/swakopmund-water-temperature.html [2016, June 03].

Seigal, L. & Zelonis, J. 1995. *Water desalination*. [Online], Available: http://www.rpi.edu/ [2008, February 13].

Servert, J.F., Cerrajero, E. & Fuentealba, E.L. 2016. Synergies of solar energy use in the desalination of seawater : A case study in northern Synergies of Solar Energy Use in the Desalination of Seawater : a Case Study in Northern Chile. *AIP Conference Proceedings*. 1734(140002).

Shannon, M.A., Bohn, P.W., Elimelech, M., Georgiadis, J.G., Marinas, B.J. & Mayes, A.M. 2008. Science and technology for water purification in the coming decades. *Nature*. 452:301–210.

Siemens AG. 2012. *SST-600 Steam Turbine (Up to 150MW)*. Erlangen. [Online], Available: http://www.energy.siemens.com/hq/en/fossil-power-generation/steam-turbines/sst-600.htm.

SolarGIS Geomodel Solar. 2013. *World map of direct normal irradiation*. [Online], Available: http://geosun.co.za/wp-content/uploads/2014/10/DNI-Solar-map-World.png [2016, November 14].

solarGIS Geomodel Solar. 2016. *Solar resource maps for Namibia*. [Online], Available: http://solargis.com/products/maps-and-gis-data/free/download/cameroon [2016, November 15].

Stellenbosch University https://scholar.sun.ac.za

SOLARRESERVE. 2016. *Molten Salt Energy Storage*. [Online], Available: http://www.solarreserve.com/en/technology/molten-salt-energy-storage [2016, November 23].

Surf-Forecast.com. 2016. *Tiger Reef Water Temperature and Wetsuit Guide*. [Online], Available: http://www.surf-forecast.com/breaks/Tiger-Reef/seatemp [2016, July 18].

Swamee, P.K. & Sharma, A.K. 2008. *Design of Water Supply Pipe Networks*. 1st ed. New Jersey: John Wiley & Sons.

Takada, M. & Drake, J.C. 1983. Application of improved high-performance evaporator. *Desalination*. 45:3–12.

Thresh, J.C. 1901. *Water and water supplies*. London: Rebman Ltd.

Torresol Energy. 2010. *Gemasolar*. [Online], Available: http://www.torresolenergy.com/EPORTAL_IMGS/GENERAL/SENERV2/IMG2-cw4e4127ca5ffdf/gemasolar-plant-july2011-2b.JPG [2016, November 14].

Trading economics. 2016. *Namibian Sales Tax Rate | VAT*. [Online], Available: http://www.tradingeconomics.com/namibia/sales-tax-rat [2016, November 23].

Turchi, C.S. & Heath, G. a. 2013. *Molten Salt Power Tower Cost Model for the System Advisor Model (SAM)*. Colorado.

UN-Water. 2015. *The United Nations World Water Development Report 2015: Water for a sustainable world*. Paris.

Usci & Diane Properties. 2016a. *MYNA4738 Usakos*. Usakos. [Online], Available: https://www.my.na/product/4738/a-perfect-weekend-get-away-plot/ [2016, November 23].

Usci & Diane Properties. 2016b. *Ref: 25178 Swakopmund*. Swakopmund. [Online], Available: https://www.my.na/product/4724/own-this-plot-close-to-swakopmund-namibia/ [2016, November 23].

Viranyi, Z. 2015. *2015 Annual Report, NamPower*. Windhoek.

Walter Short, Daniel J. Packey & Thomas Holt. 1995. *A Manual for the Economic Evaluation of Energy Efficiency and Renewable Energy Technologies*.

Wei, X., Lu, Z., Wang, Z., Yu, W., Zhang, H. & Yao, Z. 2010. A new method for the design of the heliostat field layout for solar tower power plant. *Renewable Energy*. 35(9):1970–1975.

Stellenbosch University https://scholar.sun.ac.za

WHO. 1970. *European Standards for Drinking-Water*.

Wittholz, M.K., Neill, B.K.O., Colby, C.B. & Lewis, D. 2008. Estimating the cost of desalination plants using a cost database. 229:10–20.

WSP. 2013. *Prefeasibility study for biomass power plant, Namibia. Commercial assessment.* Windhoek.